

**NASA
Technical
Paper
2186**

October 1983

Expanded Operational Capabilities of the Langley Mach 7 Scramjet Test Facility

**Scott R. Thomas
and Robert W. Guy**

**LOAN COPY: RETURN TO
AFWL TECHNICAL LIBRARY
KIRTLAND AFB, N.M. 87117**

NASA



25th Anniversary
1958-1983

NASA
TP
2186
c.1





**NASA
Technical
Paper
2186**

1983

Expanded Operational Capabilities of the Langley Mach 7 Scramjet Test Facility

**Scott R. Thomas
and Robert W. Guy**

*Langley Research Center
Hampton, Virginia*

NASA

National Aeronautics
and Space Administration

Scientific and Technical
Information Branch

SUMMARY

An experimental research program conducted to expand the operational capabilities of the NASA Langley Mach 7 Scramjet Test Facility is described. The facility, an electric-arc-heated wind tunnel with air as the test gas, is configured for testing airframe-integrated supersonic combustion ramjet (scramjet) models at conditions simulating flight velocities, temperatures, and pressures. Previous scramjet testing in this facility was limited to a single simulated flight condition of Mach 6.9 at an altitude of 115 300 ft. The arc heater research presented herein demonstrates the potential of the facility for scramjet testing at simulated flight conditions from Mach 4 (at altitudes from 77 000 to 114 000 ft) to Mach 7 (at altitudes from 108 000 to 149 000 ft). Arc heater electrical characteristics are defined and systematic procedures for setting the arc heater and power supply parameters and the facility airflow rates to achieve the test conditions of interest are outlined. Solutions to operational problems (including frequent failure of a critical O-ring and arc instability) which had limited facility productivity in the past are discussed and limits of operation are presented. Measurements of nitrogen oxide contaminants and total-temperature profiles in the test stream are evaluated.

INTRODUCTION

Development of airframe-integrated supersonic combustion ramjet (scramjet) technology continues to progress at NASA Langley Research Center (LaRC). The scramjet program focus is a fixed-geometry, hydrogen-burning, advanced engine concept (fig. 1) that has been shown analytically to be an efficient propulsion device at flight speeds above Mach 4 (refs. 1 and 2). In the Mach 4 to Mach 6 range, the engine is most efficient when operated as a ramjet (ref. 2).

The integrated design (fig. 2) uses the underside of the flight vehicle as part of the propulsion system; that is, the forebody shock wave provides aerodynamic pre-compression of the flow entering the inlet, and the aft portion of the vehicle under-surface is used as part of the nozzle expansion surface. This feature reduces both the compression required from the inlet and the physical size of the engine modules needed to produce the required thrust. Because of the bow-shock precompression, the airflow, including the vehicle forebody boundary-layer flow, enters the scramjet module inlet at a Mach number less than the flight Mach number. The total enthalpy of the entering airflow, however, is unchanged by precompression and equals that of the flight Mach number.

Experimental research on this scramjet concept is currently in progress with subscale models in wind-tunnel facilities especially adapted to provide the required test conditions. Tests are conducted at total enthalpies and total pressures which are representative of practical flight Mach numbers and altitudes. These facilities provide simulation of engine-airframe integration effects such as vehicle bow-shock precompression and boundary-layer ingestion by the scramjet. This is accomplished by testing at a tunnel Mach number less than the Mach number corresponding to the flow total enthalpy and by mounting the model so that a portion of the facility nozzle boundary layer is ingested by the scramjet model.

Past tests of the airframe-integrated scramjet have been conducted in three wind tunnels at simulated flight Mach numbers of approximately 4 and 7 (refs. 3 to 6). These test Mach numbers were chosen because they provide data representative of engine operation with different amounts of engine airflow captured and different fuel-injection techniques (ref. 4). Mach 4 testing was conducted at test facilities located at LaRC and at the General Applied Science Labs (GASL) in Westbury, New York. Both are vitiated air (hydrogen-combustion heated with oxygen replenishment) facilities. Mach 7 testing was conducted at the GASL facility and at the Langley Mach 7 Scramjet Test Facility (STF), which is an electric-arc-heated facility.

This report describes an experimental test program aimed at expanding the capability of the STF for testing at simulated flight Mach numbers from 4 to 7 rather than just at Mach 7 (ref. 4). This required that the arc heater be used over a wide range of test conditions for which its behavior was unknown. Arc heaters in general are not well understood on a theoretical basis. The results of previous research on similar types of arc heaters were useful for predicting the trend of operational characteristics for the STF arc heater due to various parameter changes. However, since every arc heater is unique when coupled with a particular power supply, this experimental test program was necessary to determine the actual performance.

The arc heater was successfully operated over a wide range of total pressures and total enthalpies using three nozzle throat sizes. This demonstrated the potential of the STF for testing over a wide range of simulated Mach numbers and altitudes. With the proper facility contoured nozzles, a complete test program over a range of Mach numbers can be accomplished without removing a model from the facility by changing only the nozzle and some components in the air supply line. Arc heater and power supply parameters and facility airflow rates necessary to achieve these test conditions are presented in this report. Two problems which had previously limited facility productivity, frequent failure of a critical O-ring on the arc heater downstream electrode and occasional arc instability, were investigated. Measurements of nitrogen oxide contaminants and total-temperature profiles in the test stream over the expanded range of simulated flight Mach numbers and altitudes are presented.

SYMBOLS

A^*	geometric throat area of facility nozzle
A_{eff}	effective exit flow area of facility nozzle
D_{throat}	throat diameter of facility nozzle
E	arc voltage
$h_{\text{air,in}}$	total enthalpy of unheated supply air
h_{HE}	total enthalpy of the main airflow at the exit of the arc heater
$h_{t,1}$	total enthalpy of facility airflow at the nozzle throat
I	arc current
M_{∞}	flight Mach number

M_1	airflow Mach number at the facility-nozzle exit simulating the flow downstream of an aircraft bow-shock wave
\dot{m}_{byp}	mass flow rate of bypass air which is added downstream of the arc heater
\dot{m}_{main}	mass flow rate of main air which flows through the arc heater
\dot{m}_t	total mass flow rate of air, $\dot{m}_{main} + \dot{m}_{byp}$
NO_x	nitrogen oxides
P	arc power
P_{HE}	pressure measured in the arc heater
$P_{t,1}$	pressure measured in the facility plenum chamber
R_{arc}	arc resistance
R_{bal}	ballast resistance
R_{total}	total electrical resistance, $R_{arc} + R_{bal}$
$T_{t,1}$	total temperature of airflow in the facility nozzle simulating the flow downstream of an aircraft bow-shock wave
α	aircraft angle of attack
ΔP	arc power fluctuation
η_{fac}	facility thermal efficiency

LANGLEY MACH 7 SCRAMJET TEST FACILITY

The Langley Mach 7 Scramjet Test Facility (STF) is an electric-arc-heated facility with air as the test gas (refs. 7 and 8). Figure 3 shows an elevation view of the tunnel circuit. The test flow from the arc heater and plenum chamber is expanded through a contoured nozzle into the test section. Downstream of the test section, the flow is diffused to subsonic velocity, cooled by an aftercooler, and exhausted into a vacuum sphere.

Facility Improvements

The first tests of the hydrogen-burning, airframe-integrated scramjet were conducted at the STF and are described in references 4 and 7. These tests were successful in demonstrating the performance potential of the scramjet and in indicating areas of engine operation requiring further research. The tests also served to define areas where facility improvements would enhance future scramjet-related research. These improvements were implemented prior to the present test program. They required structural strengthening of the arc heater, construction of a new Mach 6 contoured nozzle, modification of an existing test section, fabrication of a new instrumentation box, and design of new fuel controls. A photograph of the modified facility is shown in figure 4.

The structural strengthening of the arc heater increased the maximum allowable facility stagnation pressure from 30 to 45 atm. Higher stagnation pressure is desirable to provide a lower altitude flight simulation, which will promote more efficient ignition and reaction of the hydrogen-air mixture in the scramjet. Increased stagnation pressure was obtained at simulated Mach 7 flight conditions by increasing maximum arc power from 10 MW to approximately 13 MW and by slightly reducing throat area in the new Mach 6 contoured nozzle.

An existing test section was modified to provide several additional viewing ports so that the engine can now be observed from both sides and from below at the inlet and at the exhaust. This permits more complete flow visualization than previously available and allows more extensive use of nonintrusive measurement techniques during future testing. The access port located on top of the test section was also enlarged from a 1-ft-diameter circular opening to a rectangular opening 2 ft wide by 5 ft long. A new, larger instrumentation box was constructed to fit this larger access port. These modifications were made to provide easier access to the model and to allow more space for routing instrumentation, fuel lines, model injection hardware, and fuel controls.

The new computer-operated fuel control system allows up to four distinct total fuel flow rates to be obtained during a test, with the individual fuel flow rates to six scramjet injection stations controlled independently. A system has also been added to the facility to inject a pyrophoric fuel (a mixture of hydrogen and silane (ref. 9)) into the scramjet model to promote ignition of the hydrogen-air mixture within the engine.

Major Support Systems

Major support systems required for operation of the STF are shown in figure 5. These include high-pressure air, electrical power, high-pressure deionized cooling water, vacuum, hydrogen fuel, ignitor fuel, and model injection systems. The hydrogen fuel and model injection systems, which were not used during the present test series, are described in reference 7. The air, electrical power, cooling water, and vacuum systems were used throughout the present test series and are described in this section.

Air.- A 5000 psig air bottle field supplies the STF with air through two lines. The first air line, labeled "A" in figure 5, supplies the main airflow which passes through the arc heater and is heated to a total enthalpy higher than presently used for scramjet-related testing (nominally 3000 Btu/lbm). This heated air is then mixed in the plenum chamber with an unheated bypass airflow, supplied by line "B," to obtain the test airflow with the desired total enthalpy. During the present test series, the main airflow rate was varied between 0.44 and 2.50 lbm/s and the bypass airflow rate was varied between 0.88 and 16.50 lbm/s.

Electrical power.- Direct-current (dc) electrical power is provided by two identical power supplies connected in series with the arc heater and with two sets of ballast resistors and a reactor, which are used to achieve arc stability. The power supplies, which consist of arrays of alternating-current (ac) transformers and silicon diode rectifiers, can be regulated to provide various power levels up to 20 MW dc to the arc heater circuit. Power levels are obtained by selection of power-supply-transformer output voltages, which are termed tap settings. Each power supply has 33 available tap settings with corresponding voltage-current output characteristics as shown in figure 6. A schematic of the arc heater electrical power system is

shown in figure 7. During testing, total ballast resistances of 1.304, 1.479, and 1.594 ohms were used; the corresponding resistor arrangements are shown in figure 8.

Cooling water.- Deionized water, stored in a 50 000-gal capacity tank (fig. 5), is used to cool the arc heater components, the plenum chamber, and the facility nozzle. A pump driven by a 3000-hp motor supplies the components with cooling water at pressures up to 1400 psig. During this test series, the supply manifold pressure was 1000 psig for all tests with arc heater power less than or equal to 10 MW. This pressure was increased by 100 psig for every 1-MW increase in arc heater power above 10 MW. At a supply pressure of 1000 psig, the total cooling water flow rate to all components was 1060 gal/min.

Vacuum.- Vacuum for altitude simulation at the STF is provided by a 100-ft-diameter vacuum sphere which is evacuated using a three-stage steam ejector. During this test series, the only vacuum requirement was that flow through the metering nozzle throat be choked. In the most critical case, this required a sphere pressure below approximately 6.5 psia.

Arc Heater and Plenum Chamber Configuration

The electric arc heater and plenum chamber configuration used at the STF is shown in figure 9. The arc heater is a Linde type ($N = 3$), and the various components of the heater and of the plenum chamber are noted respectively in figures 10 and 11 and in tables I and II. As indicated in the electrical system schematic (fig. 7), the arc heater is operated with the upstream electrode as the anode and the downstream electrode as the cathode. The potential difference between ground and the downstream electrode is approximately the same as that between the upstream electrode and ground. During the present test series, the voltage drop across the electrodes ranged from 1450 to 7100 V.

The electric arc is initiated by using a 0.035-in-diameter steel rod to make initial contact between the two coaxial, cylindrical electrodes (upstream and downstream electrodes), which are separated by the electrically insulated main air-inlet chamber. The arc establishes between the electrodes and, except for the termination regions, is confined along the centerline of the heater by the vortex flow of the main airstream, which is injected with both a radial and a tangential velocity (swirled in). This type of arc heater is termed a vortex-stabilized arc heater (ref. 10). The arc termination regions (the areas where the arc attaches to the electrodes) are continuously rotated by a combination of the swirling air and the interaction of the arc with the two externally applied magnetic fields, each of which has a strength of 5000 gauss. The arc rotation spreads the intense heating rate of the arc attachment regions over a much greater surface area and prevents the copper electrodes from melting in these regions.

The arc-heated air is mixed with the bypass air to form a resultant test gas with the desired stagnation conditions. This mixing scheme is necessary because the arc heater cannot process the total facility mass flow and maintain a stable operating mode. The bypass air is injected radially from two sets of slots machined in the second and third plenum rings as shown in figure 11. This radial injection enhances mixing and also breaks up the swirl downstream of the arc heater to improve flow quality for engine testing.

ARC HEATER RESEARCH TESTS

The arc heater research tests were conducted to extend the capability of the STF for testing at simulated flight Mach numbers from 4 to 7. This required the size of the facility-nozzle throat, both the main and bypass airflow rates, the power-supply tap settings, and the ballast resistance to be varied. Previously the STF was operated to simulate a single Mach 7 flight condition (arc power of 9.77 MW, total pressure of 28.5 atm, total temperature of 3925°R, and other operating conditions tabulated in ref. 7). Data providing information on the operating characteristics of the arc heater and power-supply combination at other arc powers and heater pressures were not available.

Testing the present-size scramjet engine models at various simulated flight Mach numbers requires use of a series of nozzles with exit areas compatible with the same engine size; therefore, each nozzle has a different throat area. The pressure within the arc heater and plenum chamber is strongly dependent on the nozzle throat area where the test stream is always choked; therefore, the size of this throat could affect the operating conditions of the arc heater (providing the main airflow exiting the downstream electrode is not choked). However, since the flow velocity at the throat is sonic, flow conditions downstream of the throat have no effect on those in the arc heater and plenum chamber. Therefore, tests with converging metering nozzles (of circular cross section) with the same throat areas but without the complex expansion contours of a tunnel nozzle provide proper arc heater operation corresponding to the desired test conditions.

Results of previous scramjet tests (refs. 3 and 4) were used to determine approximate specifications for contoured facility-nozzle designs (i.e., exit Mach number, exit area, and throat area) useful for testing scramjet engine models typically 8.0 in. high by 6.4 in. wide at simulated flight Mach numbers of 4.0, 5.5, and 7.0. The chosen levels of simulated flight-vehicle-forebody precompression yielded inlet Mach numbers of 3.4, 4.9, and 6.0. (See fig. 12.) Converging metering nozzles with the throat areas specified by these results were constructed and used during this test program.

Special Test Apparatus

The converging metering nozzles discussed above and a constant-area, uncooled connector duct (coated internally with zirconium oxide) were used in place of facility contoured nozzles. This test setup is shown schematically in figure 13 and a photograph of the configuration is presented in figure 14. Metering nozzles with the following three different throat diameters were used: a 1.3-in-diameter throat for simulating Mach 7 flight conditions; a 2.2-in-diameter throat for simulating Mach 5.5 flight conditions; and a 5.6-in-diameter throat for simulating Mach 4 flight conditions. The 1.3-in-diameter throat and the 2.2-in-diameter throat consisted of a common flange into which the two individual throat inserts were installed. (See figs. 15(a) and 15(b).) These configurations were water-cooled and the surfaces exposed to the hot airflow were coated with zirconium oxide for additional thermal protection. The 5.6-in-diameter throat was machined as an integral part of a flange as shown in figure 15(c). The surfaces of this throat configuration which would be exposed to the hot air were also coated with zirconium oxide; however, the throat was not water-cooled.

In order to obtain the correct total enthalpies and total pressures for the desired range of simulated flight conditions, bypass and main airflow rates greater

than those used in previous tests were required. The increases in bypass airflow rate were accomplished with only minor changes to the bypass air system. The plenum rings (fig. 11) were modified as indicated in table III by increasing the number of rectangular injection slots located between rings 1 and 2 and between rings 2 and 3 and by increasing the size of each injection slot. A larger capacity airflow meter and a larger flow orifice in the bypass air regulator were also required. No changes were necessary in the main air system to increase this airflow rate by the required amount.

Test Parameters Setup Procedure

During the initial part of the test series, all run conditions, regardless of the arc power level and the test flow total enthalpy, were set up maintaining the ratio of attempted arc power to main airflow rate the same as for the previous single operating point (i.e., at a ratio of 10 MW/1.7 lbm/s). Expected arc resistance was calculated with a similar ratio (i.e., a ratio of 2 ohms/1.7 lbm/s). From these values, tap settings, which would yield specified arc powers, were approximated from plots such as figure 16, generated from the plots of power-supply characteristics (fig. 6). Figure 16 shows arc power as a function of arc resistance and power-supply tap settings for a ballast resistance of 1.304 ohms. The tap settings on both power supplies were taken to be equal. Assuming heater total enthalpy to be the same as the previous operating point (i.e., approximately 3000 Btu/lbm) and with main airflow rate and the unheated bypass air enthalpy known, the required bypass airflow rate for a given test total enthalpy was calculated from a simple mixing equation. This setup procedure was refined as new data were obtained.

Test Procedure

Prior to a test, the facility configuration needed to obtain the test conditions of interest was determined. Hardware selection options included metering-nozzle size, downstream electrode design, bypass air injector configuration, and ballast resistance. The various systems of the STF were then set up (i.e., the electrical power, air, cooling water, vacuum, and data acquisition systems). The output power level was adjusted by choosing a tap setting for each power supply according to the procedure outlined in the previous section, and the corresponding main and bypass airflow rates were selected.

A check run was made each day before any other testing was conducted. During this run all systems functioned except the arc heater electrical power and data acquisition systems. Although these systems were not in operation, the timing of the sequencers controlling them and all other systems was checked. If all systems performed as expected during the check run, final preparations for a hot test were completed.

After the hot test was manually initiated, the test sequence was completely automatic. Control was provided by three cam systems, an automatic sequencer, and several timers, all of which were preprogrammed. Throughout the test series, the arc was established for 10 to 15 s during each test.

Measured Parameters

The measured parameters included arc voltage and current; main and bypass air mass flow rates; cooling water flow rates to all heater components, the plenum rings, the plenum, and the throat; inlet and outlet cooling water temperatures to the same components; arc heater pressure; and plenum chamber pressure. From these measurements, which were recorded 20 times per second, arc heater electrical operating characteristics were determined. Heater and test-flow total enthalpies were calculated according to the energy balance equations given in reference 7, and test total enthalpy was calculated using the uncorrected sonic throat method (ref. 11).

Nitrogen oxide levels in the test gas were determined from gas samples obtained at the exits of the metering nozzles during some tests. (See fig. 17.) A water-cooled sample probe was positioned at the exit of the metering nozzle. With the solenoid and sample-bottle valves open, the test section vacuum was used to purge the bottle with captured test gas during the first 5 s of the hot test. The downstream solenoid valve was then closed and a gas sample obtained. Prior to extinguishing the arc, the upstream solenoid valve was closed to ensure an accurate sample of the test gas. The sample bottle was then removed and its contents analyzed to determine nitrogen oxide level.

Total temperature was measured during some tests of all three metering nozzles. The total-temperature probes were mounted in the flow just downstream of the nozzle throat. (See fig. 13.) An annealed iridium/iridium-40-percent-rhodium thermocouple was used with the 1.3-in-diameter metering nozzle for test conditions at which the airflow total temperature was greater than 2500°R (fig. 18). Although the thermocouple probe was designed to minimize velocity, conduction, and radiation losses (see ref. 12), uncertainties still exist at these temperature levels. Other factors such as changes in thermocouple emissivity due to plating of copper oxide from the arc heater electrodes onto the thermocouple bead could also have affected the accuracy of the thermocouple measurements. For tests with the total temperature below 2500°R, surveys were conducted using a chromel/alumel thermocouple rake (fig. 19). Velocity, conduction, and radiation loss were minimized by the probe design and were small at the total temperatures measured with the chromel/alumel thermocouples.

TEST RESULTS

The major results of this test series are presented in this section. Operational problems are discussed first, and solutions to these problems or imposed limits of operation are presented. Arc heater and power-supply electrical characteristics are outlined, and the effects of ballast resistance, airflow rate, and arc heater pressure on these characteristics are discussed. Results from the various techniques for determining total enthalpy of the airflow are compared, and facility thermal efficiency is discussed. Measured total-temperature profiles are analyzed to assess flow quality for future scramjet tests over a range of simulated flight Mach numbers. Measurements of nitrogen oxide contaminants in the arc-heated flow are presented for a range of simulated flight conditions for use in relating scramjet performance measured in the facility tests to expected flight performance. Maps of facility operating range in terms of total pressure and total enthalpy are presented for three potential facility nozzles. The flight Mach number and altitude-simulation capabilities corresponding to the range covered by these maps are discussed. Finally, refined facility setup procedures which can be used to determine the proper electrical and airflow parameters for this range of test conditions are outlined.

Operational Problems

Critical O-ring failure.- One very important operational problem, which was solved during the arc heater research tests, was the failure of a critical O-ring after every high-arc-power test (arc power greater than approximately 7.5 MW). The O-ring provides a seal between the high-pressure cooling water and the facility airflow at the downstream end of the downstream electrode (fig. 20(a)). The problem was eliminated by redesign and modification of the downstream electrode.

With the original downstream electrode configuration, the tip of the electrode was some distance from the cooling water passage and was directly exposed to the hot airflow exiting the electrode (entering the plenum chamber). During a hot test, the high-temperature airflow caused the downstream electrode to thermally expand. The tip of the electrode increased in diameter, extended farther from the cooling water passage, and became very hot. After the test was terminated, the downstream electrode contracted and dragged the hot tip over the O-ring surface. For every high-power test, O-ring damage occurred with water leakage after the test; therefore, the O-ring had to be replaced. This required securing all major facility systems, disassembling part of the arc heater, replacing the O-ring, reassembling the arc heater, and setting up the facility systems again before the next test could be made. Replacing the O-ring involved much time and effort and this problem significantly limited the productivity of the STF.

A downstream electrode design with a new tip configuration completely resolved the O-ring problem. In this design, shown in figure 20(b), the downstream electrode tip was constricted to a smaller internal exit diameter (to 1.600 in. from 2.315 in.) to allow space for an external cooling water passage between the O-ring and the hot airflow. This cooling water passage also moves with the electrode tip as the electrode expands thermally and maintains the surface in contact with the O-ring at a reasonably cool temperature at all times. No O-ring failure has occurred with the newly designed electrode tip. At the completion of this test series, 125 tests, 50 of which were at high arc power, had been made without O-ring damage.

Arc instability.- An arc-instability problem, characterized by significantly increased fluctuations in arc power and by arc attachment further downstream than normal, was observed for some test conditions during the arc heater research tests as well as during earlier test programs. This problem occasionally resulted in damage to the tip of the downstream electrode. In a few cases, arc attachment downstream of the electrode caused damage to the plenum rings or to the metering-nozzle flange. During this test series, the stable operating range of the facility was defined for the test conditions of interest.

Maximum arc power fluctuations normalized with the corresponding mean arc powers are shown in figure 21 as functions of the ratio of arc resistance to total resistance for various run conditions. Curves are presented for data obtained using the original downstream electrode with the 1.3-in-diameter throat and using the new constricted downstream electrode with all three metering nozzles. Data obtained with some of these configurations exhibited considerable scatter; therefore, only curves which were faired through the mean of the data are shown. The normalized arc power fluctuations were relatively constant for all electrode-throat combinations below an arc-to-total resistance ratio of 0.65. With the 1.3-in-diameter throat, however, the arc power fluctuations with both electrodes increased dramatically at higher resistance ratios. Insufficient data exist to determine stability limits for the two larger throats. The data emphasize the importance of maintaining sufficient ballast resistance in the arc heater electrical circuit. Generally, power fluctuations were

smaller when operating with the new constricted downstream electrode design than with the original design and decreased as metering-nozzle diameter was increased. The arc was contained within the arc heater and no damage to the downstream electrode, plenum rings, or metering-nozzle flange occurred because of an arc-instability problem after the newly designed downstream electrode was placed in service.

Arc Heater Electrical Characteristics

The arc heater electrical characteristics (voltage, current, and power) are specified by power-supply tap settings, ballast resistance, and arc resistance. Although the tap settings and the ballast resistance are selected prior to a test, arc resistance is a function of several variables. In this test series, arc resistance was determined as a function of main airflow rate, arc heater pressure, and metering-nozzle throat size in the operating range explored.

Arc power as a function of tap settings, ballast resistance, and arc resistance is shown by the curves in figures 22(a) to 22(c), which were generated using power-supply characteristics (fig. 6). Lower ballast resistance yields higher arc power for any particular value of arc resistance. However, sufficient ballast resistance must be present in the arc heater circuit to maintain stable arc operation. In the tests the amount of ballast resistance was varied between 1.304 and 1.594 ohms. These data, shown in figures 22(a) to 22(c), demonstrated that a ballast resistance of 1.304 ohms was sufficient to maintain stable arc operation with the new downstream electrode installed while achieving any scramjet test condition in the range of interest. The dashed curves in the figures represent the limit of the arc-to-total resistance ratio (approximately 0.65) where arc instability was shown to be a potential problem in tests using the 1.3-in-diameter throat. Test conditions above the dashed line may result in the arc being less stable whereas those below the dashed line result in stable arc operation. Some data points are shown where arc resistance was greater than that defined by the dashed stability curve. Although the newly designed downstream electrode contained the arc during the tests, large arc power fluctuations were observed ($\Delta P/P \approx 12$ percent for $R_{arc} = 6.5$ ohms in fig. 22(a)).

Arc resistance as a function of main air mass flow rate and metering-nozzle throat size is shown in figure 23(a). These data were obtained with constant power-supply tap settings of 16 and a ballast resistance of 1.304 ohms. Arc resistance increased almost proportional to main airflow rate for the larger two throats over the range investigated. However, with the 1.3-in-diameter throat, arc resistance increased rapidly at main airflow rates above approximately 1.4 lbm/s. This rapid increase occurred as operation approached unstable conditions. Data obtained at other power-supply tap settings exhibited similar trends.

Arc heater pressure effects on arc resistance are shown in figure 23(b). These data were obtained at various power-supply tap settings and bypass airflow rates with a ballast resistance of 1.304 ohms and nominal main airflow rates. All the data fall into a correlation band which shows a gradual increase in arc resistance with heater pressure. The shaded symbols are the data shown in figure 23(a). These data indicate that the main airflow rate effect is independent of the pressure effect.

The effects of main airflow rate on several fluid and electrical properties are shown in figures 24 and 25. The data in figure 24 were obtained using the 5.6-in-diameter throat with tap settings of 16 and a constant bypass airflow rate. The flow from the downstream electrode was choked when this throat was installed (see fig. 26); therefore, all property variations are solely a function of the main air-

flow rate. The large variations in the properties demonstrate that main airflow rate can be an important parameter for achieving a range of test conditions. The data in figure 25 show the effect of main airflow rate on arc power at the maximum power-supply tap setting of 33. Increased main airflow rate leads to higher arc power. Since 33 is the maximum tap setting for the power supplies, this effect can be useful to achieve maximum power within the previously defined arc-stability limits.

The large effects of main airflow rate on arc resistance and other heater properties require that nominal main airflow rate be defined as a function of power-supply tap setting. (See fig. 27.) The use of these nominal airflow rates should provide a consistent approach to achieving the desired test conditions.

Arc resistance, arc power, arc voltage, and arc current are presented as functions of tap setting in figures 28 and 29 at the nominal main airflow rates with a ballast resistance of 1.304 ohms. The magnitudes of all these parameters increase with increasing tap setting. In general, operation with larger throat sizes at a particular tap setting resulted in lower arc resistance, arc voltage, and arc power but in higher arc current. At the highest tap setting (33 on both power supplies), only 11.1 MW of arc power was obtained with the 5.6-in-diameter throat, whereas 12.8 MW was obtained with the 1.3-in-diameter throat at the same nominal main airflow rate. As shown in figure 25, the power obtained with the 5.6-in-diameter throat can be increased by increasing the main airflow rate above the nominal value. However, this is not the case with 1.3-in-diameter throat because of potential problems with arc instability.

Test-Flow Total Enthalpy and Facility Thermal Efficiency

Three methods were used to determine total enthalpy: the energy-balance technique (ref. 7), the equilibrium sonic-throat technique (ref. 11), and the total-temperature measurements. A comparison of the results is shown in figure 30, in which total enthalpy at the nozzle throat is plotted versus $\dot{m}_t/(p_{t,1}A^*)$. Data obtained for all three metering nozzles are presented. The energy balance and uncorrected thermocouple data are correlated by the $\dot{m}_t/(p_{t,1}A^*)$ parameter, and all three methods are in relative agreement over the lower portion of the enthalpy range. However, total enthalpy determined using the total-temperature measurements is lower than the other two methods at the higher enthalpies. As discussed previously, the total-temperature measurements are subject to radiation, velocity, and heat conduction losses which are difficult to account for accurately. Because of these errors, the measured values of total temperature are less than the actual values. The energy-balance technique is believed to be the most accurate of the three methods for determining total enthalpy because it is independent of the kinetic state of the gas and because facility thermal efficiency is high. (Approximately 50 percent of the energy available from the arc remains in the main airflow at the exit of the heater.) Therefore, the energy-balance total enthalpy is used throughout the remainder of this report.

Facility thermal efficiencies obtained during operation with all three metering nozzles are shown in figure 31 as a function of throat total enthalpy. Facility thermal efficiency is defined as the fraction of the arc power which is in the airflow at the nozzle throat. The trends of the efficiency curves may be explained as follows. Increasing throat size decreases plenum pressure and, generally, arc heater pressure (unless the flow from the downstream electrode is choked) for a given operating condition. Lower operating pressures yielded a reduction in heat loss to all water-cooled components. Therefore, at a constant test enthalpy, increased

throat size will yield higher facility thermal efficiency. Increasing the bypass airflow rate while holding tap settings and main airflow rates constant decreases test enthalpy and increases total airflow rate, plenum chamber pressure, and arc heater pressure (if the flow from the downstream electrode is not choked). During operation with the 5.6-in-diameter metering nozzle, the flow exiting the downstream electrode was always choked (fig. 26). Therefore, increased bypass airflow yielded higher plenum pressure but had no effect on the pressure within the arc heater or on the heat loss to the arc heater components (which comprises most of the facility heat losses). As a result, efficiency remained approximately constant over the total-enthalpy range. During operation with both the 2.2-in- and 1.3-in-diameter metering nozzles, larger bypass flows resulted in higher pressures in both the plenum chamber and the arc heater, and thus in greater heat losses to all water-cooled components. This effect was greater for the smaller metering nozzle, yielding the variations of η_{fac} with $h_{t,1}$ shown in the figure.

Total-Temperature Profiles

Total-temperature profiles were measured at the exits of the metering nozzles to determine if the flow uniformity was sufficient to warrant constructing facility contoured nozzles for testing scramjets at simulated flight Mach numbers of 4 and 5.5. (A nozzle for Mach 7 flight simulation exists.) The facility air injection configuration, in which the unheated bypass air is injected into the arc-heated flow, requires that a high degree of mixing occur in the plenum chamber to achieve a satisfactory test flow. Methods to enhance mixing of the main and bypass airflows within the plenum chamber to improve the total-temperature profiles were also explored. These methods included modifying the number and size of the bypass air injection slots located between plenum rings 1 and 2 and between plenum rings 2 and 3. The various bypass air injection configurations used are outlined in table III.

In a previous test series (refs. 4 and 7), pitot pressure and stagnation point heating-rate surveys were used to obtain a total-enthalpy profile at the exit of the Mach 6 facility contoured nozzle. The throat area of this nozzle was the same as that of the 1.3-in-diameter metering nozzle, and the resultant flow uniformity was determined to be sufficient for Mach 7 scramjet engine testing. During the present test series, only centerline total temperatures were measured at the exit of the 1.3-in-diameter metering nozzle for several testing conditions using configuration number 1 in table III. These measurements were generally somewhat lower than the total temperatures calculated with the energy-balance method. (See fig. 30.) Potential thermocouple error at these extreme conditions make this data somewhat inconclusive; however, the best estimates of thermocouple error still leave the thermocouple measurements lower than the energy-balance temperatures. This is also consistent with a well-mixed flow. A high centerline temperature (relative to the energy balance prediction) would be expected if the arc-heated flow and the bypass flow were not well mixed because the unheated bypass air is injected from the plenum rings at the periphery of the arc-heated flow.

To explore the flow uniformity of the facility test stream at simulated Mach 5.5 flight conditions, total temperatures were measured at the exit of the 2.2-in-diameter metering nozzle with the chromel/alumel thermocouple rake shown in figure 19 and with bypass air injection configuration number 3 in table III. Tests were made with the rake rotated from 0° to 135° in 45° increments to obtain profile data across the entire nozzle exit. Total-temperature profiles obtained at a flow total pressure representative of flight at an altitude of 91 000 ft indicate that the flow uniformity was exceptionally good. (See fig. 32.) Therefore, facility operation at this

simulated flight condition is adequate for scramjet testing. Bulk total temperature derived with the energy-balance technique was in excellent agreement with the thermocouple measurements.

To explore the flow quality of the facility test stream at simulated Mach 4 flight conditions, total temperatures were measured at the exit of the 5.6-in-diameter metering nozzle with the chromel/alumel thermocouple rake. The chance of poor flow uniformity because of inadequate mixing of the arc-heated main airflow with the unheated bypass airflow within the plenum chamber was greatest with this throat because the bypass air was injected into a choked main airflow issuing from the constricted downstream electrode. (See fig. 26.) The larger throat flow area relative to the flow area of the 10.38-in-diameter plenum chamber could also unfavorably affect flow uniformity.

Initial total-temperature profiles obtained with the 5.6-in-diameter throat for bypass air injection configuration number 2 are shown in figure 33. Flow total pressure was representative of Mach 4 flight at an altitude of 91 000 ft. These profiles show an asymmetry with the thermocouple rake mounted in the horizontal plane which is only slightly detectable with the rake in the vertical plane. This was first believed to be caused by deterioration of the boron nitride insulators (located between the plenum rings) creating an imbalance in the distribution of the injection of bypass air. In an attempt to eliminate this problem, a set of 0.125-in-thick copper discs was added between the plenum rings and the insulators. (See bypass air injection configuration number 3, table III.) Even with insulator breakage the area of the slot injection should remain constant. Total-temperature profiles obtained after addition of these copper rings are shown in figure 34; the resultant flow uniformity was not substantially changed. To improve mixing further without redesign of the air injection components of the arc heater, the distribution of bypass air injection was changed so that all the bypass air was injected between plenum rings 1 and 2. This required machining slots in the copper disc covering plenum ring 2 (so that the injection area at this station was doubled) and closing off the bypass air lines to plenum ring 3 (bypass air injection configuration number 4, table III). Thus, all the bypass air was injected as close to the centerline as possible with the existing plenum ring design. The corresponding total-temperature profile, obtained only for the 135° rake orientation (shaded symbols in fig. 34), indicates that mixing was much improved.

Total-temperature profiles obtained with the 5.6-in-diameter metering nozzle were still less uniform than those obtained with the 2.2-in-diameter metering nozzle. However, the maximum variation of total temperature from the average value was only ± 4 percent. This flow uniformity is considered to be adequate for scramjet engine and inlet testing.

Total-temperature profiles were also obtained at the exit of the 5.6-in-diameter metering nozzle with various bypass airflow rates at a fixed arc power and a fixed main airflow rate. This resulted in run conditions over a range of total enthalpies (total temperatures). These profiles, which are shown in figure 35, indicate that mixing is more complete at higher bypass airflow rates in the range of interest.

Some tests with the 5.6-in-diameter throat were made at higher arc powers to demonstrate heater operation at near maximum capability. However, without some modification, the present air system could not provide enough bypass airflow at these arc power levels to reach Mach 4 enthalpy. Therefore, the tests, which were conducted with bypass air injection configuration number 2, resulted in total-temperature levels greater than those required for Mach 4 flight simulation. The corresponding

profiles are shown in figure 36. Since the downstream electrode flow is choked during operation with the 5.6-in-diameter throat, the potential of the arc heater to reach high power levels for Mach 4 flight simulation was demonstrated even though the bypass airflow level was not achieved. The increased bypass airflow rate would have no effect on arc heater operating characteristics; however, as stated above, increased bypass airflow rate (to reach Mach 4 conditions) should improve flow uniformity for the run conditions shown in figure 36.

These flow uniformity studies indicate that the scramjet test facility can be used for effective scramjet engine testing at conditions simulating flight Mach numbers from 4 to 7 and a range of altitudes. Therefore, with the proper contoured nozzles, engine tests can be conducted over this Mach number range without removing the model from the facility.

Nitrogen Oxide Contaminants

Nitrogen oxide contaminants in the test stream entering a scramjet engine affect the ignition of the hydrogen-air mixture (ref. 13) and also affect the engine performance by reducing the oxygen available for the combustion process (ref. 14). Therefore, a knowledge of the quantity of nitrogen oxides in the flow is necessary so that engine test results from ground facilities can be properly related to actual flight situations where the nitrogen oxides would not be present. Flow samples at test conditions over the expanded facility operating range were captured in a sample bottle (fig. 17) and analyzed to determine nitrogen oxide content. At each enthalpy level, facility arc power and airflow rate were varied to achieve a range of total pressures and, therefore, a range of altitude simulation.

The results of these nitrogen oxide measurement tests are shown in figure 37. Generally, nitrogen oxide level increases as simulated Mach number (i.e., flow total temperature) is increased from 4 to 7. This trend is most pronounced at the lower arc powers. For all the data shown in figure 37, the total enthalpy of the flow leaving the downstream electrode was essentially constant. Also, most of the nitric oxide present in the flow was produced in the heater. Therefore, lower percentages of nitrogen oxides would be expected at the test total enthalpies corresponding to lower Mach numbers because of the dilution effect of the higher bypass airflows required to achieve these enthalpies. All three curves tend to peak at the middle arc powers and to converge at the higher arc powers.

The levels of nitrogen oxide contamination in the facility test stream reach a maximum of more than 3.5 percent by volume for Mach 7 flight simulation. An attempt was made to reduce these levels by decreasing the total enthalpy of the air exiting the heater. This was accomplished by increasing the main airflow rate while keeping the power-supply tap settings constant and adjusting the bypass airflow rate to maintain the test total enthalpy. The results are shown in figures 38(a) and 38(b) for respective tap settings on both power supplies of 16 and 33. For the power-supply tap setting of 16, the data obtained with the 1.3-in-diameter metering nozzle show a dramatic decrease (56 percent) in nitrogen oxide content as the main airflow rate increased 32 percent. A smaller variation of nitrogen oxide level with main airflow rate was observed with the two larger metering nozzles. For the power-supply tap setting of 33, data from both the 2.2-in- and 5.6-in-diameter metering nozzles show a slight decrease in nitrogen oxide levels as main airflow increased and, therefore, heater flow total temperature decreased. Data from the 1.3-in-diameter metering nozzle were not obtained since the main airflow rate at this tap setting could not be increased because of arc-stability problems.

Range of Test Conditions

This test series demonstrated the versatility of the STF arc heater and electrical system combination through successful operation over a wide range of test conditions at arc powers from 2.3 to 13 MW. The test conditions which resulted in a stable operating mode (and which are useful to reproduce during future test series) are shown in terms of facility stagnation conditions for the 1.3-in-, 2.2-in-, and 5.6-in-diameter metering nozzles in figures 39(a), 39(b), and 39(c). Future testing will be done with equal power-supply tap settings, a ballast resistance of 1.304 ohms, and the new downstream electrode design. All the data shown in figure 39 were obtained at these conditions.

The dashed curves in figures 39(a) to 39(c) indicate the enthalpy level required for simulating flight conditions at the facility-nozzle exit Mach number. This corresponds to a flight situation with no forebody precompression, that is, the scramjet inlet Mach number is the same as the aircraft flight Mach number. Engine testing at total-enthalpy levels less than those corresponding to the facility-nozzle exit Mach numbers (to the left of the dashed curves) represents a flight situation in which the flow is expanded prior to entering the scramjet, that is, a scramjet inlet Mach number greater than the vehicle flight Mach number (an undesirable and unlikely situation). Scramjet engine tests will be most meaningful at enthalpy levels equal to or greater than that corresponding to the facility nozzle exit Mach number, that is, to the right of the dashed curve. Testing in this region is representative of a flight situation in which the flow is compressed prior to entering the scramjet, that is, the scramjet inlet Mach number is less than the vehicle flight Mach number.

The degree of simulated forebody precompression increases as total enthalpy is increased above the level corresponding to the facility-nozzle exit Mach number. Flight conditions with the values of precompression chosen for the present study and for others (refs. 3 to 6) are represented by the total enthalpy indicated by the solid curves in figures 39(a) to 39(c). These curves correspond to simulated flight Mach numbers of 7, 5.5, and 4. These figures outline the range of test stagnation pressures available at each of these simulated flight Mach numbers.

The range of simulated flight conditions available for scramjet engine testing (i.e., the resultant flight Mach number and altitude operational envelope) depends on the chosen degree of flight-vehicle-forebody precompression. As discussed, the limiting case is that of zero precompression; this test envelope is outlined in figure 40(a). The scramjet engine test envelope corresponding to flight-vehicle configurations with the levels of precompression chosen for the present study is shown in figure 40(b). Similar test envelopes could be constructed for other levels of precompression. The shaded symbols in figures 39(a) and 40(b) represent the single-point operation of the STF prior to the arc heater research test series.

Scramjet inlet tests at the particular nozzle-exit Mach numbers (supplied by nozzles with identical throat areas as those used to obtain the data in fig. 39) could be conducted over the entire total-enthalpy range shown in these figures. However, for inlet testing, the total enthalpy need only be high enough to prevent flow liquefaction. Of more importance are the inlet Mach number and the Reynolds number. Therefore, inlet tests can be conducted at total enthalpies less than that of the dashed curves. The much less severe test environment associated with the lower total enthalpies allows the use of less elaborate, uncooled inlet designs with more conventional instrumentation than can be used in a high-temperature flow.

Refined Test Setup Procedure

An important result of this test series was the development of systematic procedures for adjusting the main and bypass airflow rates and the power-supply tap settings to obtain specific flow conditions within the facility operating range. These procedures, which maintain a constant total ballast resistance of 1.304 ohms and equal tap settings on both power supplies, are outlined as follows:

1. The facility stagnation conditions (total enthalpy and total pressure) corresponding to the desired flight simulation condition (Mach number, altitude, and degree of precompression) are established.
2. Figure 30 is used to determine the necessary total air flow rate corresponding to these conditions.
3. Figure 31 is used to approximate facility thermal efficiency η_{fac} for the required total enthalpy, where

$$\eta_{fac} = \frac{100 \dot{m}_t (h_{t,1} - h_{air,in})}{P}$$

This equation is used to determine the required arc power.

4. The required power-supply tap settings are obtained from figure 29(a), and the corresponding main airflow rate is determined from figure 27. Bypass airflow rate is calculated as the difference between the known total and main air mass flow rates.
5. The arc heater electrical characteristics (arc resistance, voltage, and current) corresponding to these setup procedures can be determined approximately from figures 28, 29(b), and 29(c).

In steps 3 to 5, parameters for other throat areas within the range of those tested must be determined approximately by interpolation. The data used in these setup procedures were obtained using nominal main airflow rates (fig. 27). For the procedures to be accurate, it is essential that these nominal main airflow rates be used. Results are less sensitive to bypass airflow rate; however, some small adjustments of bypass airflow rate may be necessary to obtain the exact total enthalpy desired.

CONCLUDING REMARKS

The arc heater research test series showed the versatility of the arc heater and electrical system combination of the Langley Mach 7 Scramjet Test Facility. The potential of the facility for scramjet engine testing was demonstrated at simulated flight conditions from Mach 4 (at altitudes from 77 000 to 114 000 ft) to Mach 7 (at altitudes from 108 000 to 149 000 ft). The feasibility of conducting inlet tests in the facility over a similar range of Mach numbers was also shown. Arc heater electrical operating characteristics were determined over the corresponding range of facility stagnation conditions, and systematic procedures for generating this wide range of operating conditions were presented. Test-flow total-temperature profiles were determined to be sufficiently uniform for both scramjet engine and inlet test-

ing, and levels of nitrogen oxide contaminants in the facility test stream were determined over the range of conditions useful for engine testing.

These tests also provided a solution to a problem of O-ring failure and defined facility operational limits to avoid arc instability. The elimination of these operational problems results in cost savings by minimizing hardware damage during operation, increasing dependability and consistency of the facility, and significantly increasing facility productivity.

Langley Research Center
National Aeronautics and Space Administration
Hampton, VA 23665
August 18, 1983

REFERENCES

1. Henry, John R.; and Anderson, Griffin Y.: Design Considerations for the Airframe-Integrated Scramjet. NASA TM X-2895, 1973.
2. Jones, Robert A.; and Huber, Paul W.: Airframe-Integrated Propulsion System for Hypersonic Cruise Vehicles. ICAS Proceedings - 1978, Volume 1, Fuel Conservation, Hypersonic Vehicles, Environmental Effects, Materials and Structures, Computational Aerodynamics, Wind Tunnels, Flight Testing, Stability and Control, J. Singer and R. Staufenbiel, eds., Sept. 1978, pp. 130-136.
3. Andrews, E. H.; Northam, G. B.; Torrence, M. G.; and Trexler, C. A.: Mach 4 Tests of a Hydrogen-Burning Airframe-Integrated Scramjet. 18th JANNAF Combustion Meeting, Volume IV, Debra Sue Eggleston, ed., CPIA Publ. 347 (Contract N00024-81-C-5301), Appl. Phys. Lab., Johns Hopkins Univ., Oct. 1981, pp. 87-96.
4. Guy, Robert W.; Torrence, Marvin G.; Mueller, James N.; and Sabol, Alexander P.: Initial Ground-Facility Tests at Mach 7 of a Hydrogen-Burning, Airframe-Integrated, Scramjet-Engine Model. NASA TM-84644, 1983.
5. Guy, Robert W.; and Mackley, Ernest A.: Initial Wind Tunnel Tests at Mach 4 and 7 of a Hydrogen-Burning, Airframe-Integrated Scramjet. Fourth International Symposium on Air Breathing Engines, AIAA, Apr. 1979, pp. 347-358. (Available as AIAA Paper 79-7045.)
6. Beach, H. Lee, Jr.; Mackley, Ernest A.; and Guy, Robert W.: Mach 7 Tests of Langley Airframe-Integrated Scramjet. NASA TM-84595, 1983.
7. Guy, Robert W.; Torrence, Marvin G.; Sabol, Alexander P.; and Mueller, James N.: Operating Characteristics of the Langley Mach 7 Scramjet Test Facility. NASA TM-81929, 1981.
8. Boatright, William B.; Sabol, Alexander P.; Sebacher, Daniel I.; Pinckney, Shimer Z.; and Guy, Robert W.: Langley Facility for Tests at Mach 7 of Subscale, Hydrogen-Burning, Airframe-Integratable, Scramjet Models. AIAA Paper No. 76-11, Jan. 1976.
9. Beach, H. L., Jr.; Mackley, E. A.; Rogers, R. C.; and Chinitz, W.: Use of Silane in Scramjet Research. 17th JANNAF Combustion Meeting, Volume I, Debra Sue Eggleston, ed., CPIA Publ. 329 (Contract N00024-78-C-5384), Appl. Phys. Lab., Johns Hopkins Univ., Nov. 1980, pp. 639-659.
10. Hirsh, Merle N.; and Oskam, H. J., eds.: Gaseous Electronics, Volume I - Electrical Discharges. Academic Press, Inc., c.1978.
11. Winovich, Warren: On the Equilibrium Sonic-Flow Method for Evaluating Electric-Arc Air-Heater Performance. NASA TN D-2132, 1964.
12. Moffat, Robert J.: Gas Temperature Measurement. Temperature - Its Measurement and Control in Science and Industry, Volume 3, Pt. 2, Reinhold Pub. Corp., c.1962, pp. 553-571.

13. Slack, M.; and Grillo, A.: Investigation of Hydrogen-Air Ignition Sensitized by Nitric Oxide and by Nitrogen Dioxide. NASA CR-2896, 1977.
14. Orth, R. C.; Billig, F. S.; and Grenleski, S. E.: Measurement Techniques for Supersonic Combustion Testing. Instrumentation for Airbreathing Propulsion, Allen E. Fuhs and Marshall Kingery, eds., MIT Press, c.1974, pp. 263-282.

TABLE I.- ARC HEATER COMPONENTS

[See fig. 10]

Number	Description	Material
1	Rear closure	Copper
2	Rear housing	Naval brass alloy forging, no. 464
3	Split flange	Stainless steel, type 303
4	Field coil assembly	Copper tubing, insulated
5	Rear water jacket	Stainless steel, type 304
6	Rear water sleeve	Stainless steel, type 304
7	Upstream electrode	Copper, no. 102
8	Rear flange, chamber	Stainless steel, type 303
9	Rear insulator	Plastic, NEMA G-10 grade
10	Front insulator	Plastic, NEMA G-7 and G-10 grades
11	Rear shell seal	Naval brass alloy forging, no. 464
12	Shell	Naval brass alloy forging, no. 464
13	Chamber liner	Copper forging, no. 150
14	Ignitor	Carbon steel
15	Front shell seal	Copper forging, no. 150
16	Front flange, chamber	Stainless steel, types 303 and 321
17	Front water jacket	Stainless steel, type 304
18	Downstream electrode	Copper, no. 102
19	Front housing	Stainless steel, type 304
20	Front flange, heater	Stainless steel, type 304

TABLE II.- PLENUM CHAMBER COMPONENTS

[See fig. 11]

Number	Description	Material
1	Plenum housing	Stainless steel, types 304 and 321
2	Plenum chamber liner	Copper forging, type 182
3	Plenum ring number 1	Copper, no. 102
4	Plenum ring number 2	Copper, no. 102
5	Plenum ring number 3	Copper, no. 102
6	Insulator ring	Boron nitride, HBR grade
7	Insulator ring	Boron nitride, HBR grade
8	Insulator	Plastic, NEMA G-5 grade
9	Insulator	Plastic, NEMA G-5 grade
10	Insulator ring	Plastic, NEMA G-5 grade

TABLE III.- BYPASS AIR INJECTION CONFIGURATIONS

Configuration	Number of slots	Dimensions of slots, in.	Component covering slots
Slots between plenum rings 1 and 2			
1	12	0.140 × 0.065	Insulator
2	24	.250 × .065	Insulator
3	24	.250 × .065	Copper disc
4	24	.250 × .130	Copper disc
Slots between plenum rings 2 and 3			
1	12	0.140 × 0.065	Insulator
2	24	.250 × .065	Insulator
3	24	.250 × .065	Copper disc
4	(a)	(a)	(a)

^aNot used.

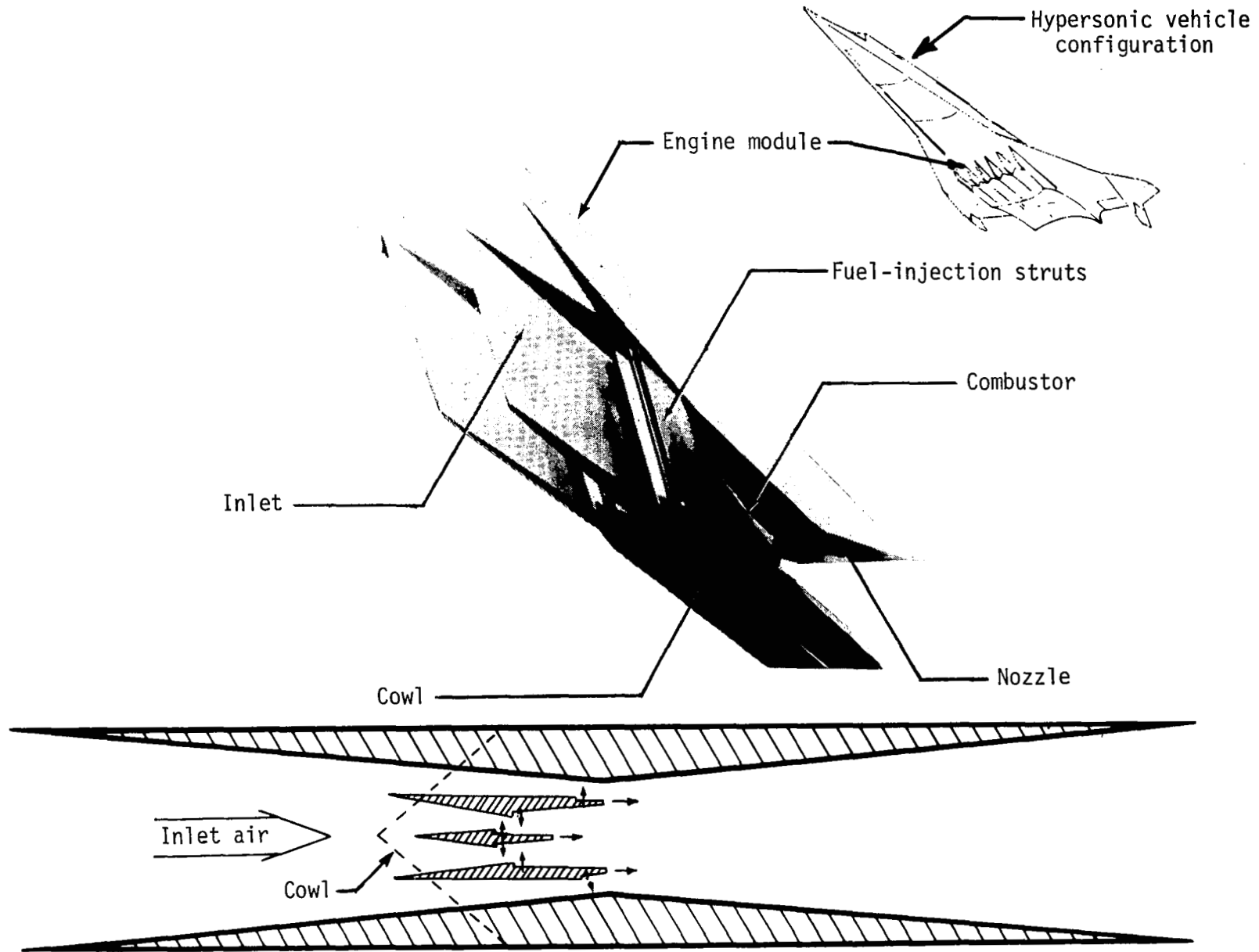


Figure 1.- Airframe-integrated supersonic combustion ramjet.

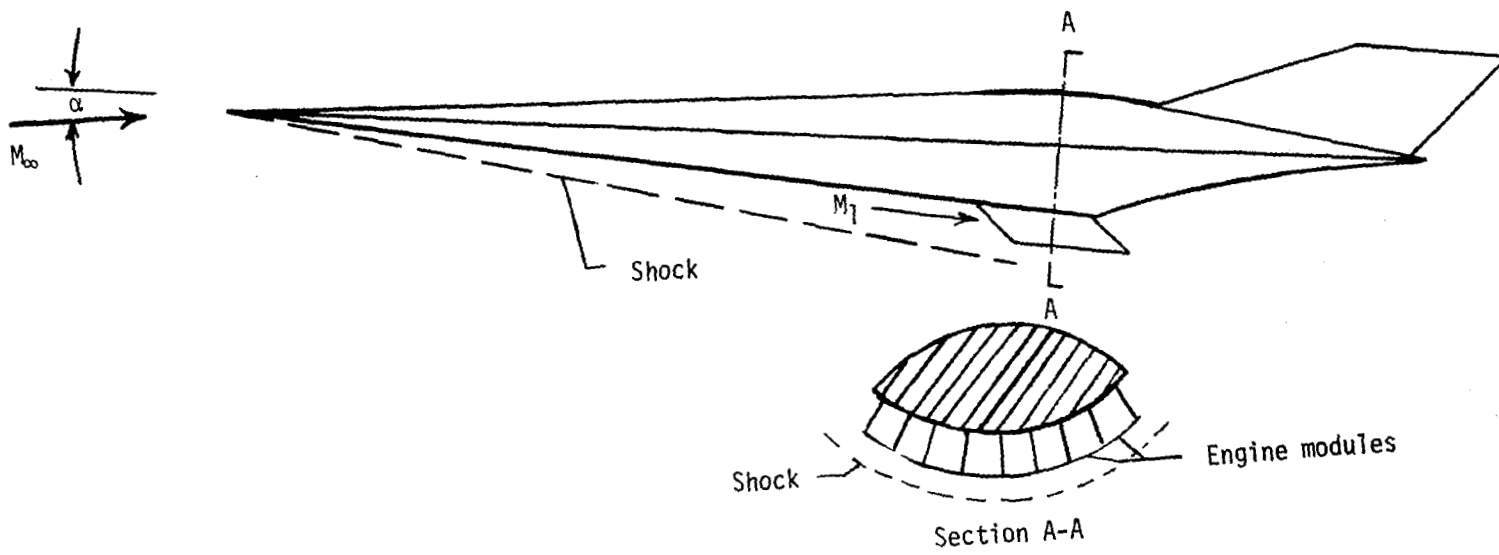


Figure 2.- Scramjet engine and flight vehicle integration concept.

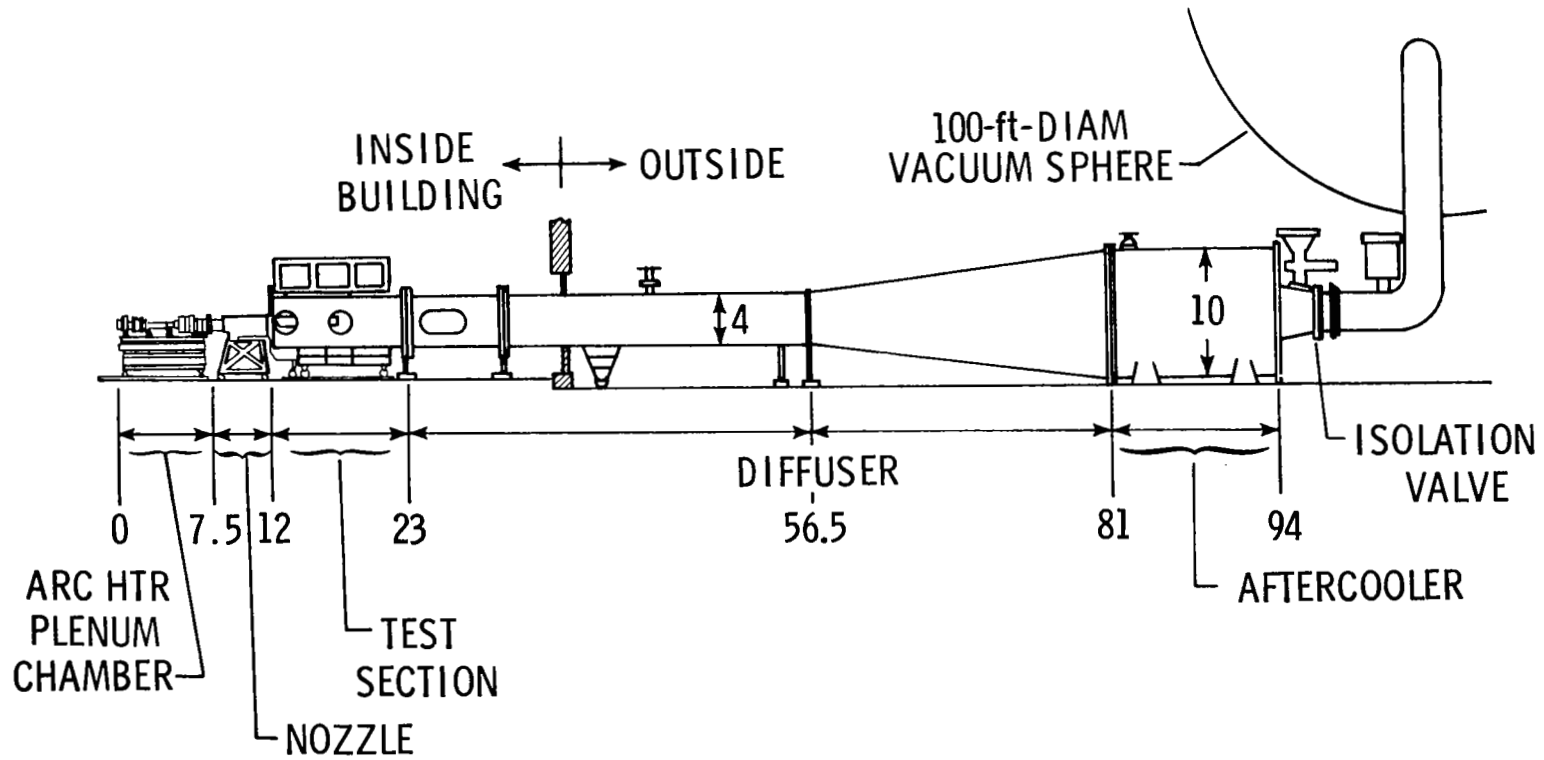
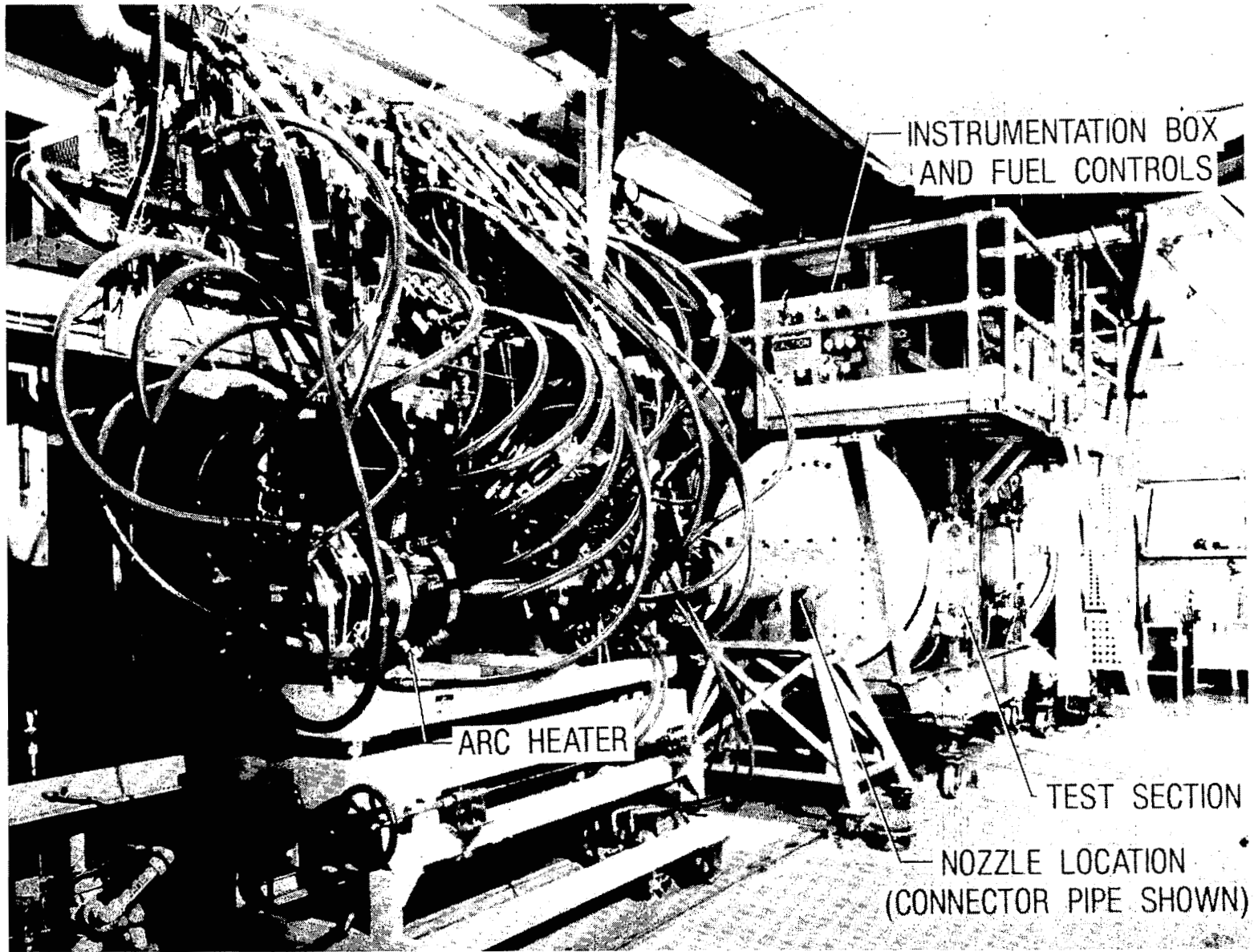


Figure 3.- Elevation view of the Langley Mach 7 Scramjet Test Facility. Dimensions are in feet.



L-82-5209

Figure 4.- Photograph of Langley Mach 7 Scramjet Test Facility after improvements.

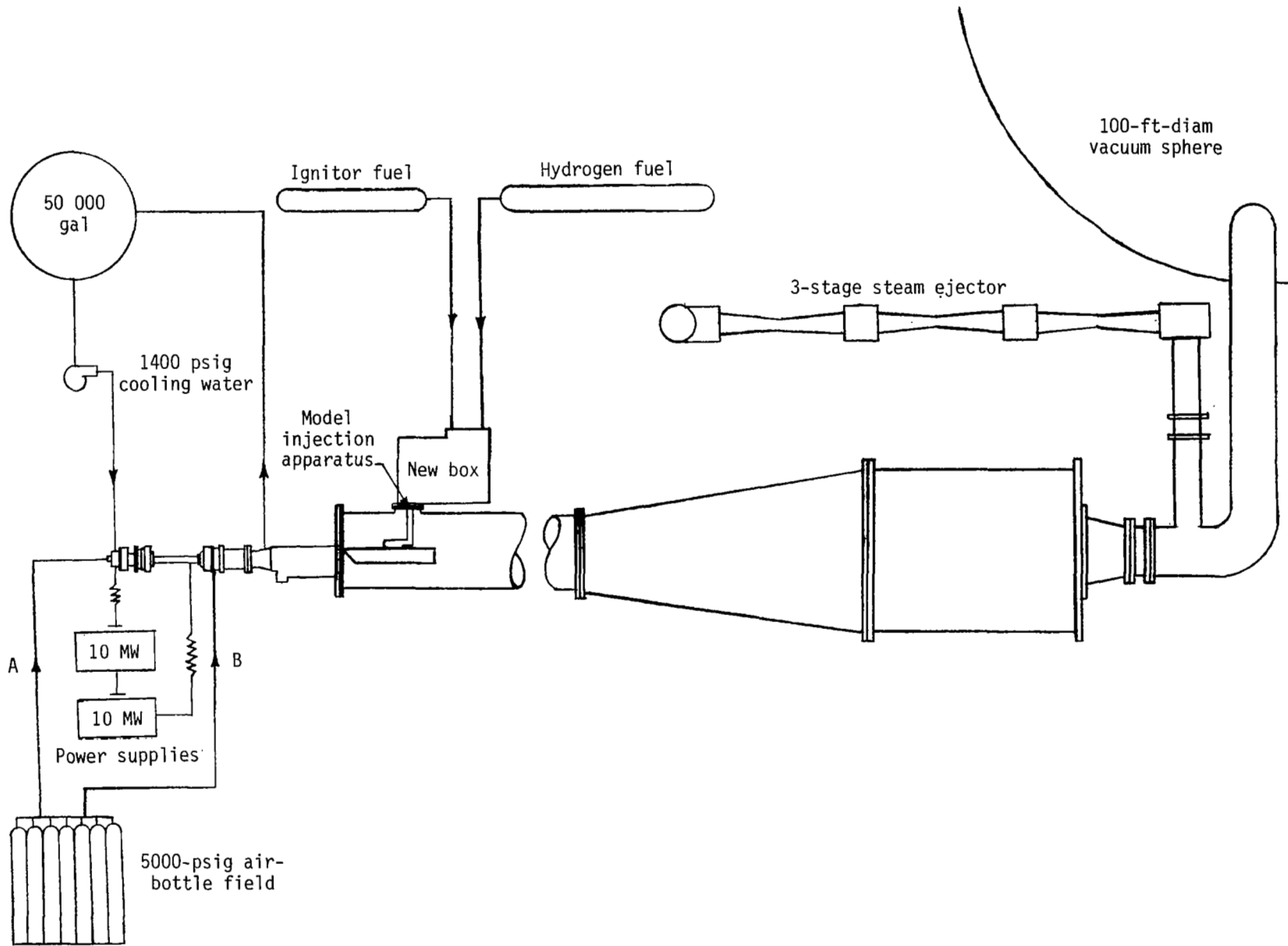


Figure 5.- Major support systems of the Langley Mach 7 Scramjet Test Facility.

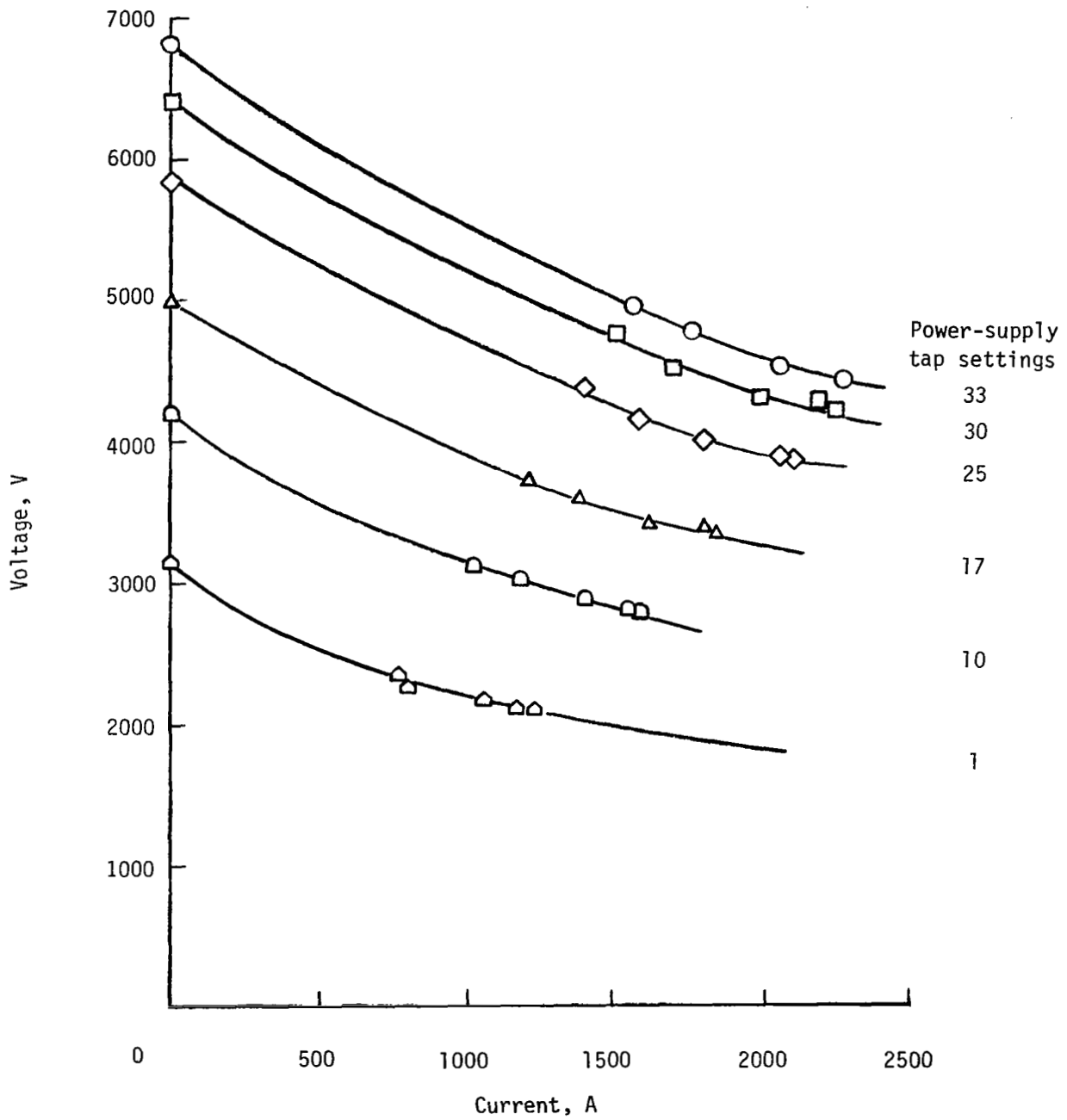


Figure 6.- Voltage-current characteristics for each of the two identical power supplies.

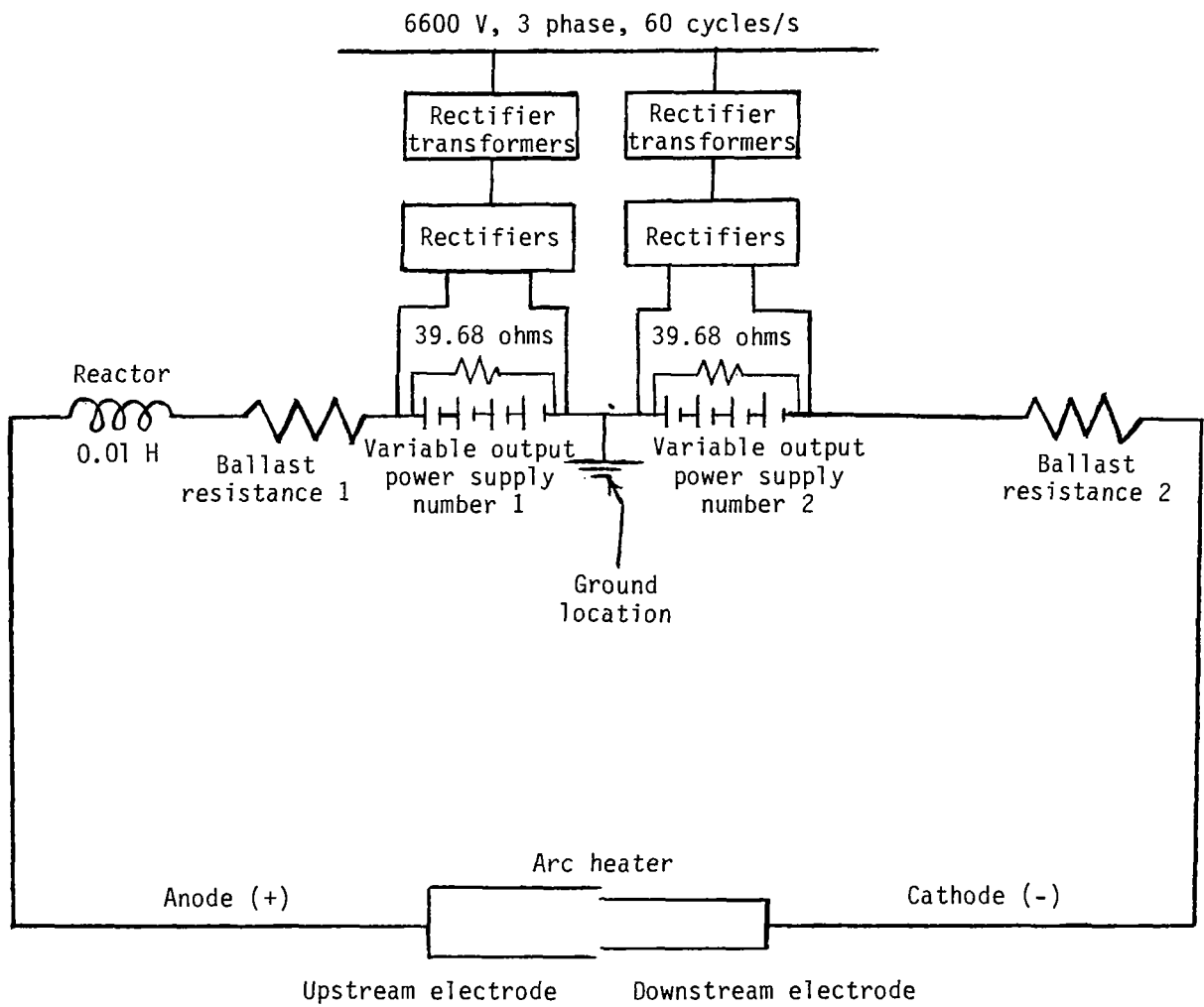
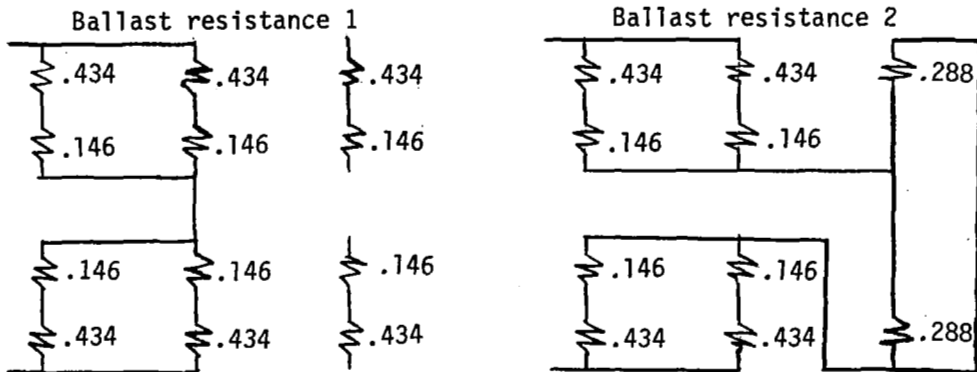
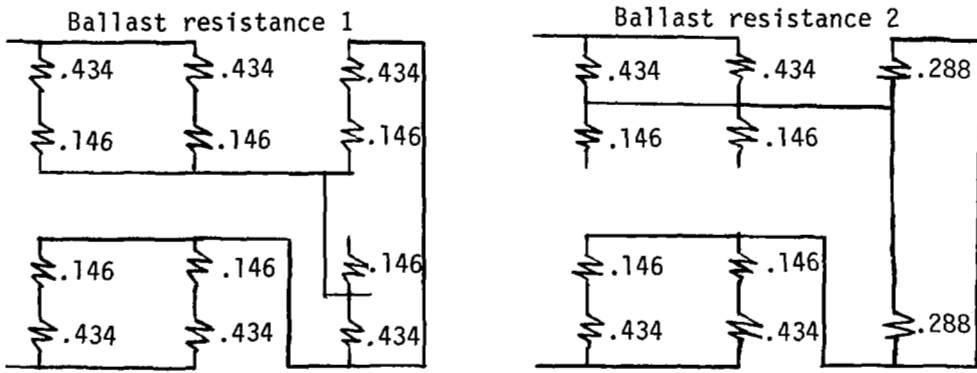


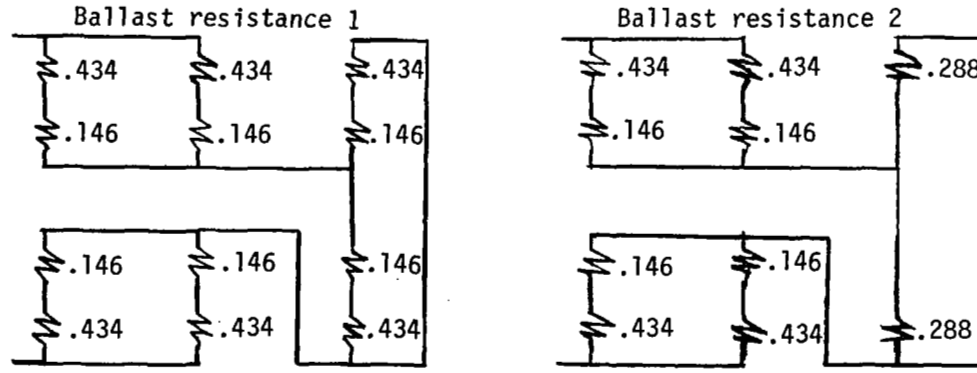
Figure 7.- Arc heater electrical power system.



(a) $R_{bal} = 1.304$ ohms.



(b) $R_{bal} = 1.479$ ohms.



(c) $R_{bal} = 1.594$ ohms.

Figure 8.- Ballast resistance arrangements. Resistance is in ohms.

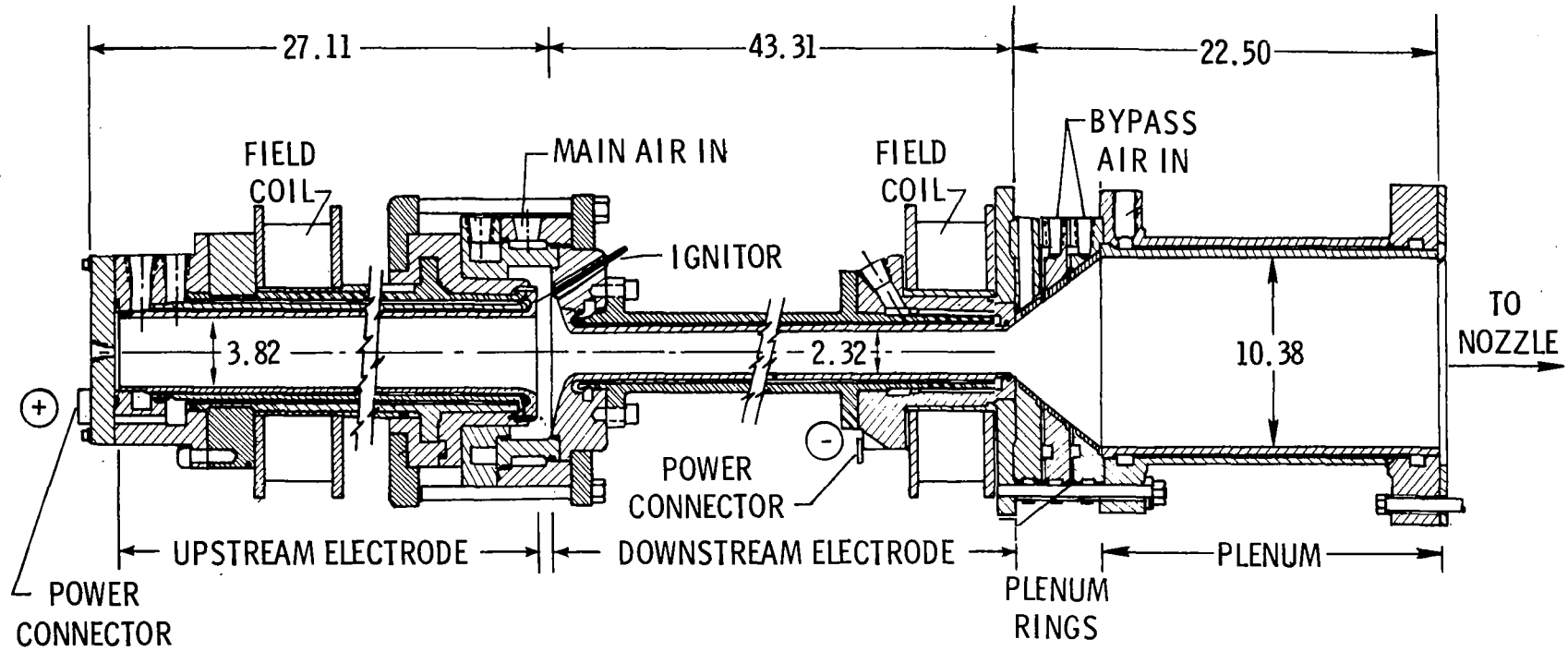


Figure 9.- Longitudinal-section view of Langley Mach 7 Scramjet Test Facility arc heater and plenum chamber. Dimensions are in inches.

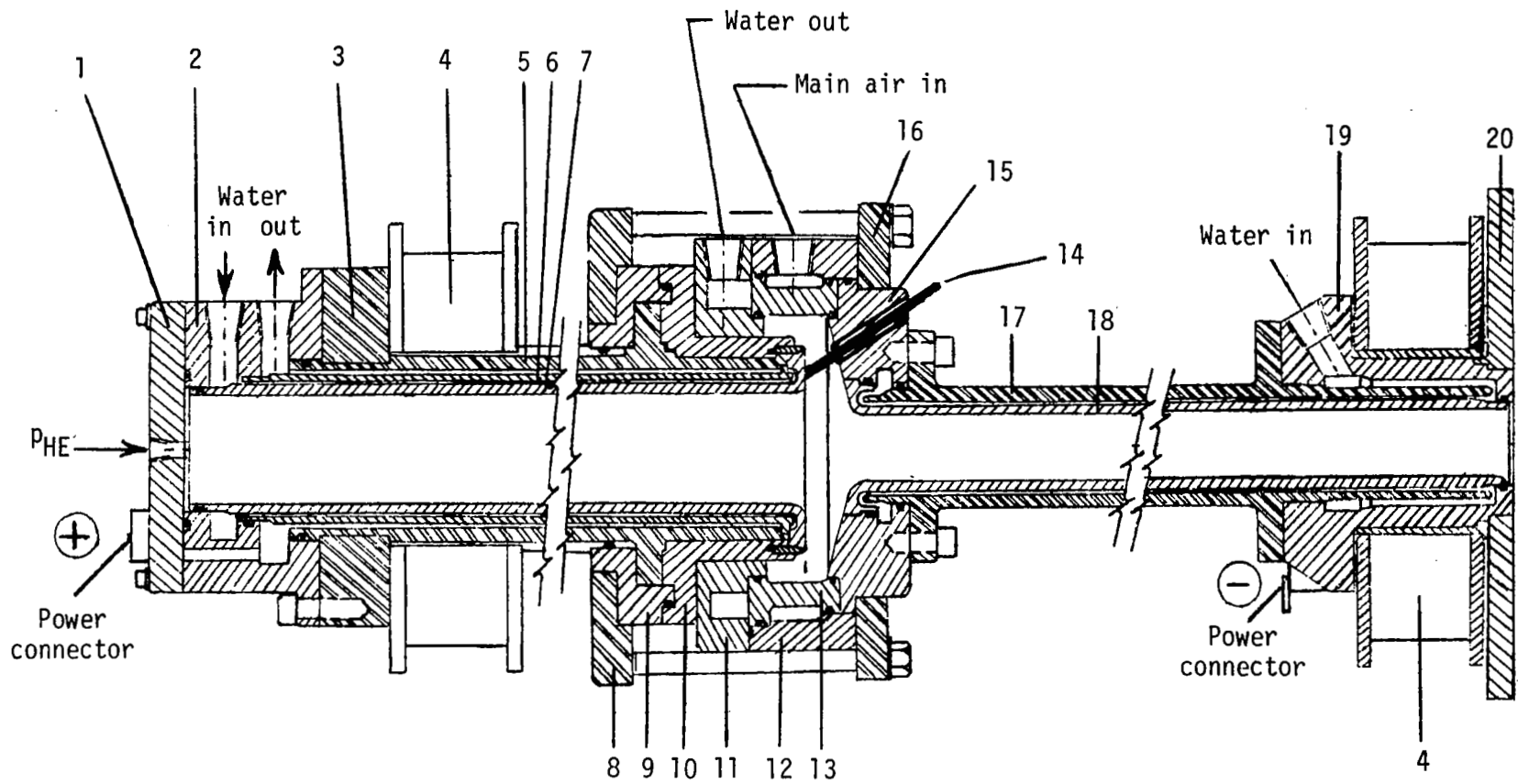


Figure 10.- Longitudinal-section view of arc heater. (See table I for description of components.)

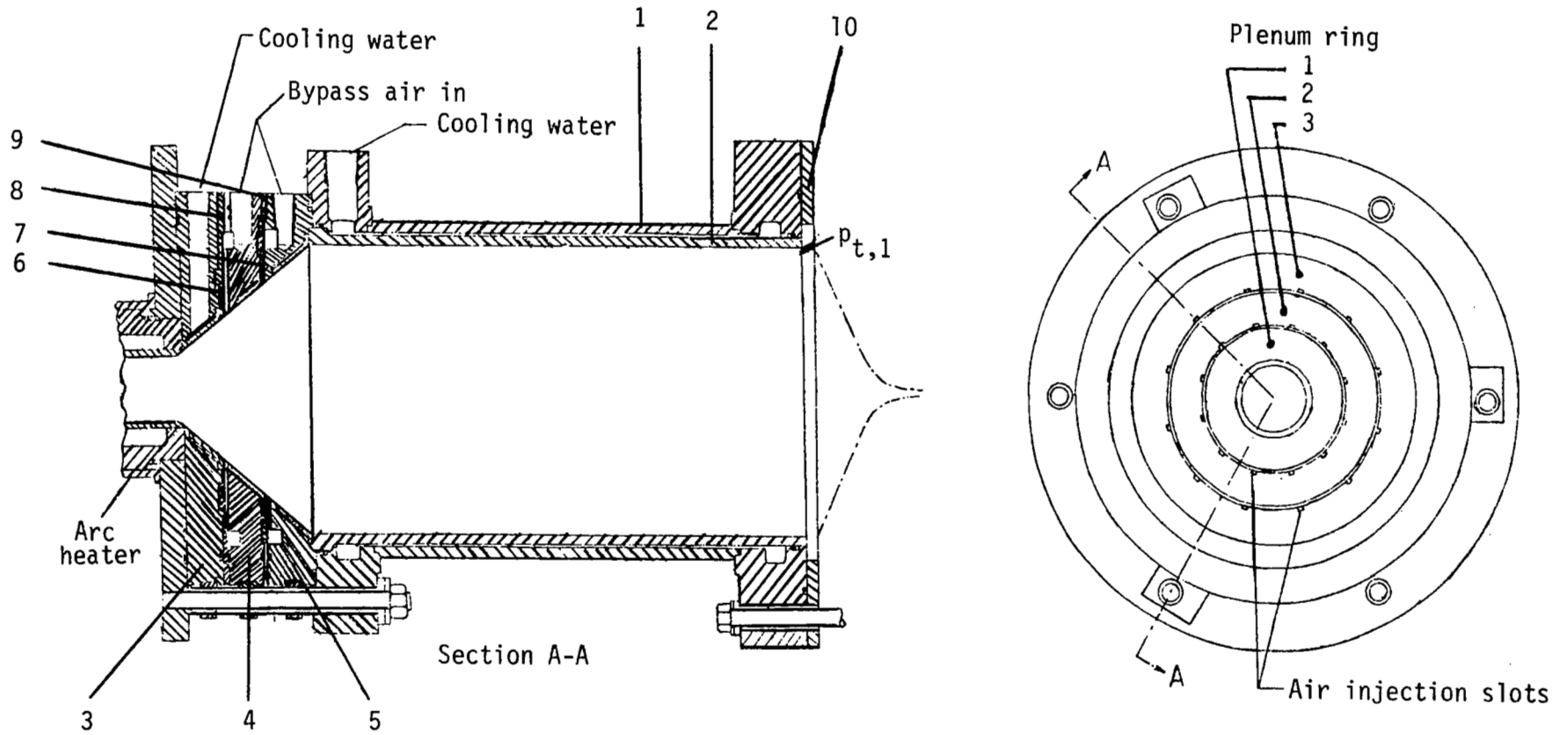
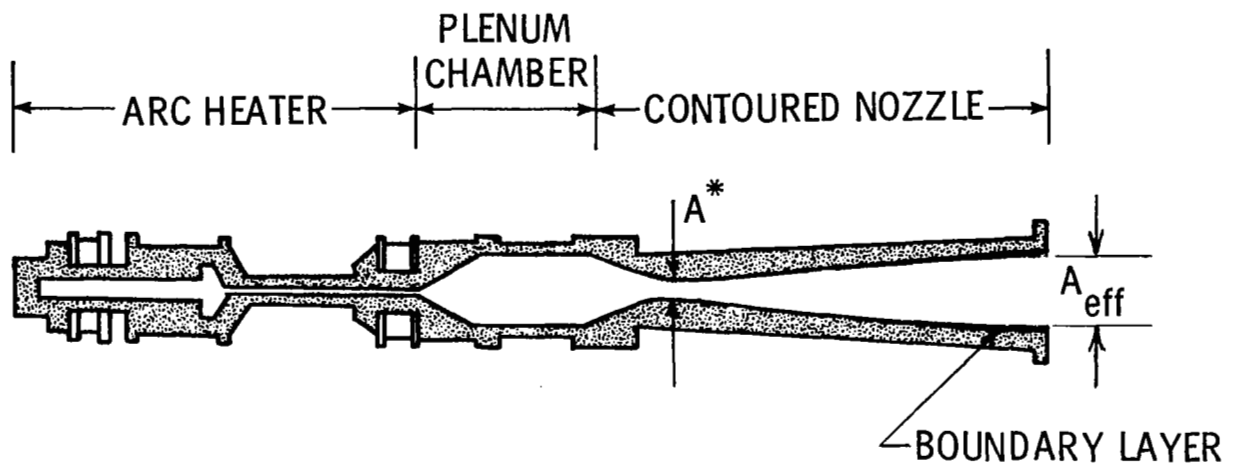


Figure 11.- Longitudinal-section view of bypass air injection slots and plenum chamber. (See table II for description of components.)



M_∞	M_1	A^*, in^2	A_{eff}, in^2
4.0	3.4	24.63	160
5.5	4.9	3.80	104
7.0	6.0	1.33	104

Figure 12.- Approximate specifications for contoured facility nozzles.

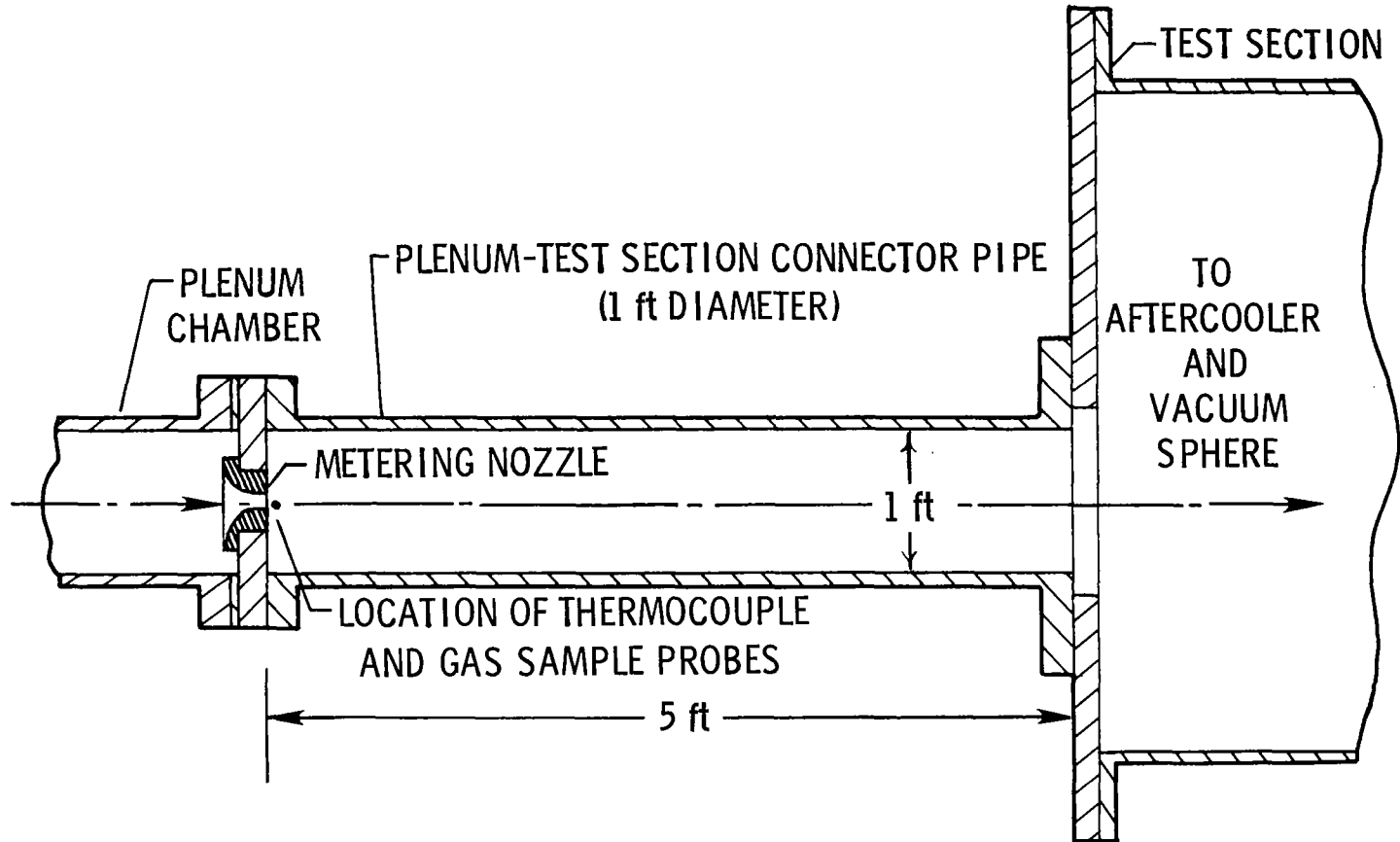
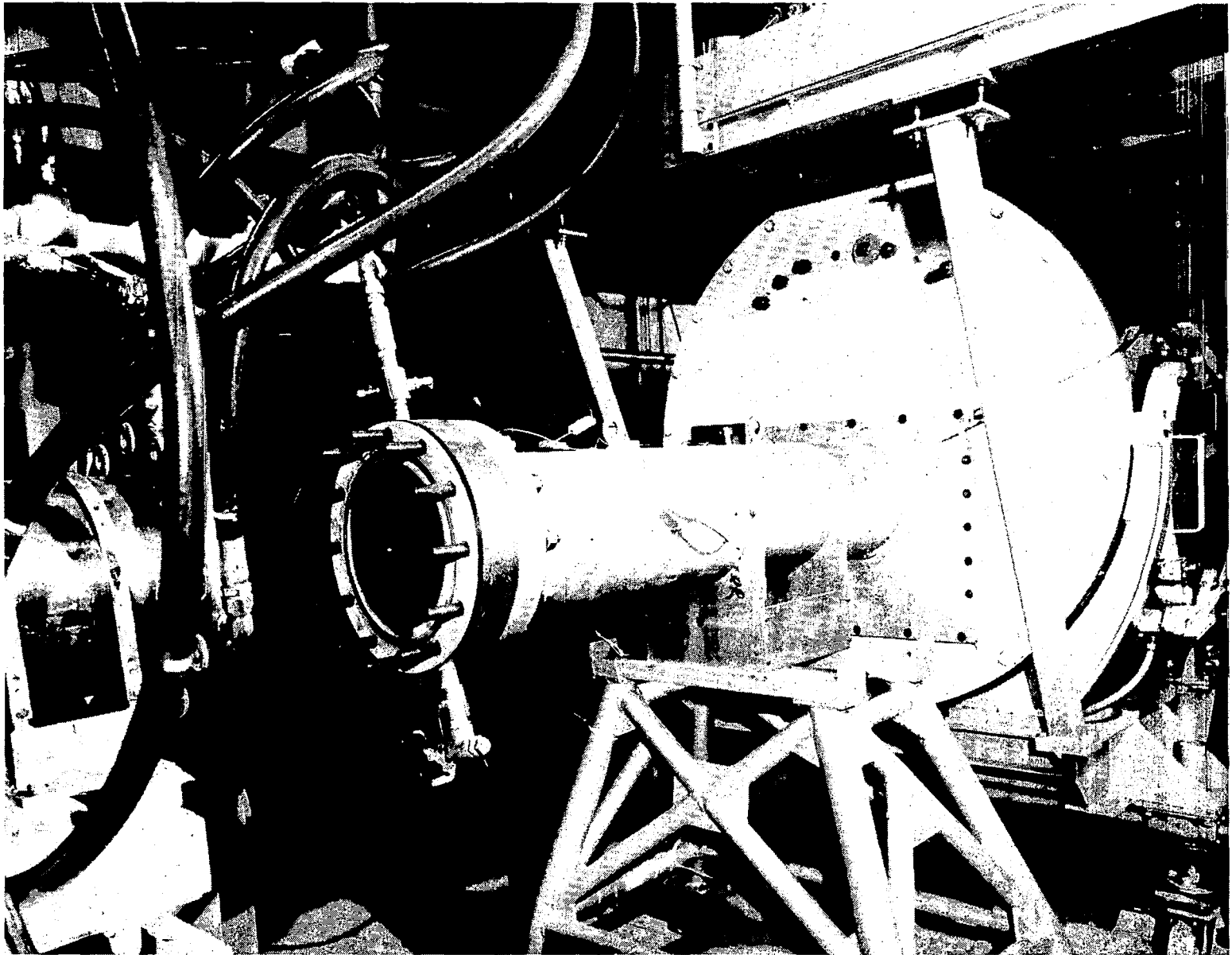
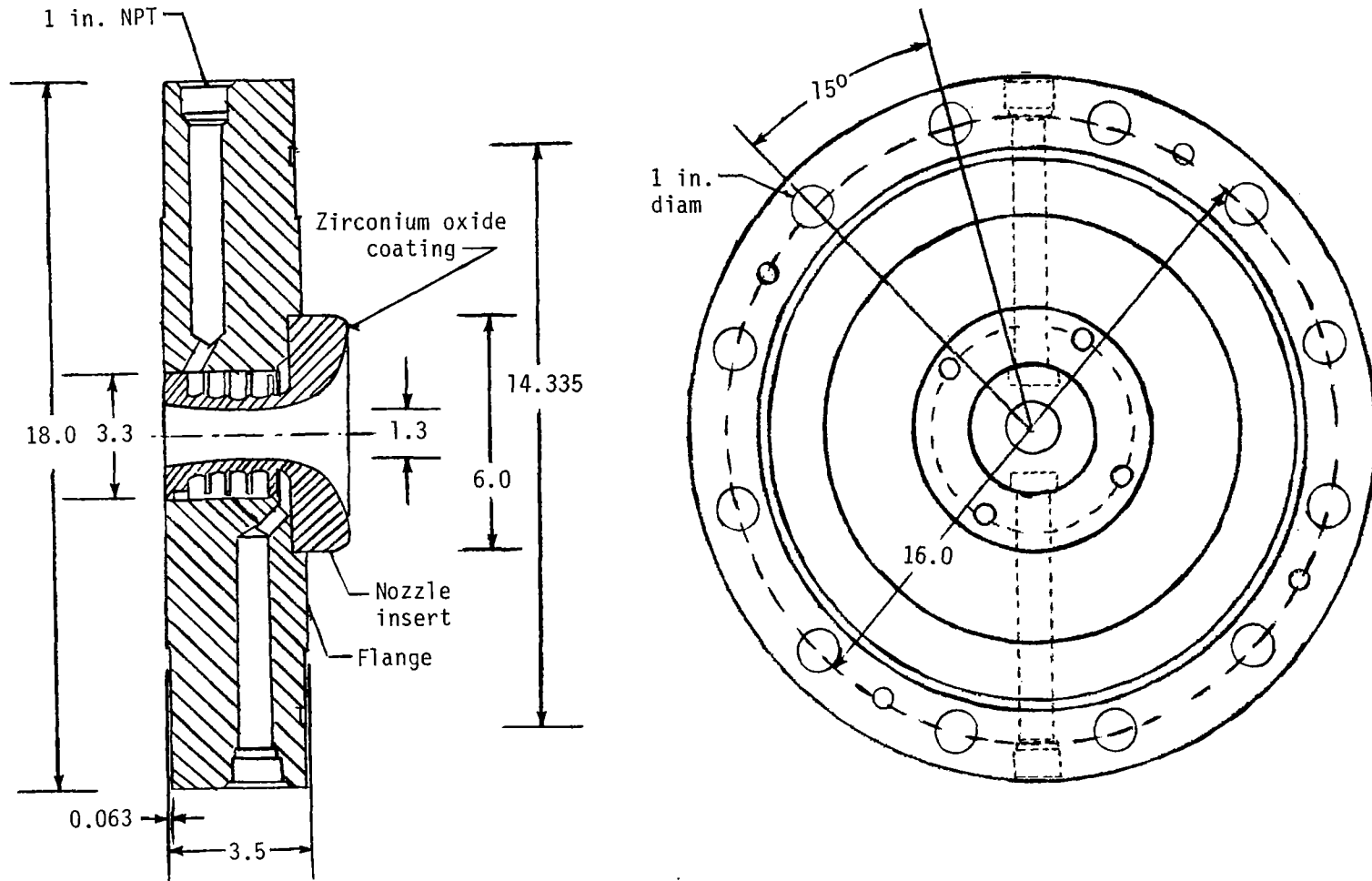


Figure 13.- Hardware arrangement for arc heater research tests.



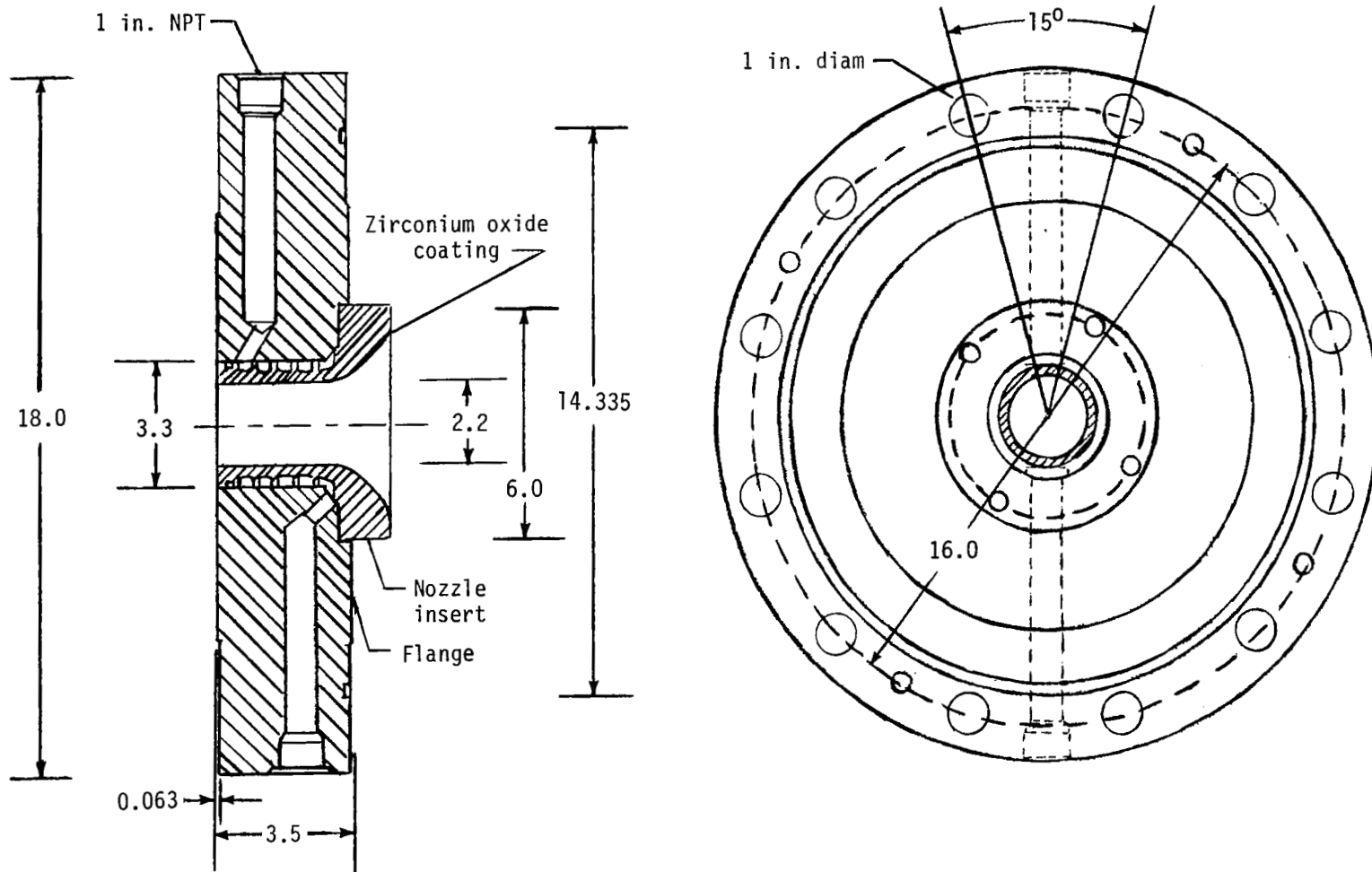
L-81-2799

Figure 14.- Photograph of 2.2-in-diameter metering nozzle and connector pipe.



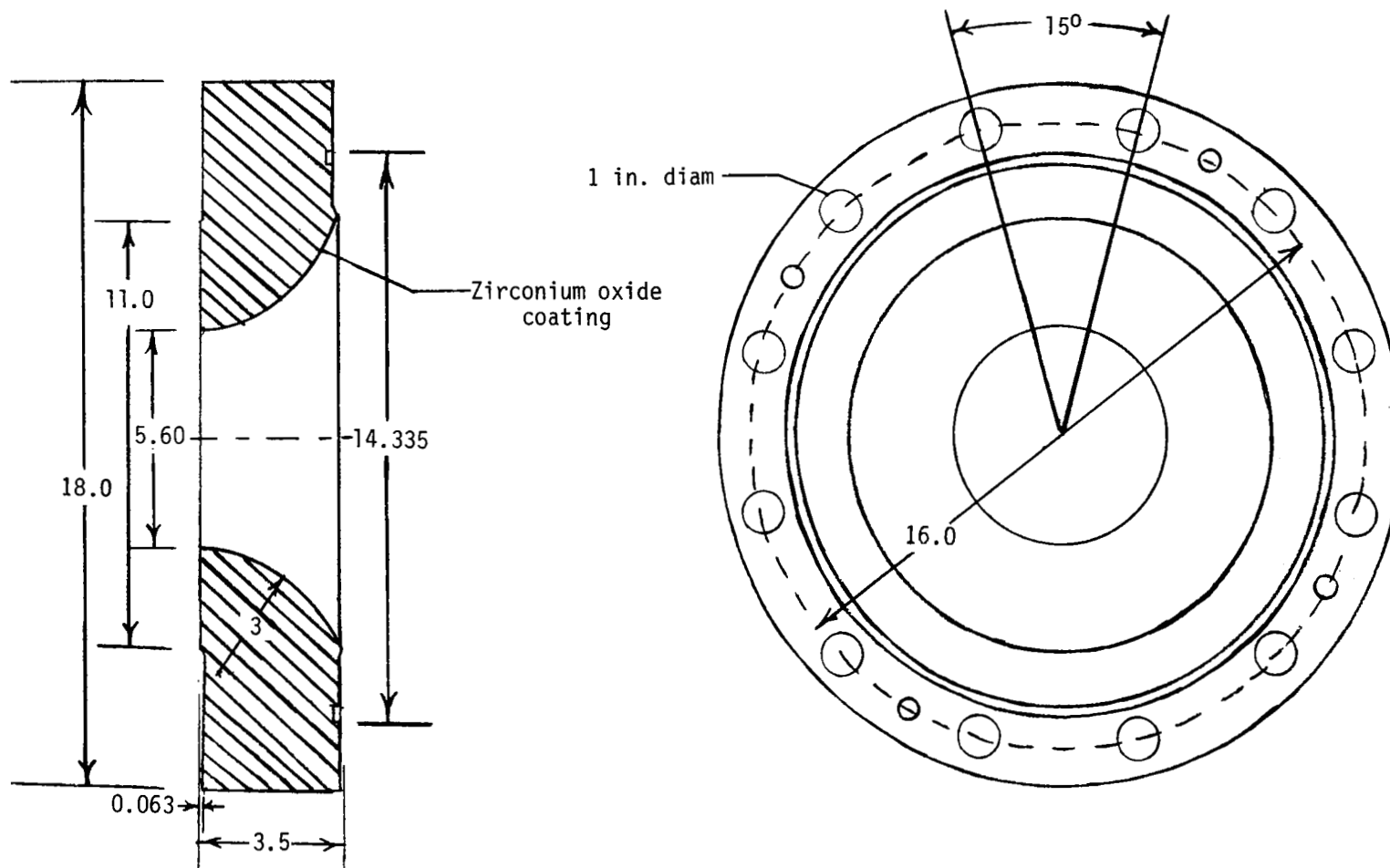
(a) 1.3-in-diameter metering nozzle.

Figure 15.- Schematics of metering-nozzle configurations. Dimensions are in inches unless otherwise noted.



(b) 2.2-in-diameter metering nozzle.

Figure 15.- Continued.



(c) 5.6-in-diameter metering nozzle.

Figure 15.- Concluded.

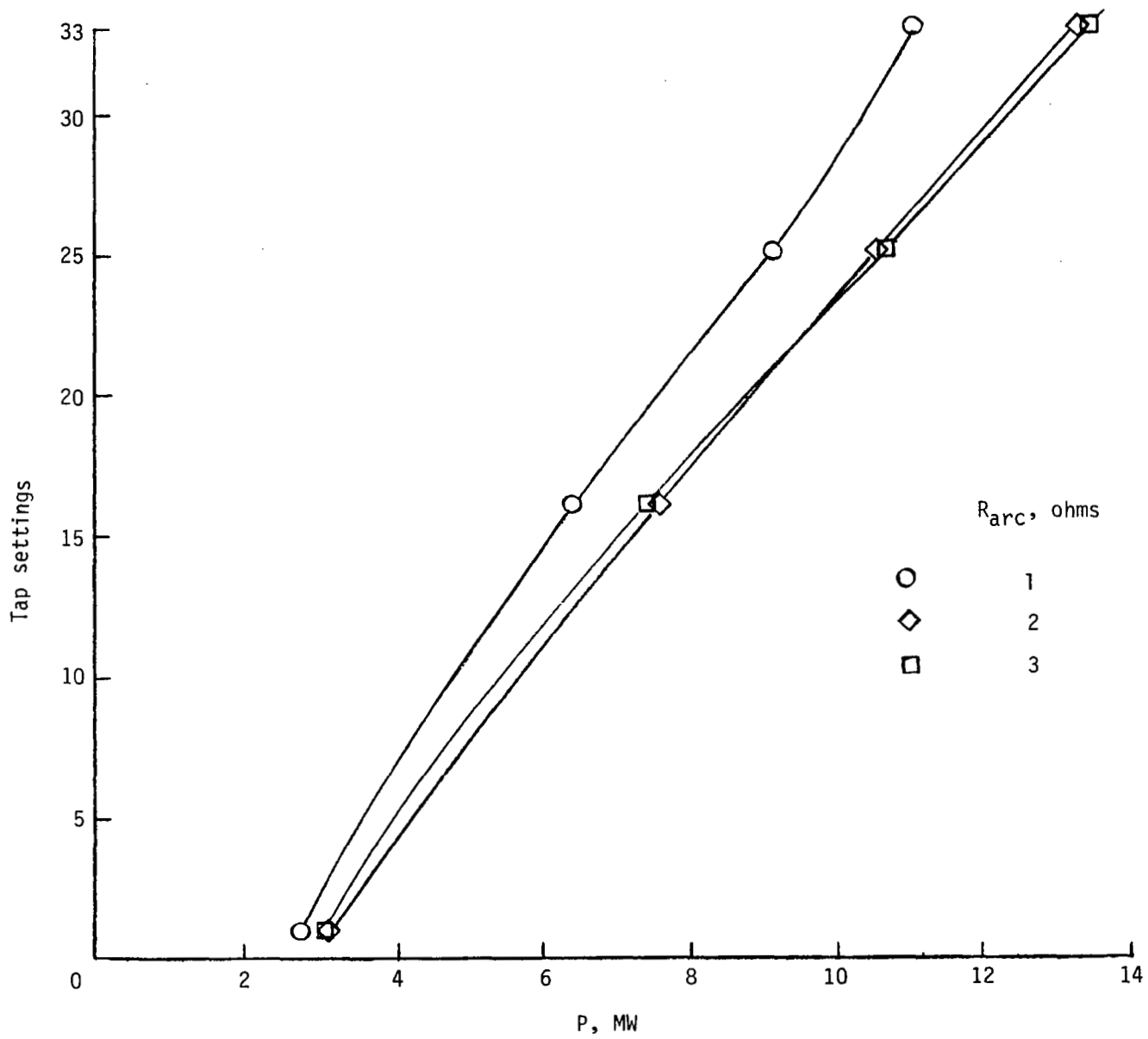


Figure 16.- Power-supply tap settings required to obtain various arc powers as a function of arc resistance. $R_{bal} = 1.304$ ohms. (Calculated from fig. 6.)

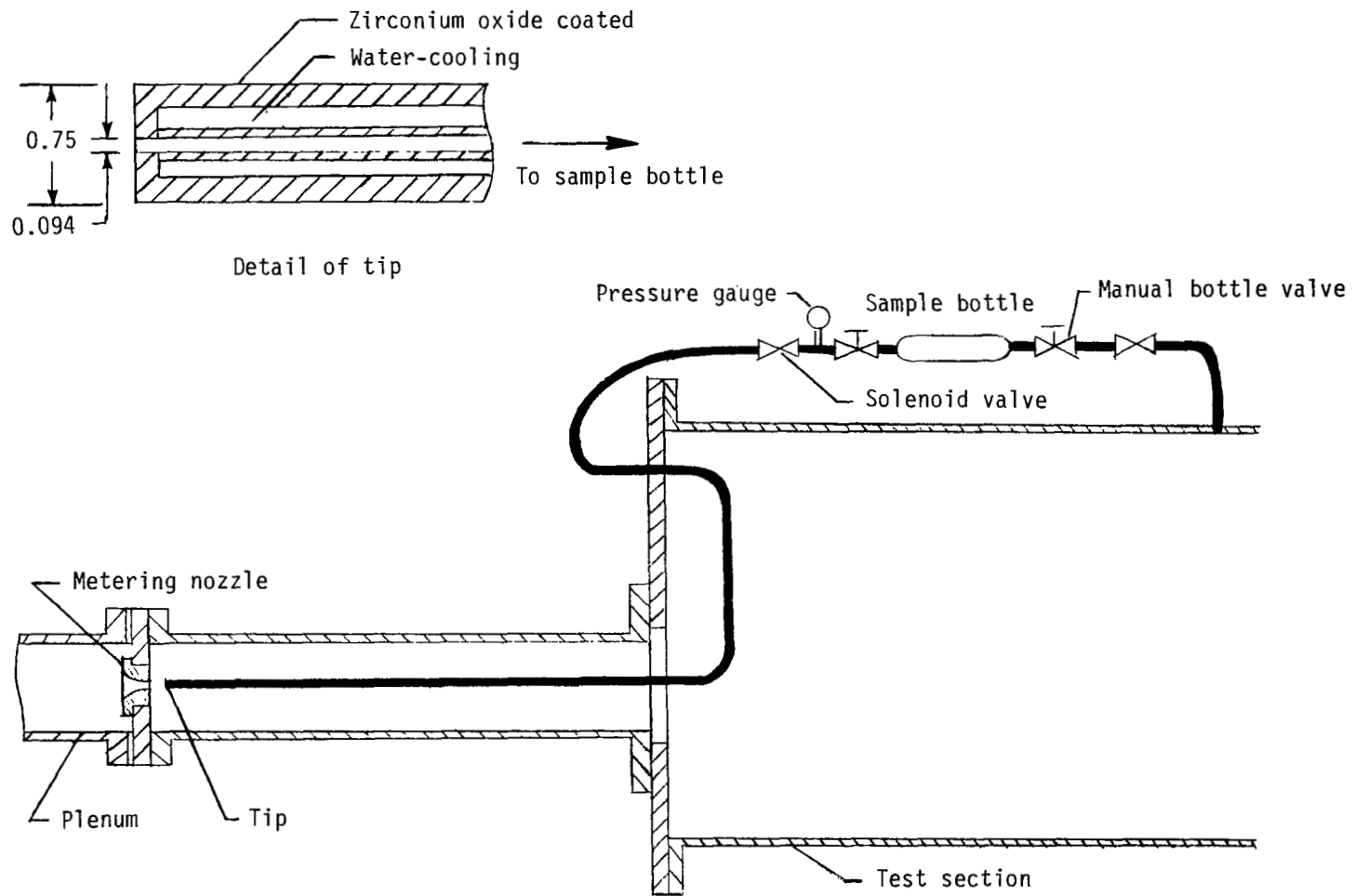


Figure 17.- Nitrogen oxide gas sample system. Dimensions are in inches.

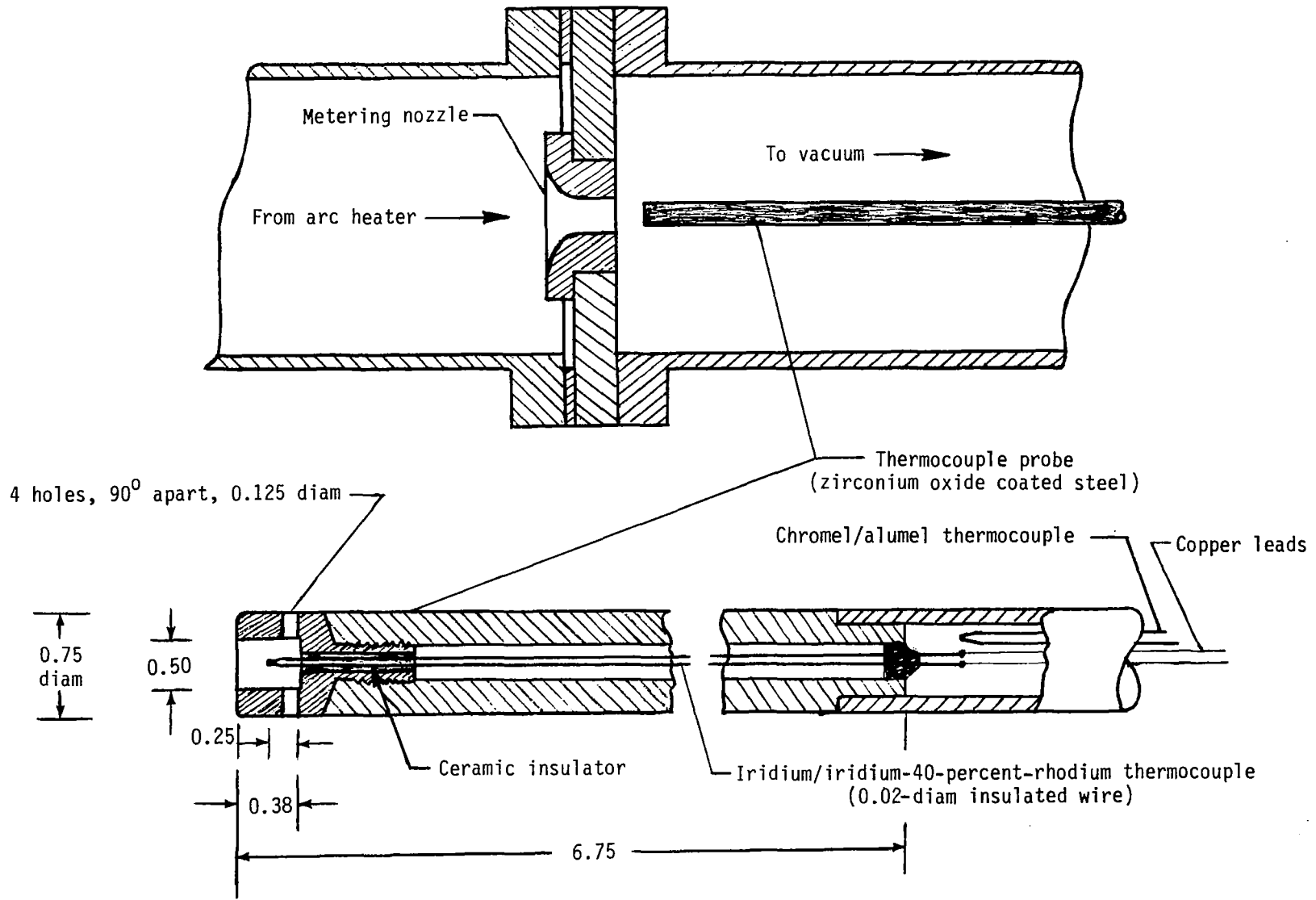


Figure 18.- Details of iridium/iridium-40-percent-rhodium thermocouple probe and test arrangement. All dimensions in inches unless otherwise noted.

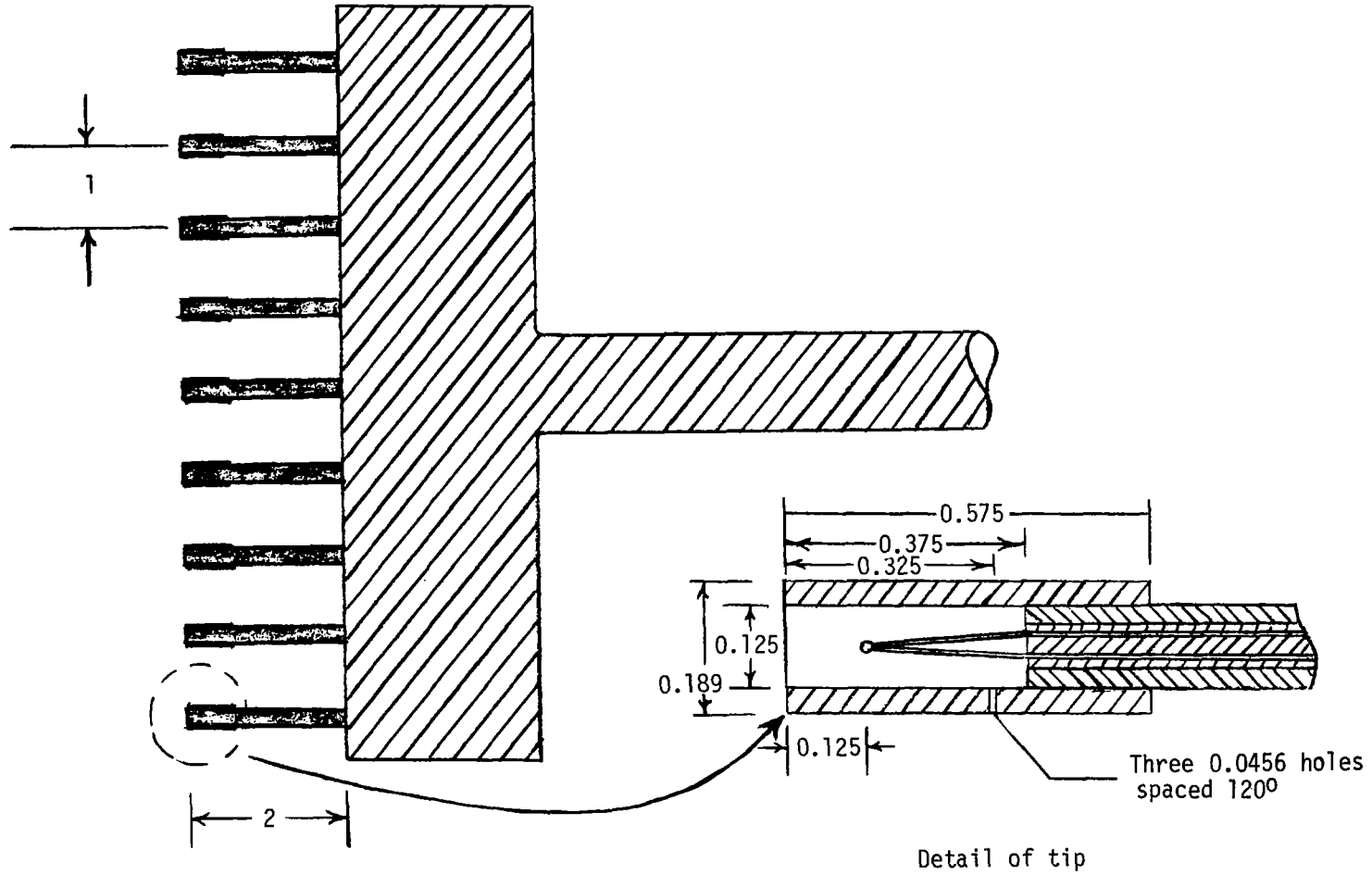
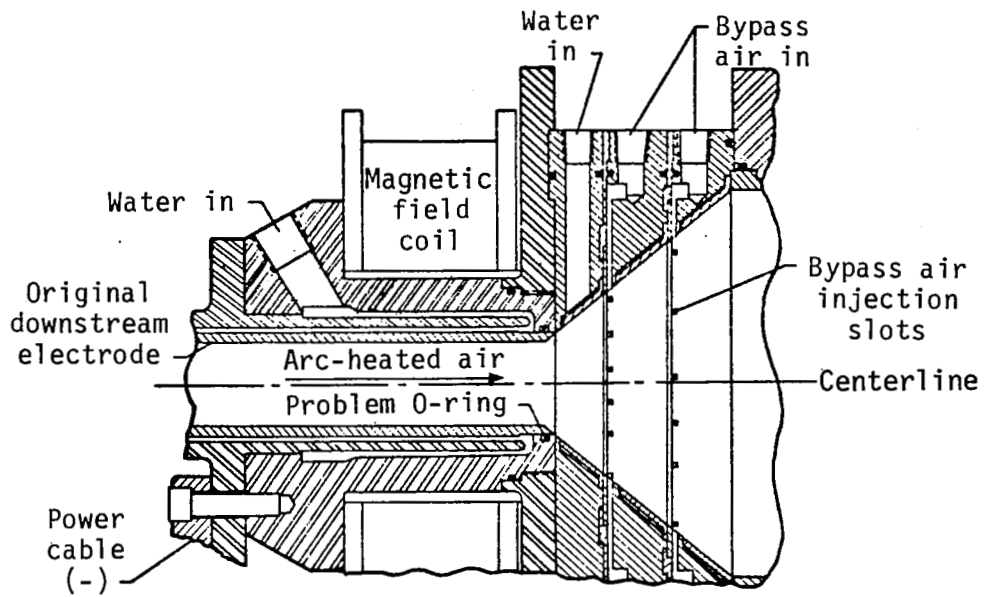
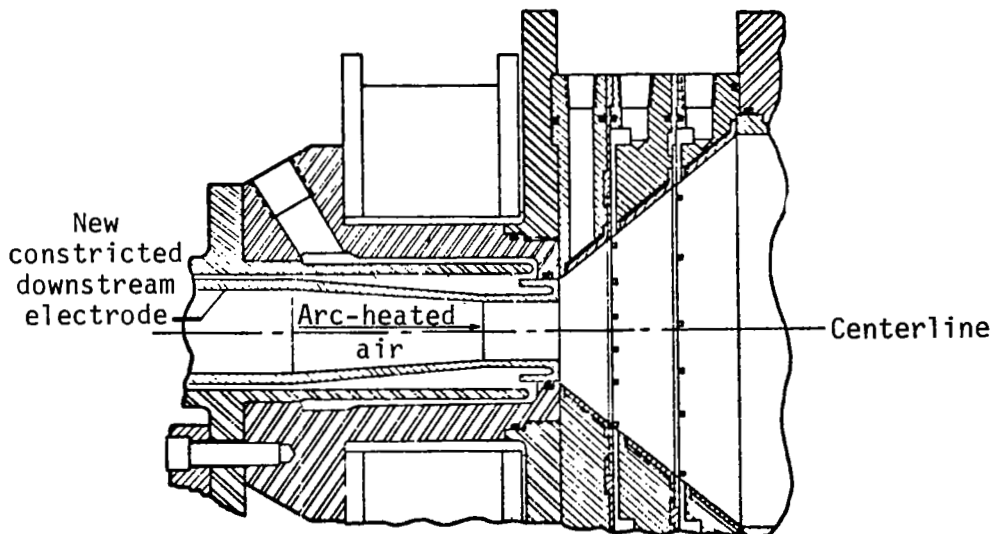


Figure 19.- Details of chromel/alumel thermocouple rake. Dimensions are in inches.



(a) Original downstream electrode tip.



(b) New constricted downstream electrode tip.

Figure 20.- Modification of downstream electrode.

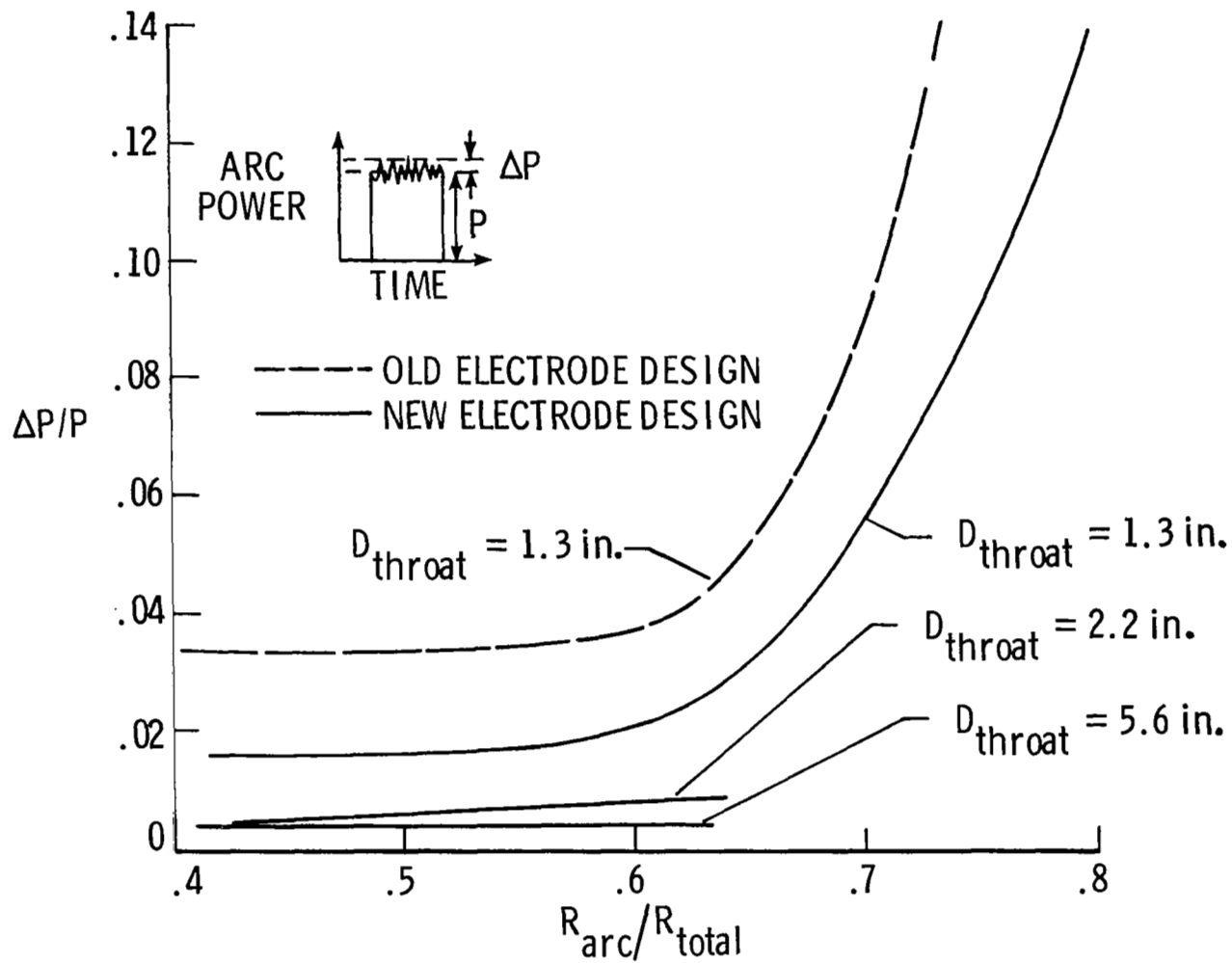
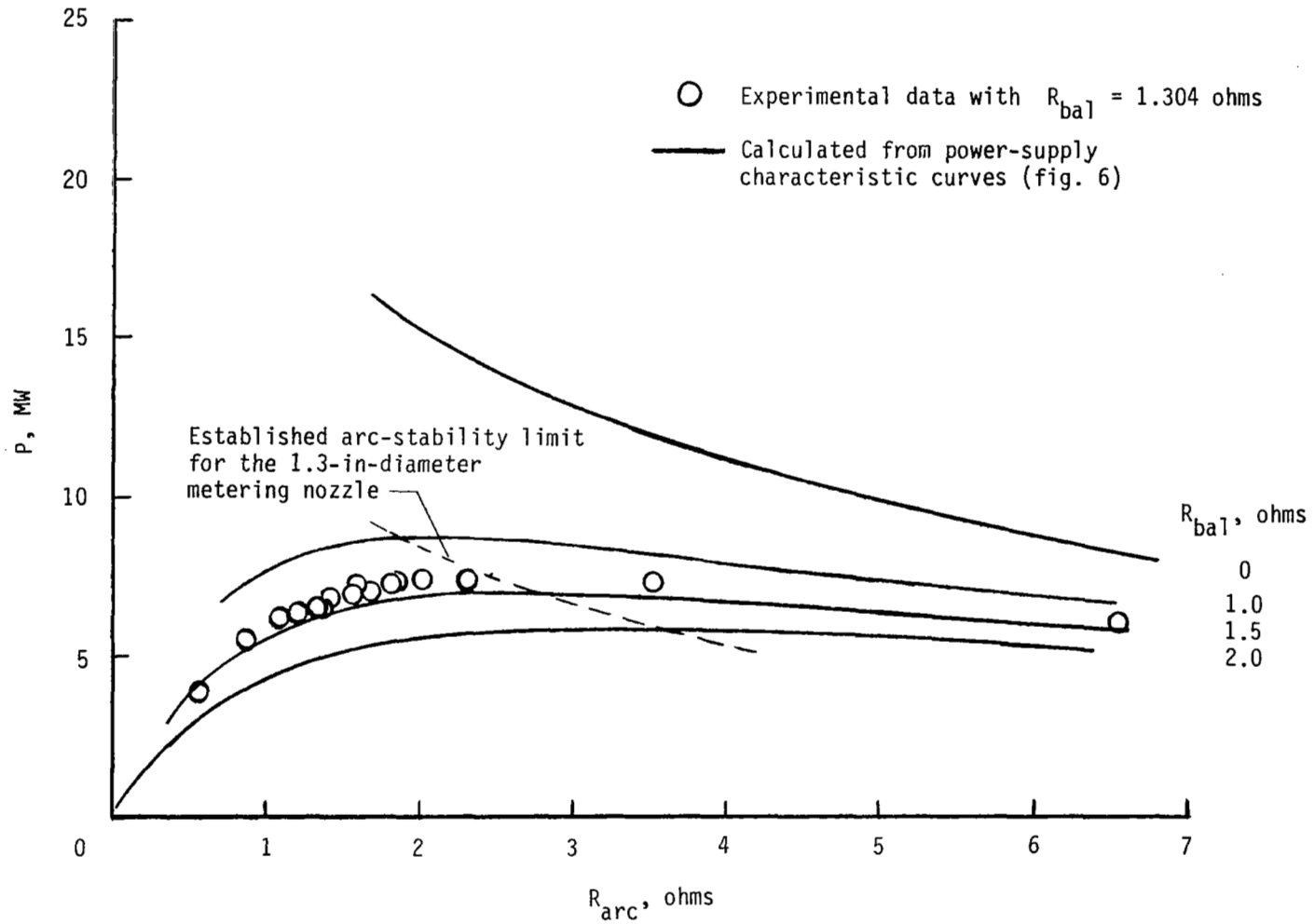
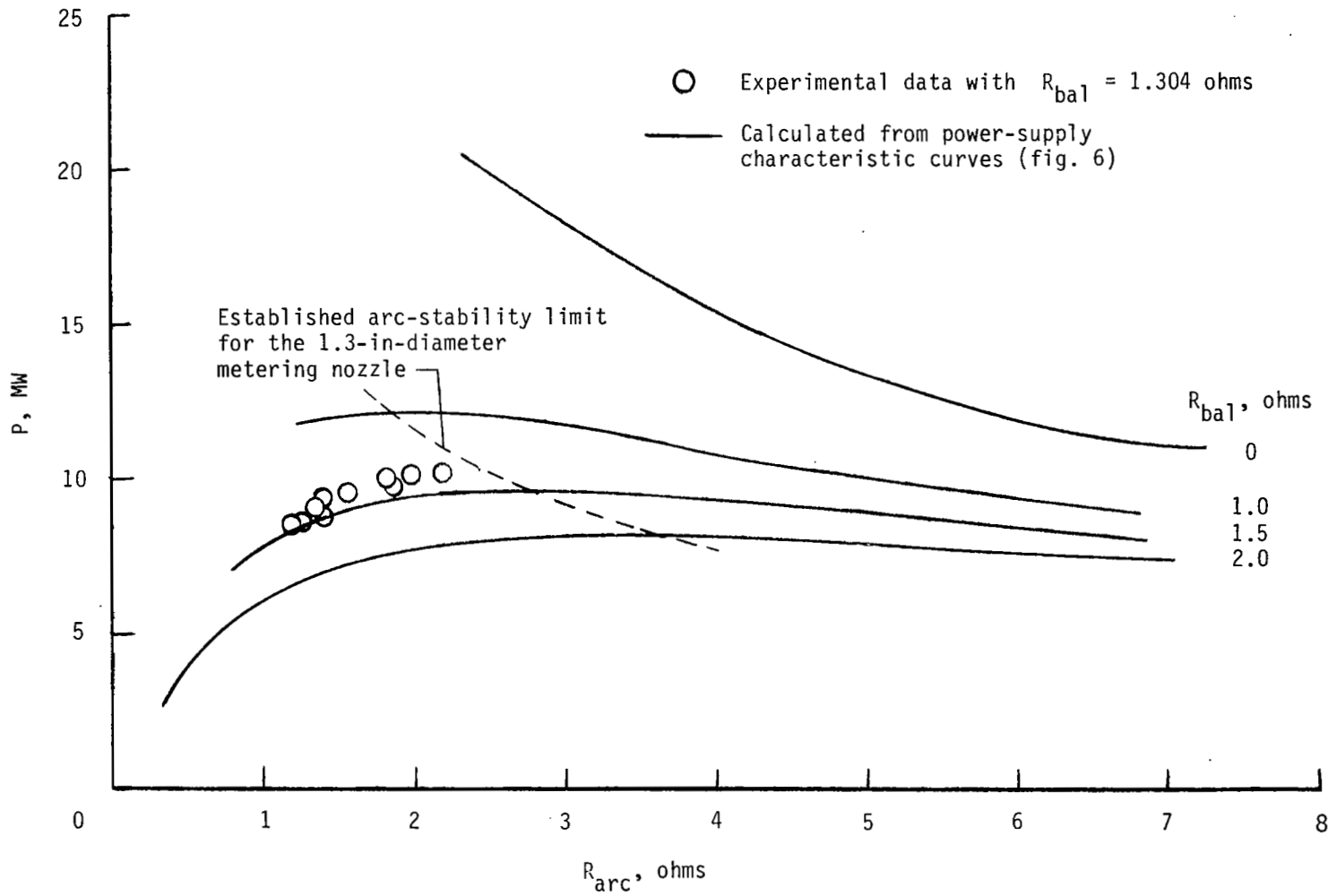


Figure 21.- Normalized arc power fluctuations as a function of arc-to-total resistance ratio.



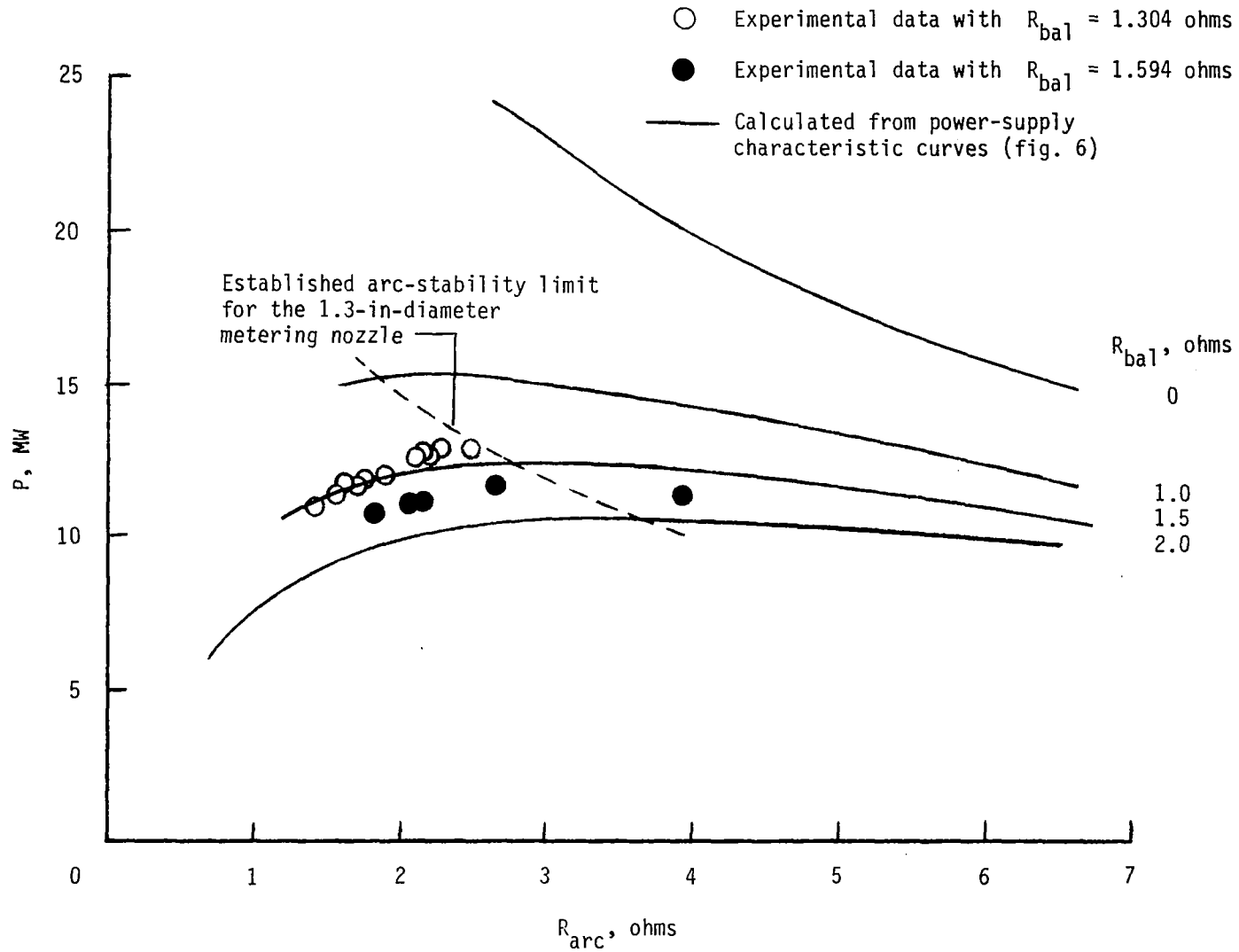
(a) Tap setting of 16 on both power supplies.

Figure 22.- Variation of arc power with arc resistance and ballast resistance.



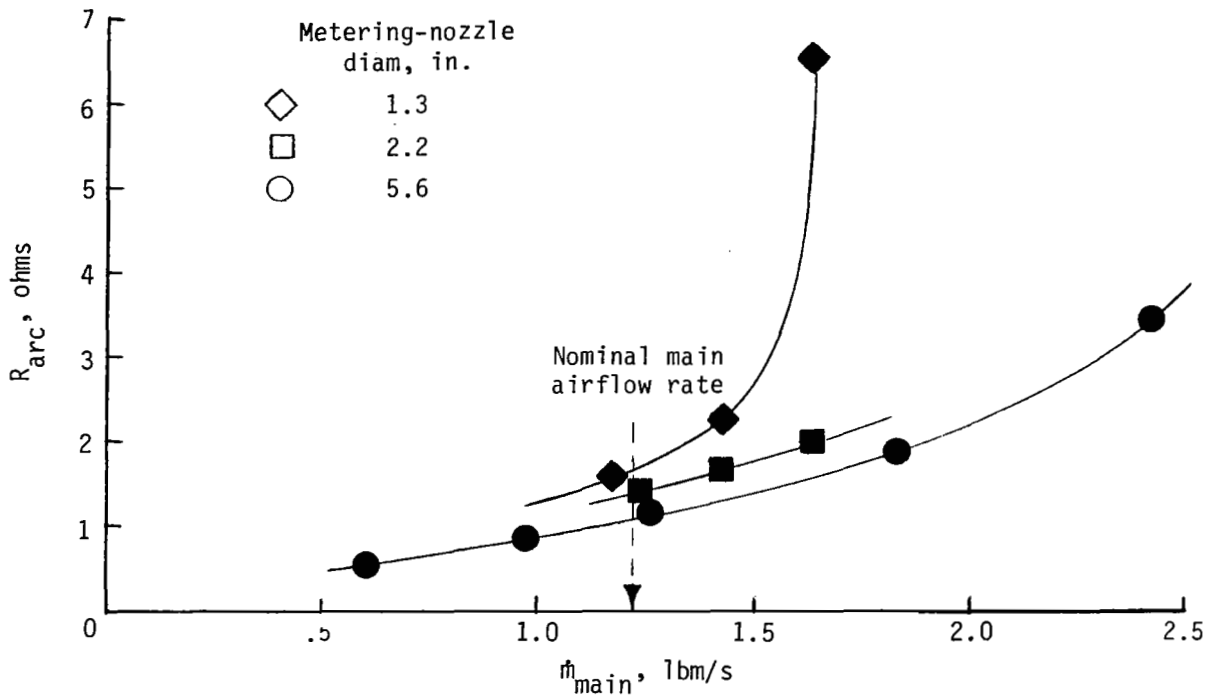
(b) Tap setting of 25 on both power supplies.

Figure 22.- Continued.

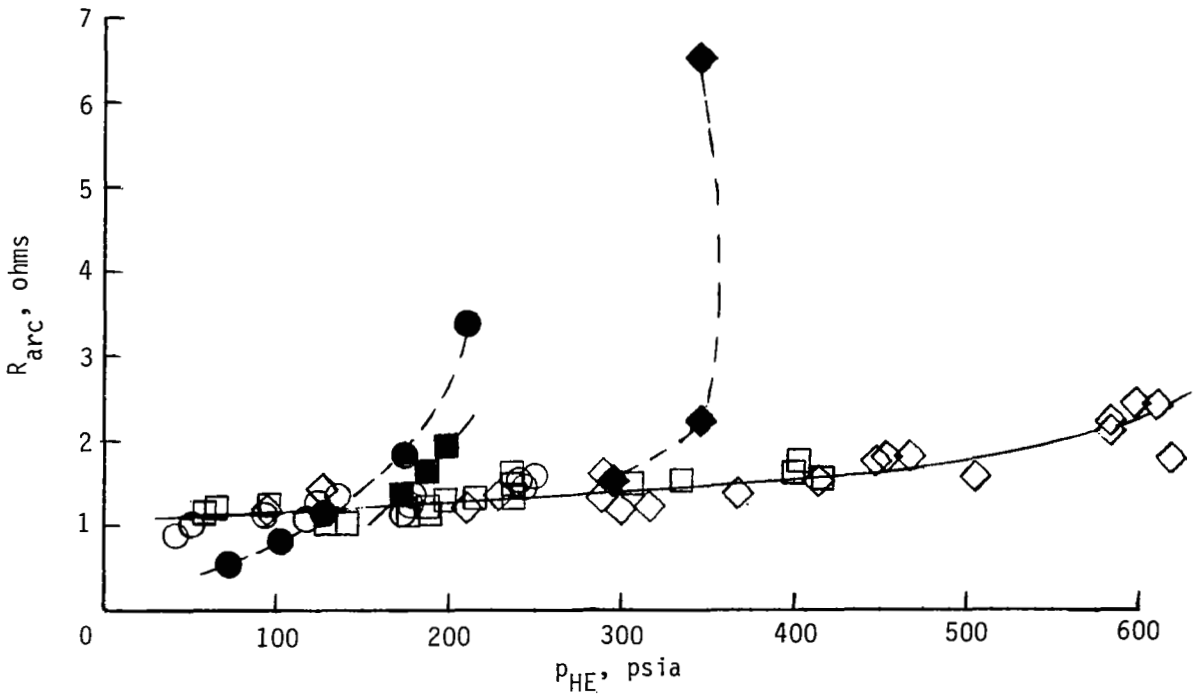


(c) Tap setting of 33 on both power supplies.

Figure 22.- Concluded.



(a) Arc resistance as a function of arc heater airflow rate and metering-nozzle throat size.



(b) Arc resistance as a function of heater pressure.

Figure 23.- Variation of arc resistance with arc heater airflow rate, heater pressure, and metering-nozzle throat size. Open symbols for nominal main airflow rates, variable tap settings, and variable bypass airflow rates; shaded symbols for power supply tap settings of 16 and variable main airflow rate; $R_{bal} = 1.304$ ohms.

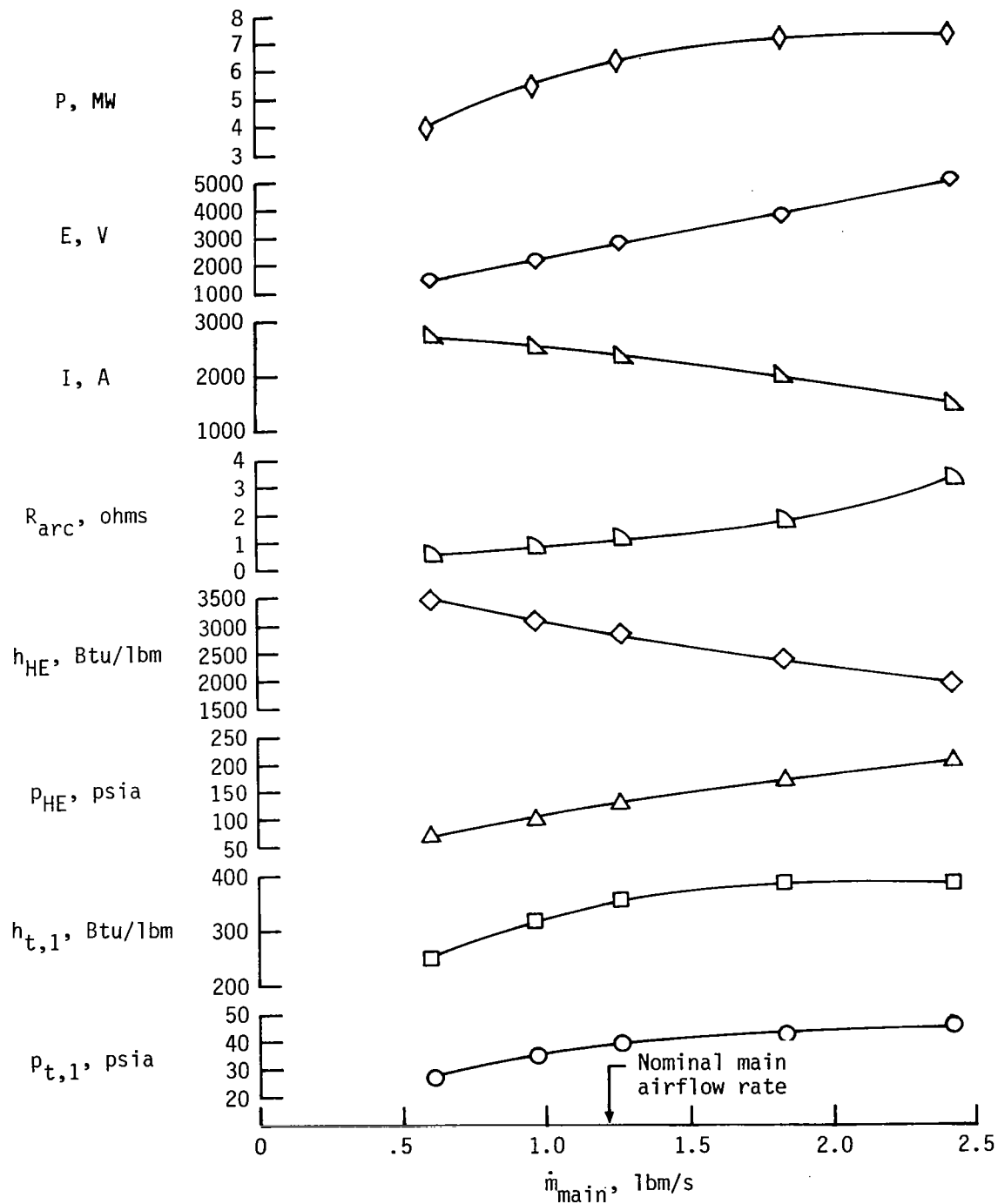


Figure 24.- Effects of main airflow rate on arc heater and plenum chamber properties for 5.6-in-diameter metering nozzle, tap setting of 16 on both power supplies, constant bypass airflow rate, and $R_{bal} = 1.304$ ohms.

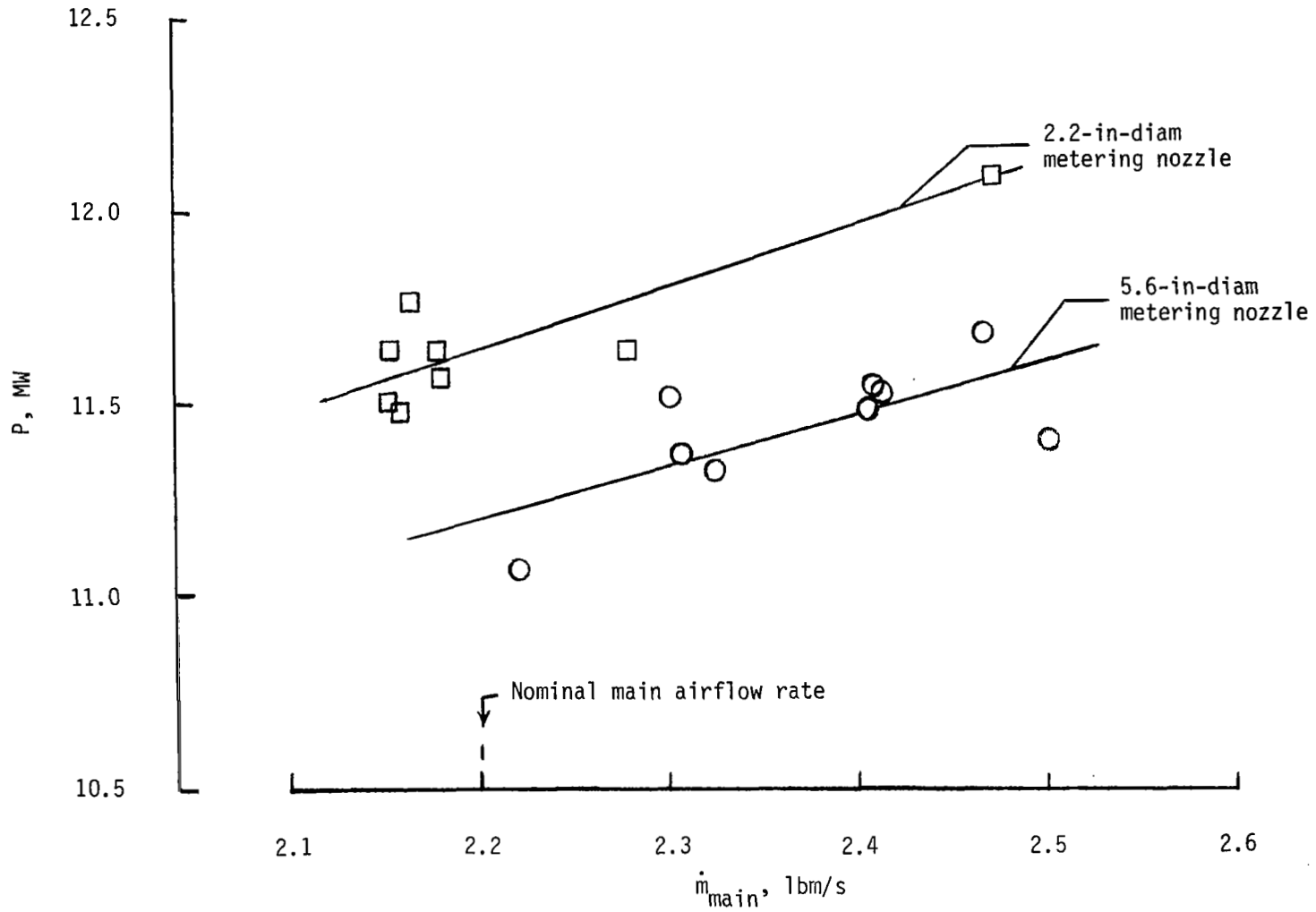


Figure 25.- Effect of main airflow rate on arc power for tap setting of 33 on both power supplies and $R_{bal} = 1.304$ ohms.

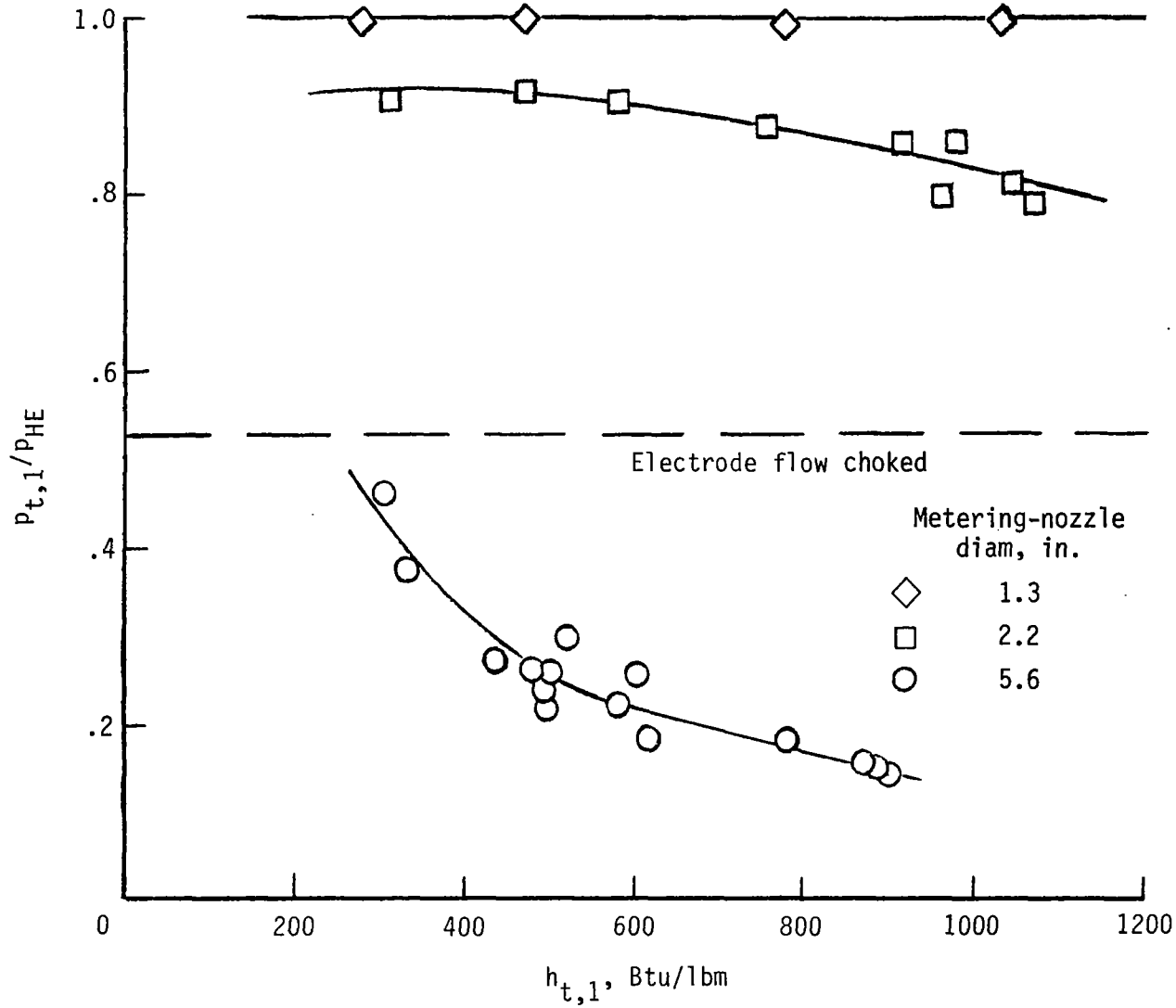


Figure 26.- Heater-plenum total-pressure ratio for nominal main airflow rates.

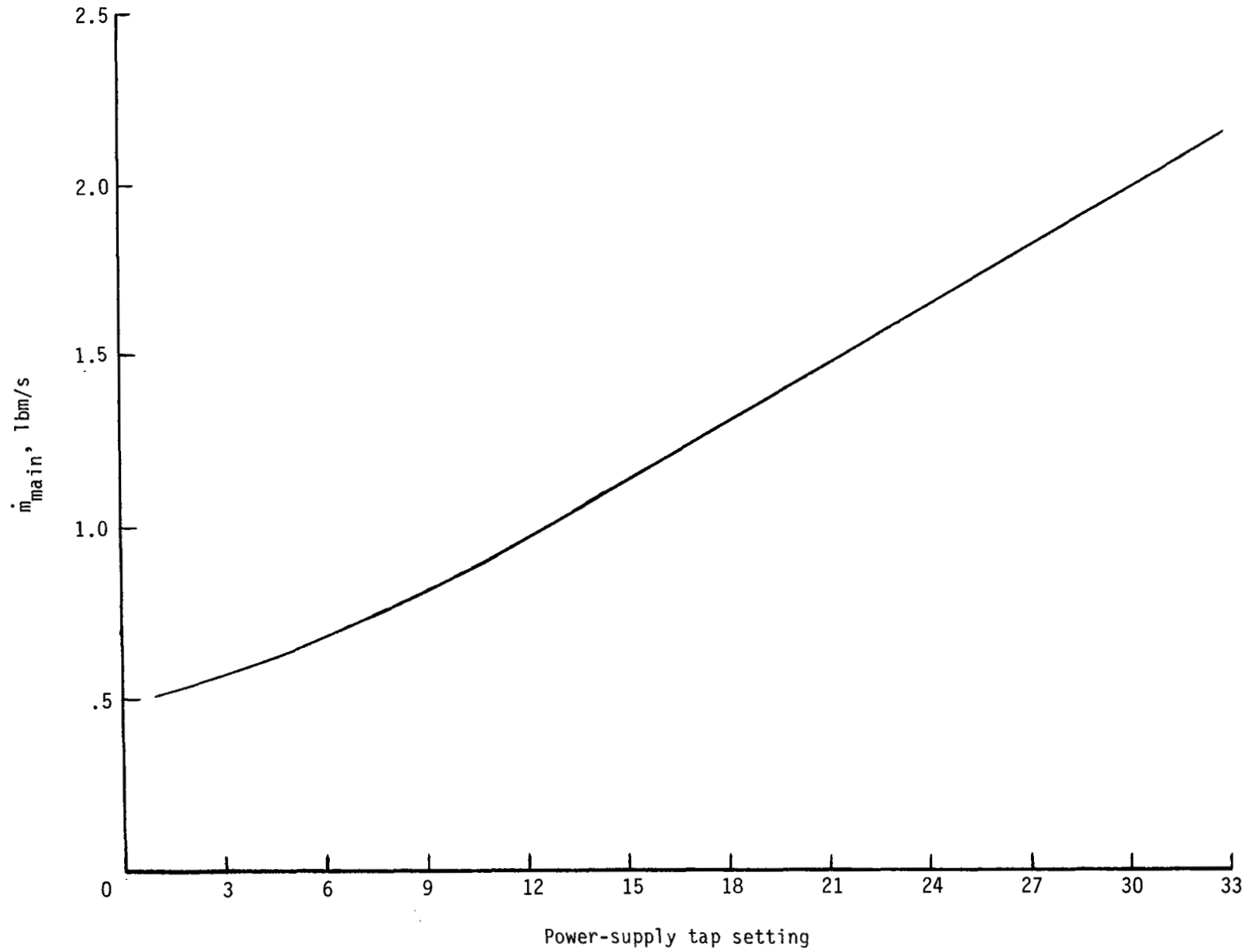


Figure 27.- Nominal main airflow rate as a function of power-supply tap setting.

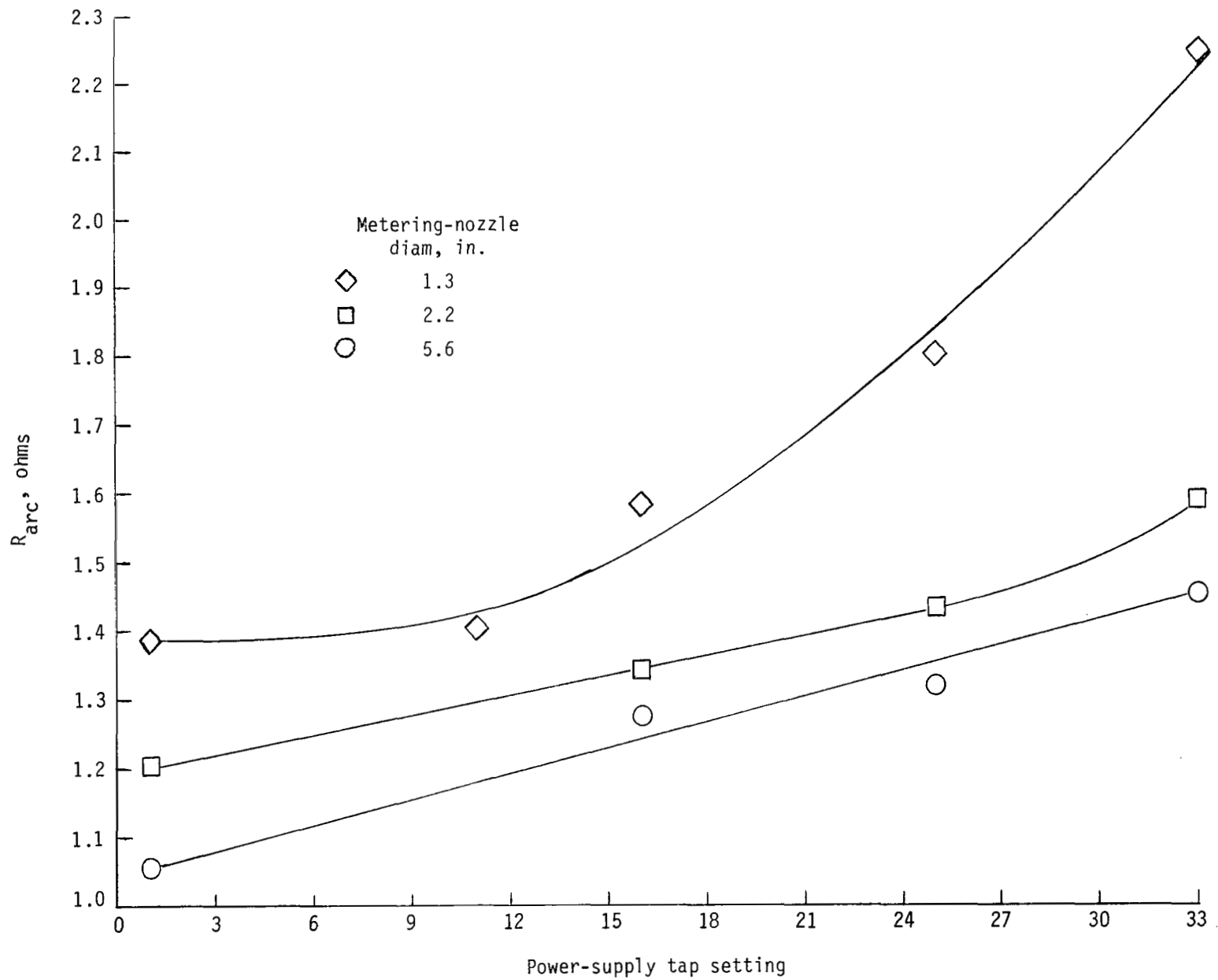
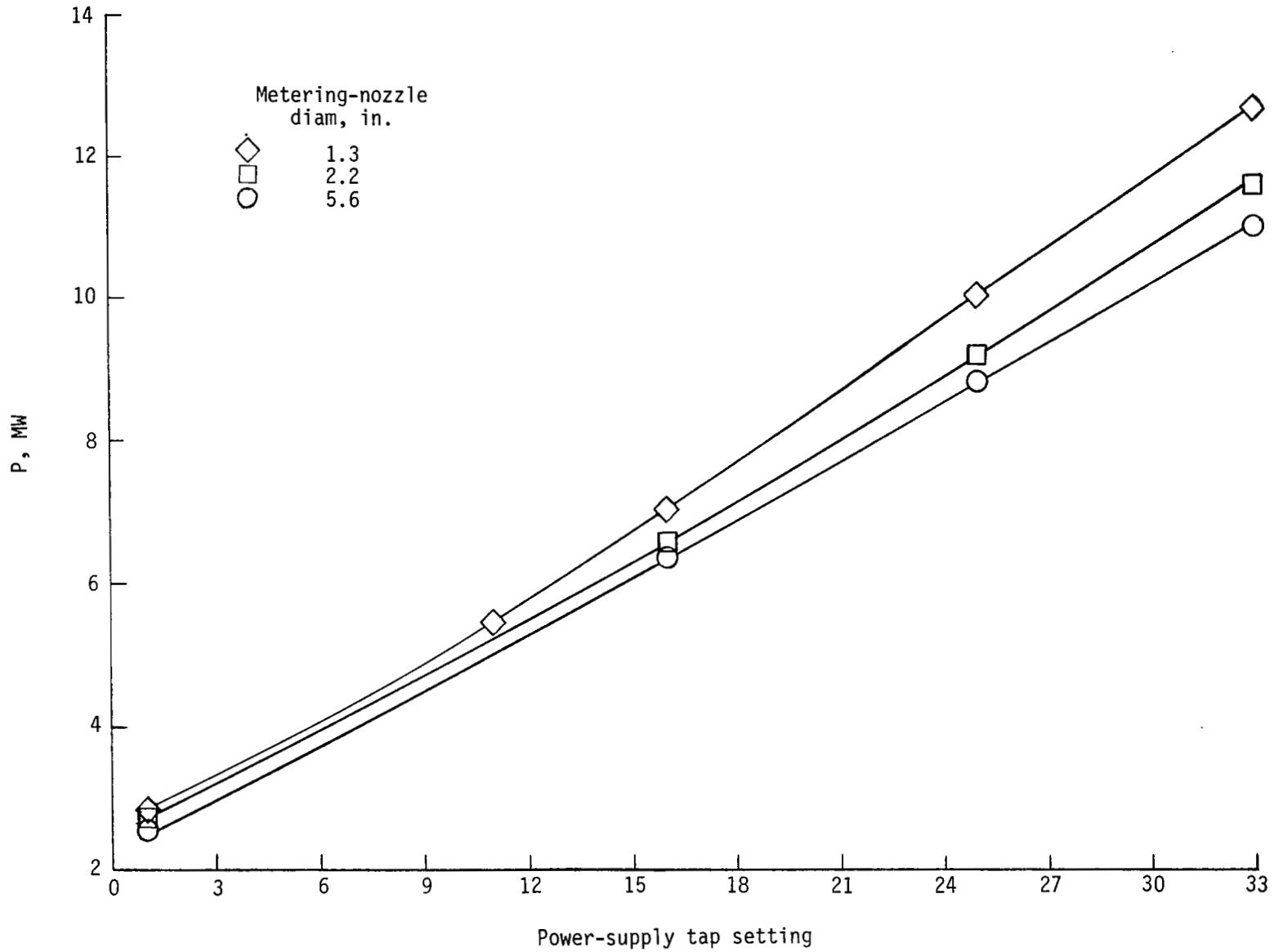
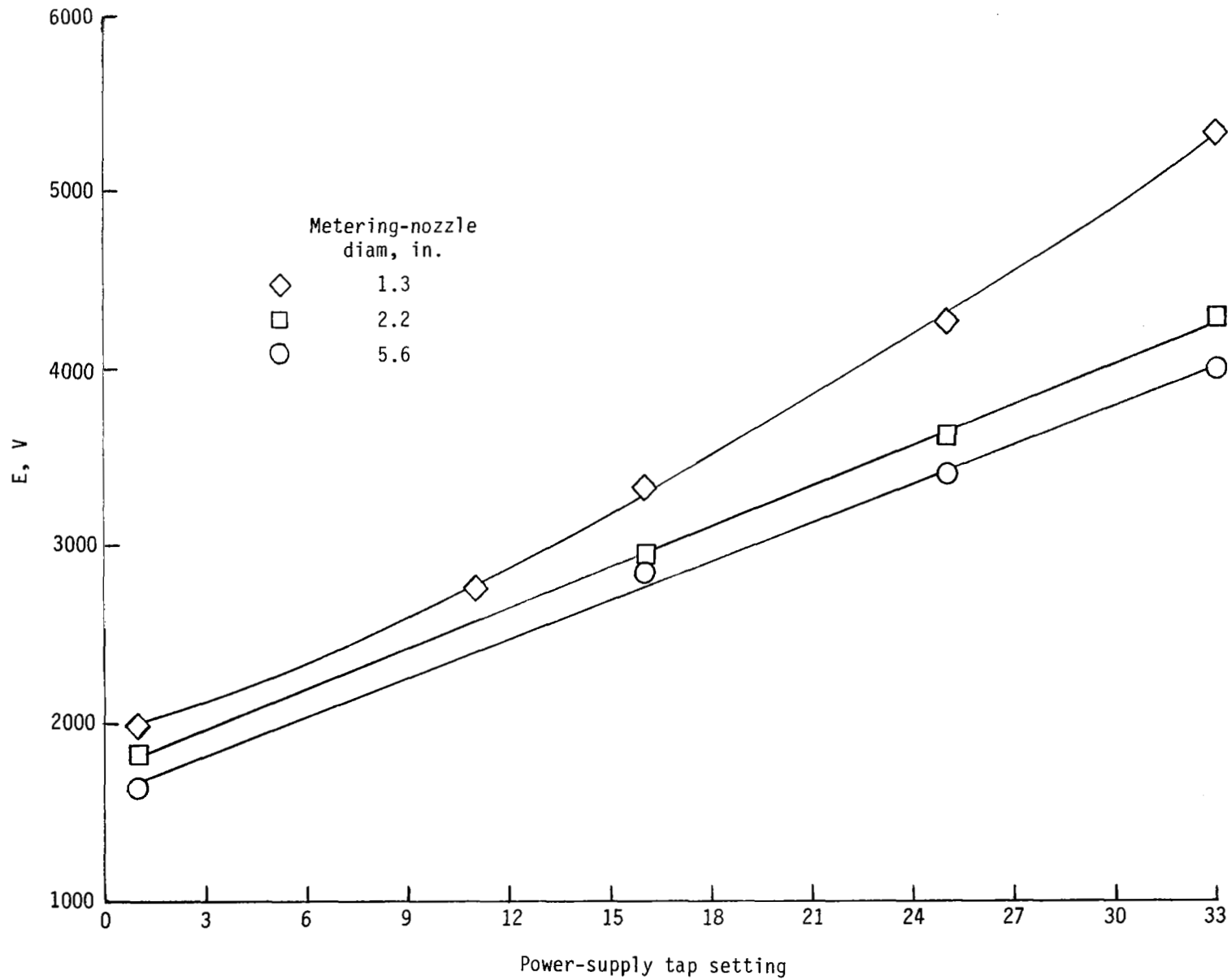


Figure 28.- Arc resistance as a function of power-supply tap setting for nominal main airflow rates and $R_{bal} = 1.304$ ohms.



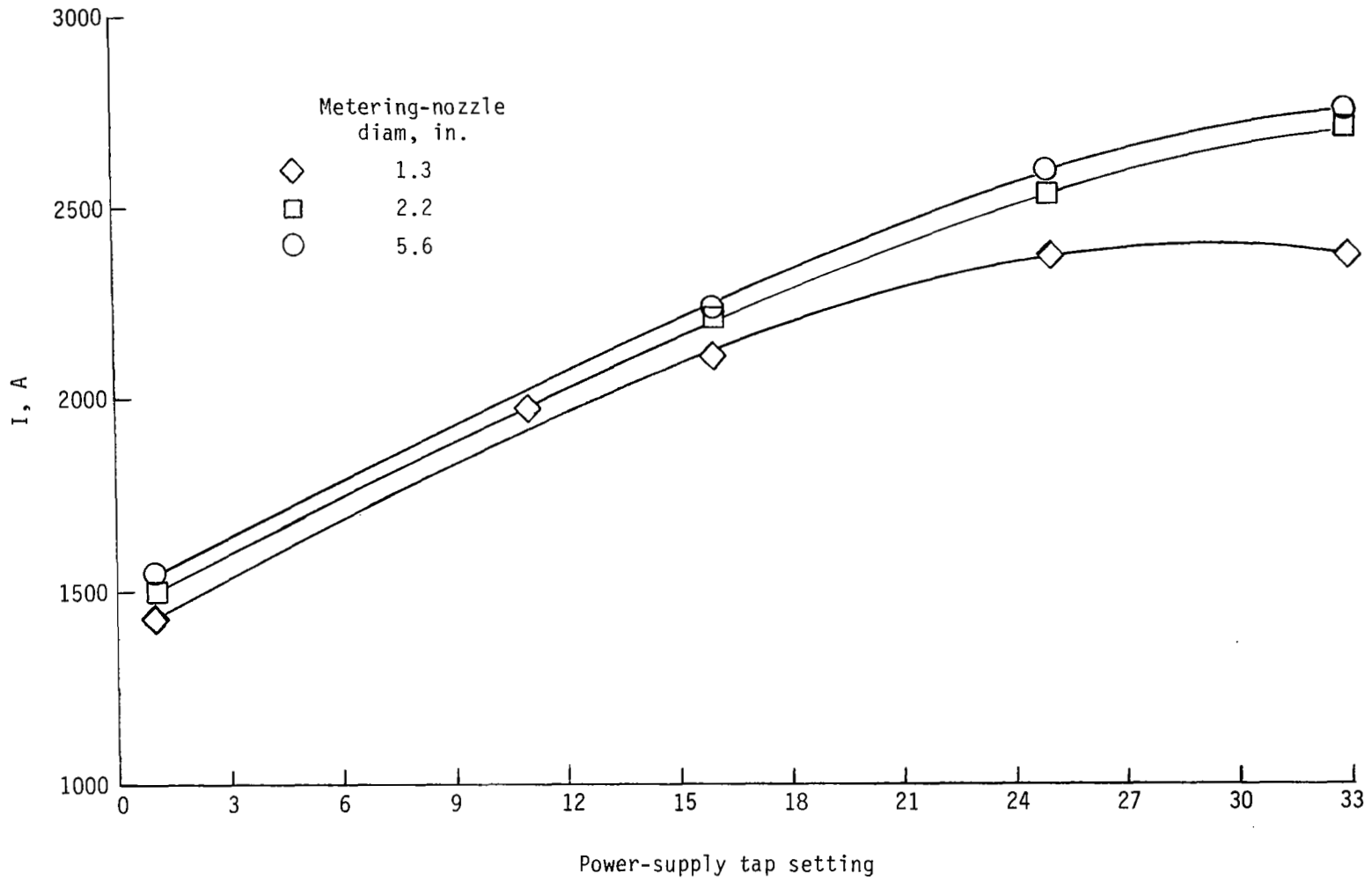
(a) Arc power versus tap setting.

Figure 29.- Arc heater electrical characteristics as functions of power-supply tap setting for nominal main airflow rates and $R_{bal} = 1.304$ ohms.



(b) Arc voltage versus tap setting.

Figure 29.- Continued.



(c) Arc current versus tap setting.

Figure 29.- Concluded.

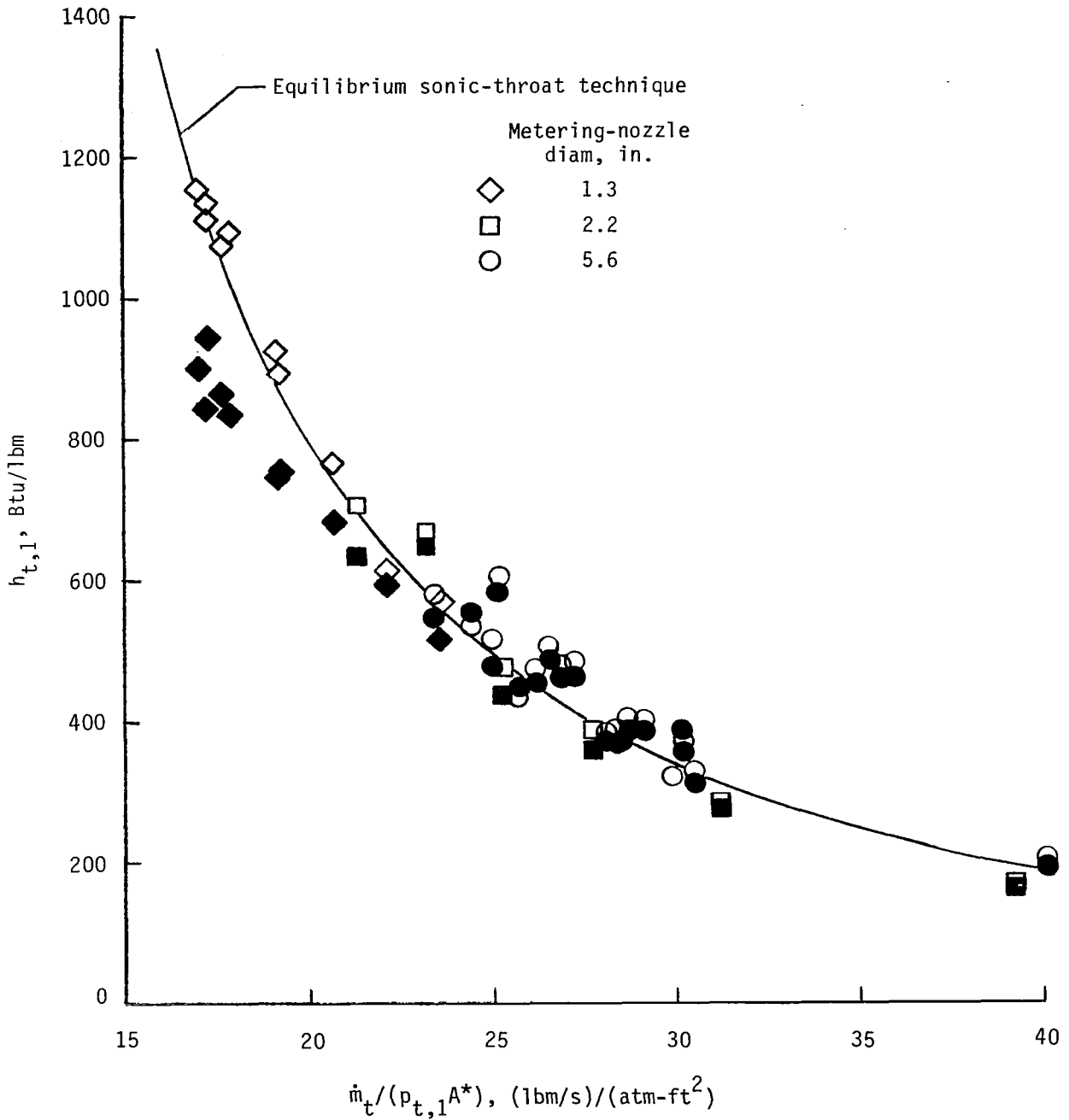


Figure 30.- Comparison of total enthalpy determined by various methods. Shaded symbols are for thermocouple measurements and open symbols are for energy-balance results.

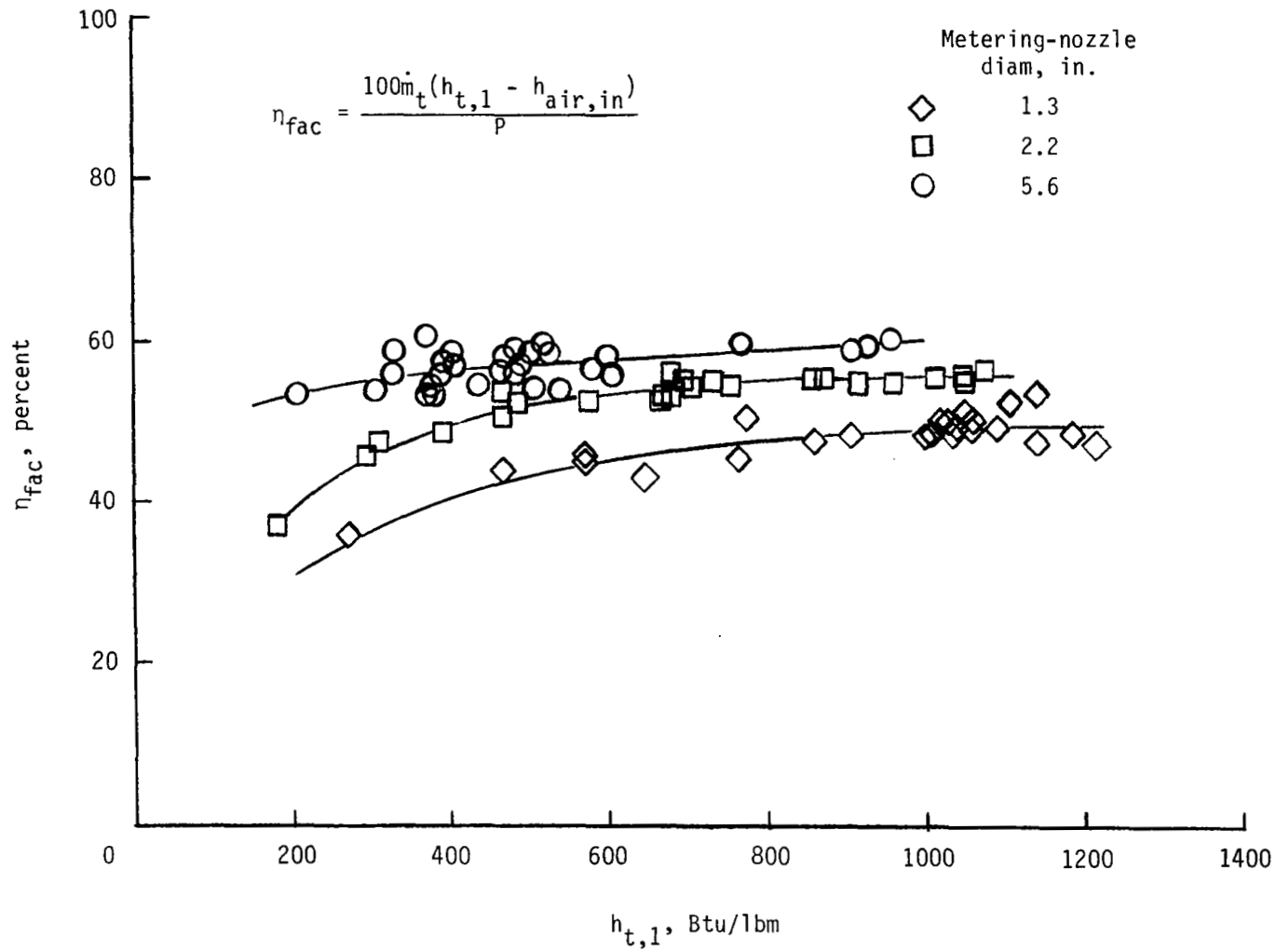


Figure 31.- Facility thermal efficiency as a function of total enthalpy.

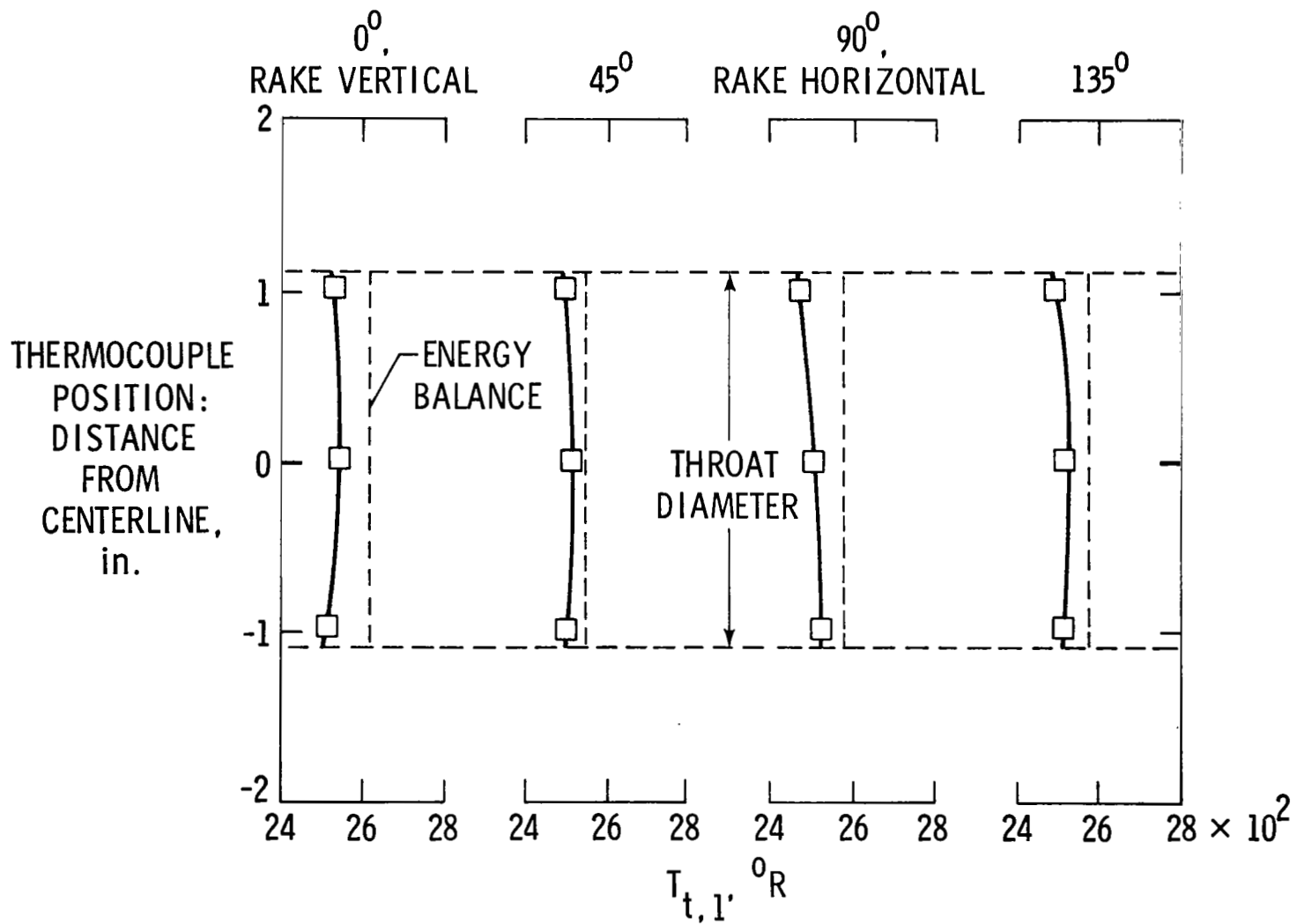


Figure 32.- Total-temperature profiles at exit of 2.2-in-diameter metering nozzle for bypass air injection configuration number 3. (See table III.) $P = 11.6$ MW; $\dot{m}_{\text{main}} = 2.2$ lbm/s; $\dot{m}_{\text{byp}} = 8.5$ lbm/s.

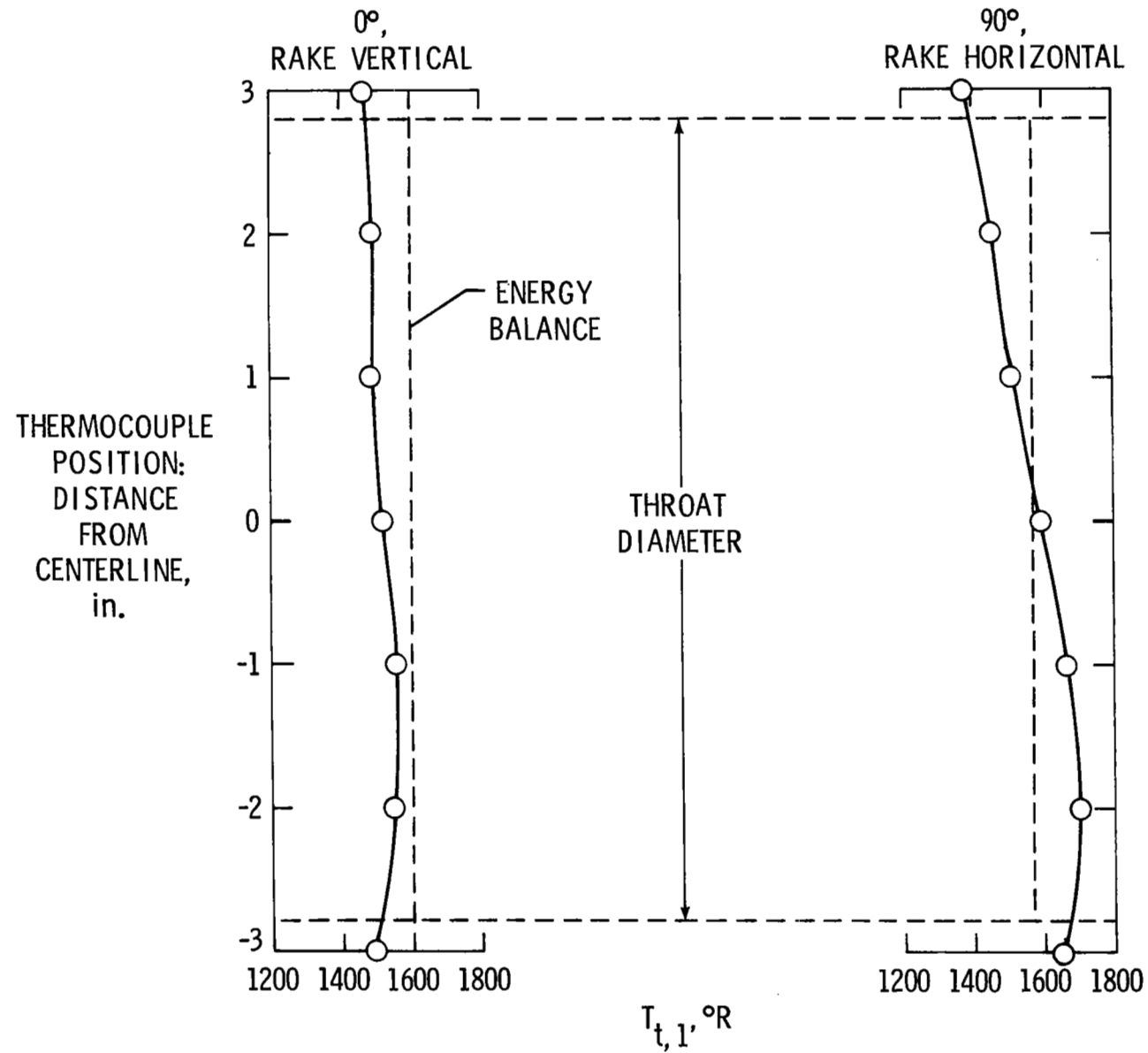


Figure 33.- Total-temperature profiles at exit of 5.6-in-diameter metering nozzle for bypass air injection configuration number 2. (See table III.) $P = 6.4$ MW; $\dot{m}_{\text{main}} = 1.3$ lbm/s; $\dot{m}_{\text{byp}} = 11.3$ lbm/s.

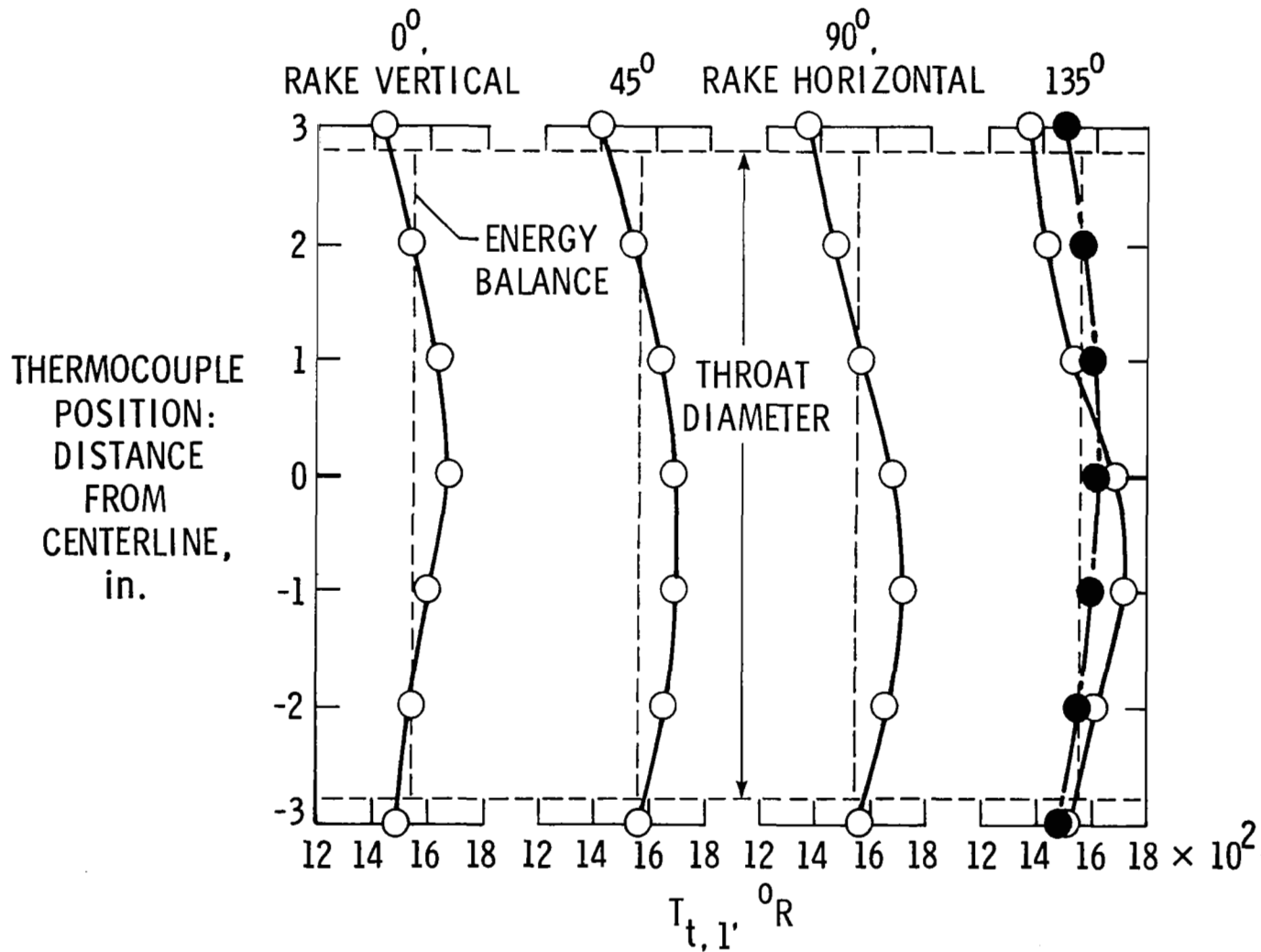


Figure 34.- Total-temperature profiles at exit of 5.6-in-diameter metering nozzle for bypass air injection configurations 3 and 4. (See table III.). Open symbols for configuration number 3: $P = 6.4$ MW; $\dot{m}_{\text{main}} = 1.2$ lbm/s; $\dot{m}_{\text{byp}} = 11.4$ lbm/s. Shaded symbols for configuration number 4: $P = 7.3$ MW; $\dot{m}_{\text{main}} = 1.8$ lbm/s.

	P, MW	\dot{m}_{main} , lbm/s	\dot{m}_{byp} , lbm/s	$\dot{m}_{\text{main}}/\dot{m}_t$
○	6.36	1.26	15.19	0.076
●	6.38	1.27	11.36	.101
●	6.29	1.24	6.48	.160

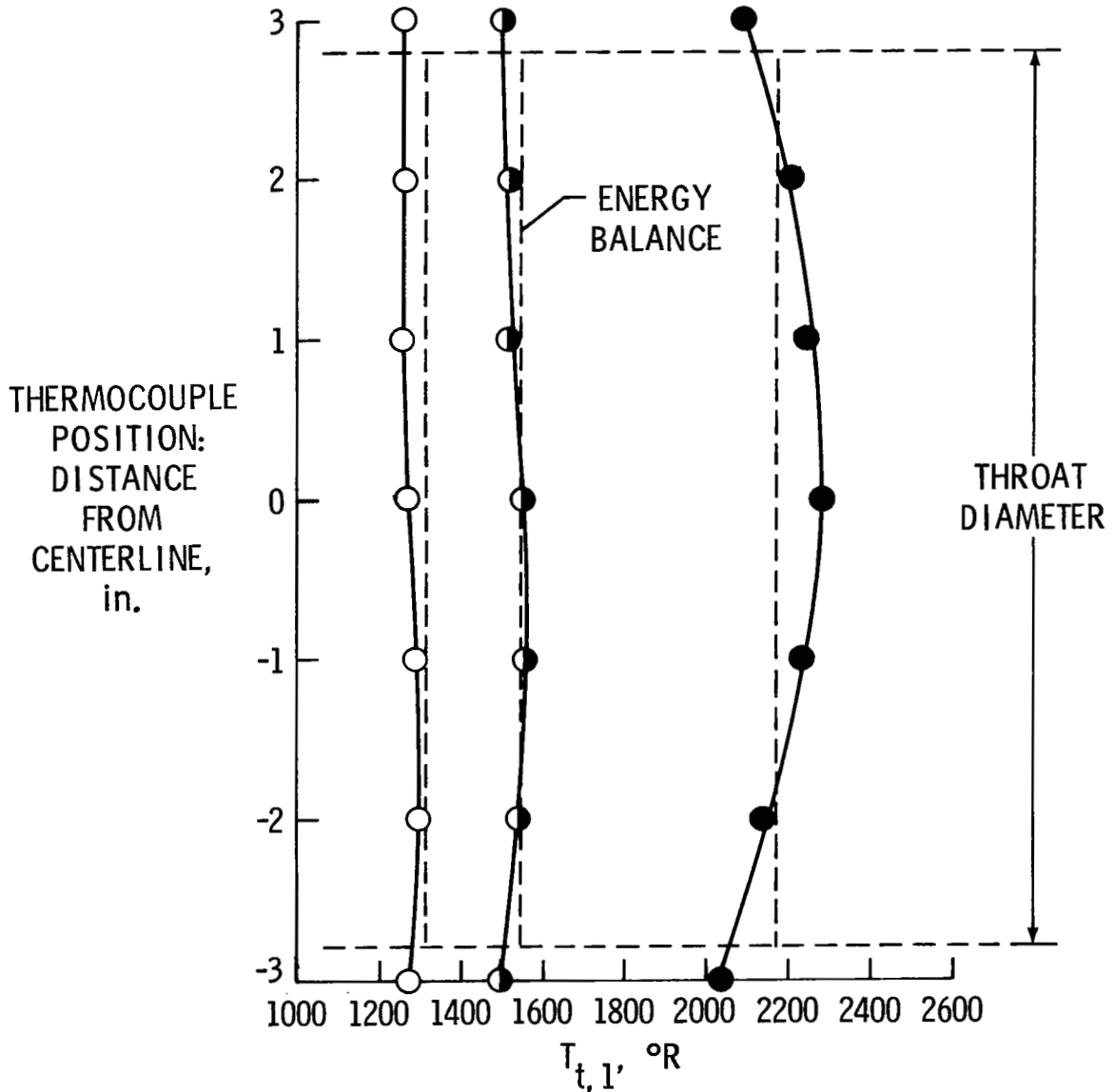


Figure 35.- Effect of bypass airflow rate on total-temperature profiles at exit of the 5.6-in-diameter metering nozzle for bypass air injection configuration number 2. (See table III.) Thermocouple rake at 0° (vertical).

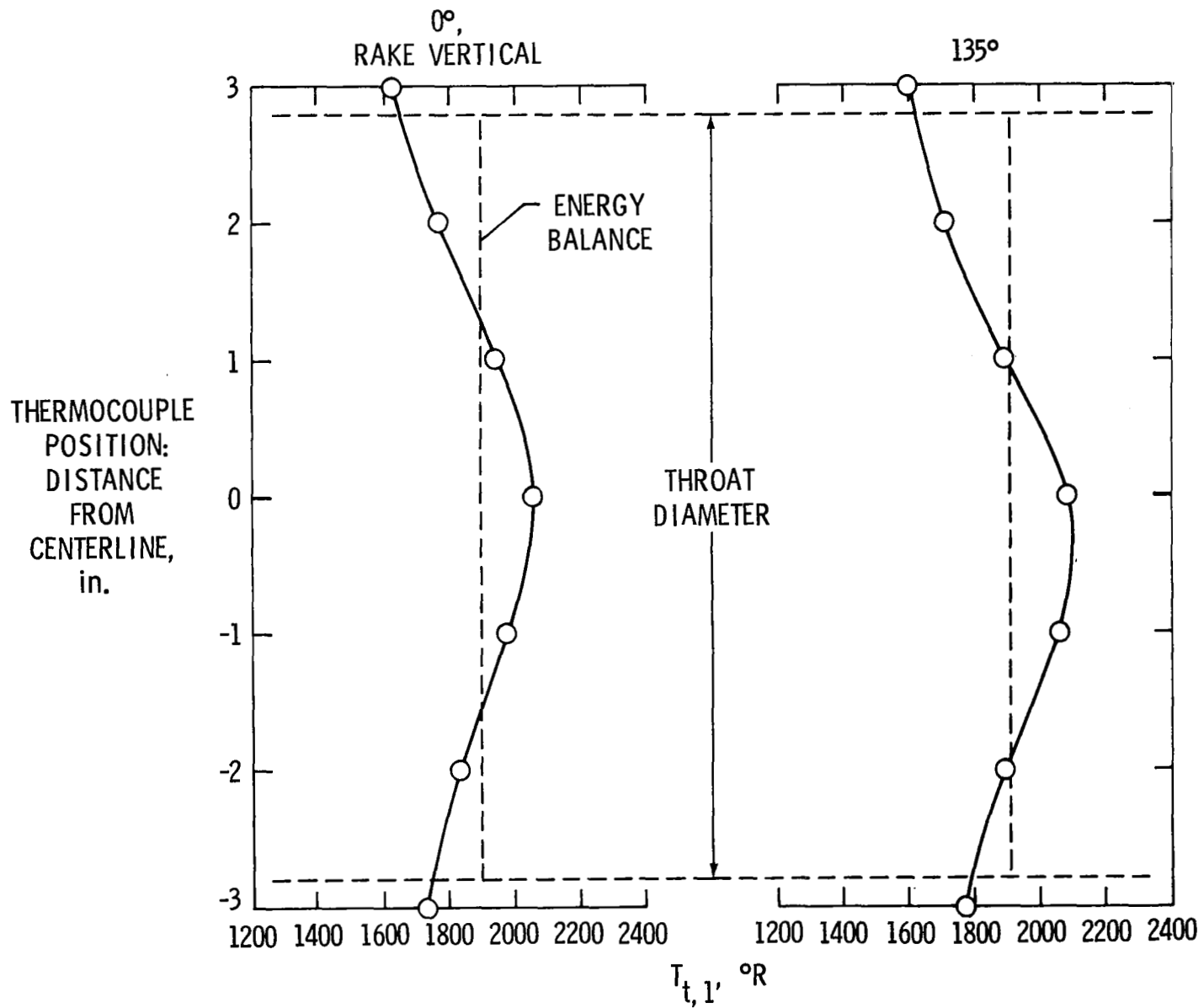


Figure 36.- Total-temperature profiles at exit of 5.6-in-diameter metering nozzle with high arc power for bypass air injection configuration number 2. (See table III.) $P = 11.5$ MW; $\dot{m}_{\text{main}} = 2.4$ lbm/s; $\dot{m}_{\text{byp}} = 15.3$ lbm/s.

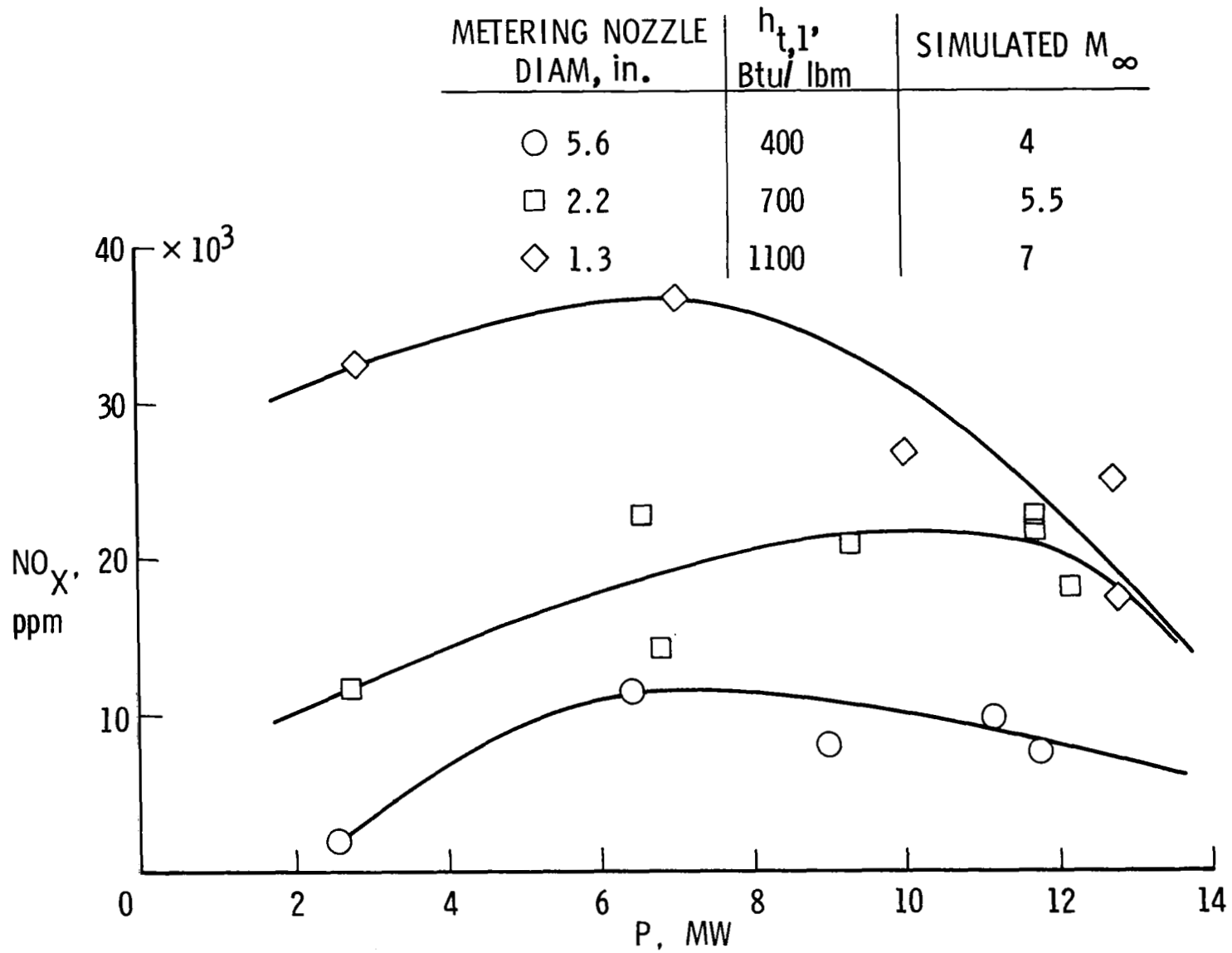
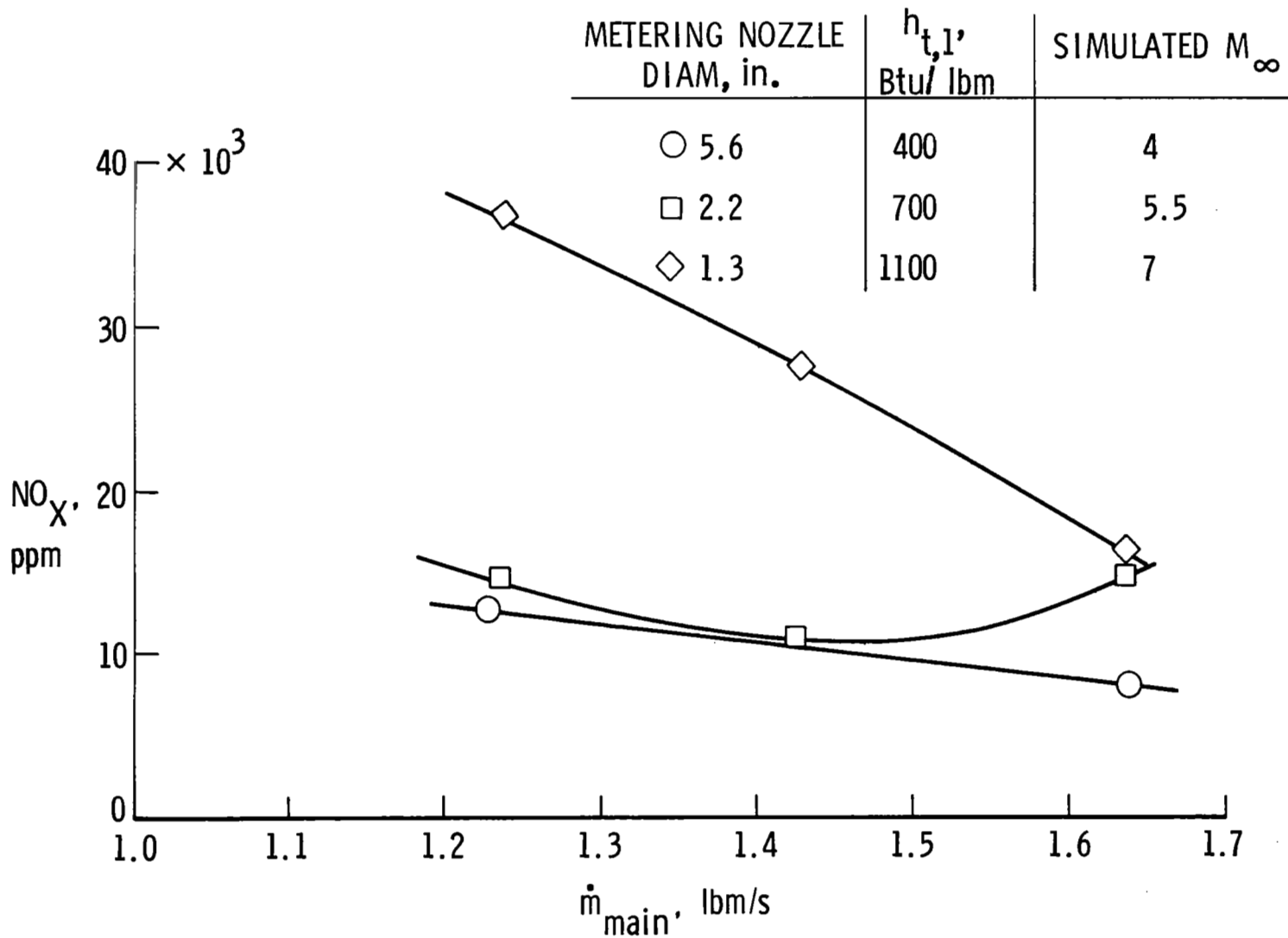
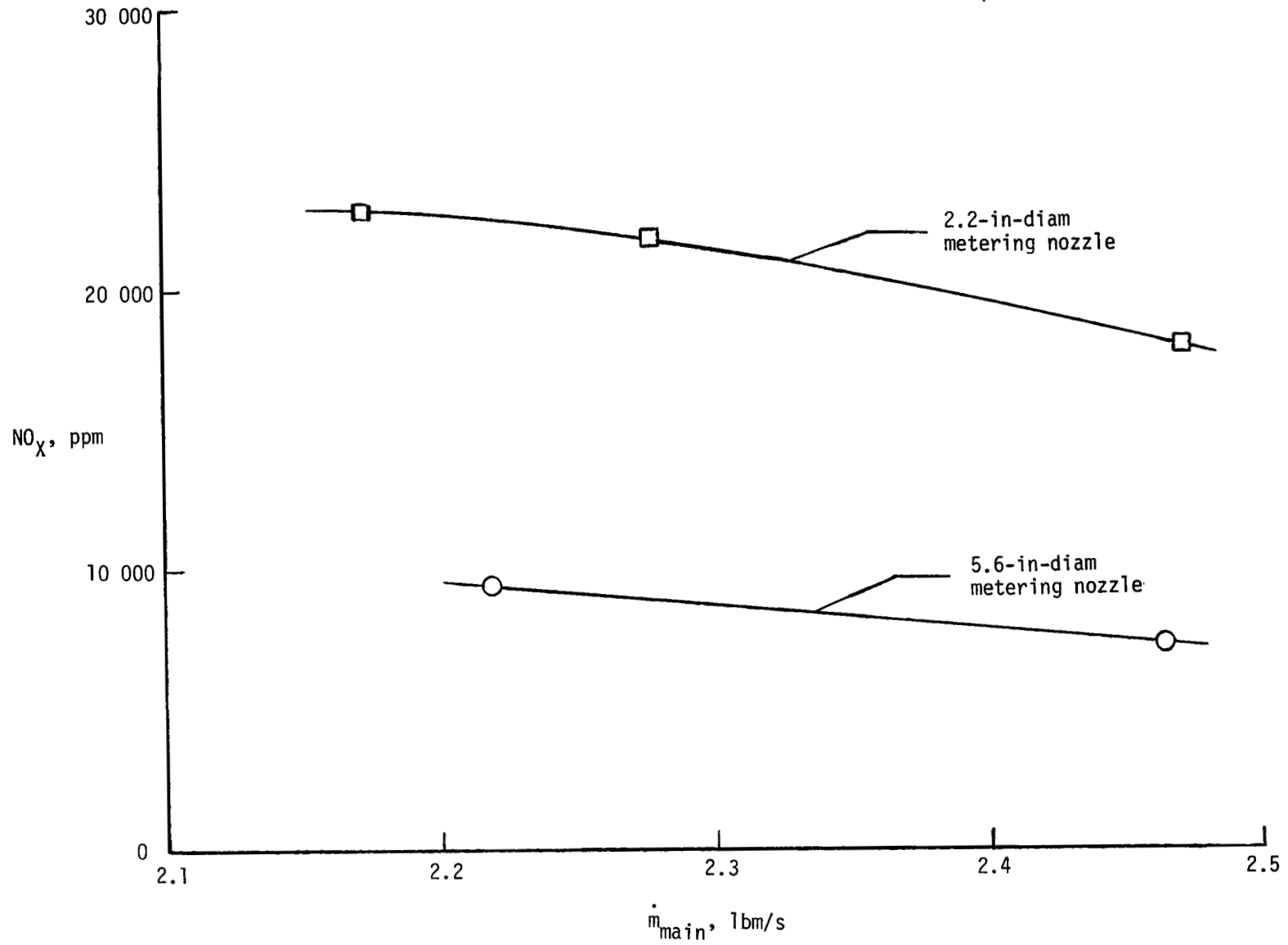


Figure 37.- Nitrogen oxide contaminants in the facility test stream for the range of simulated flight conditions and nominal main airflow rates.



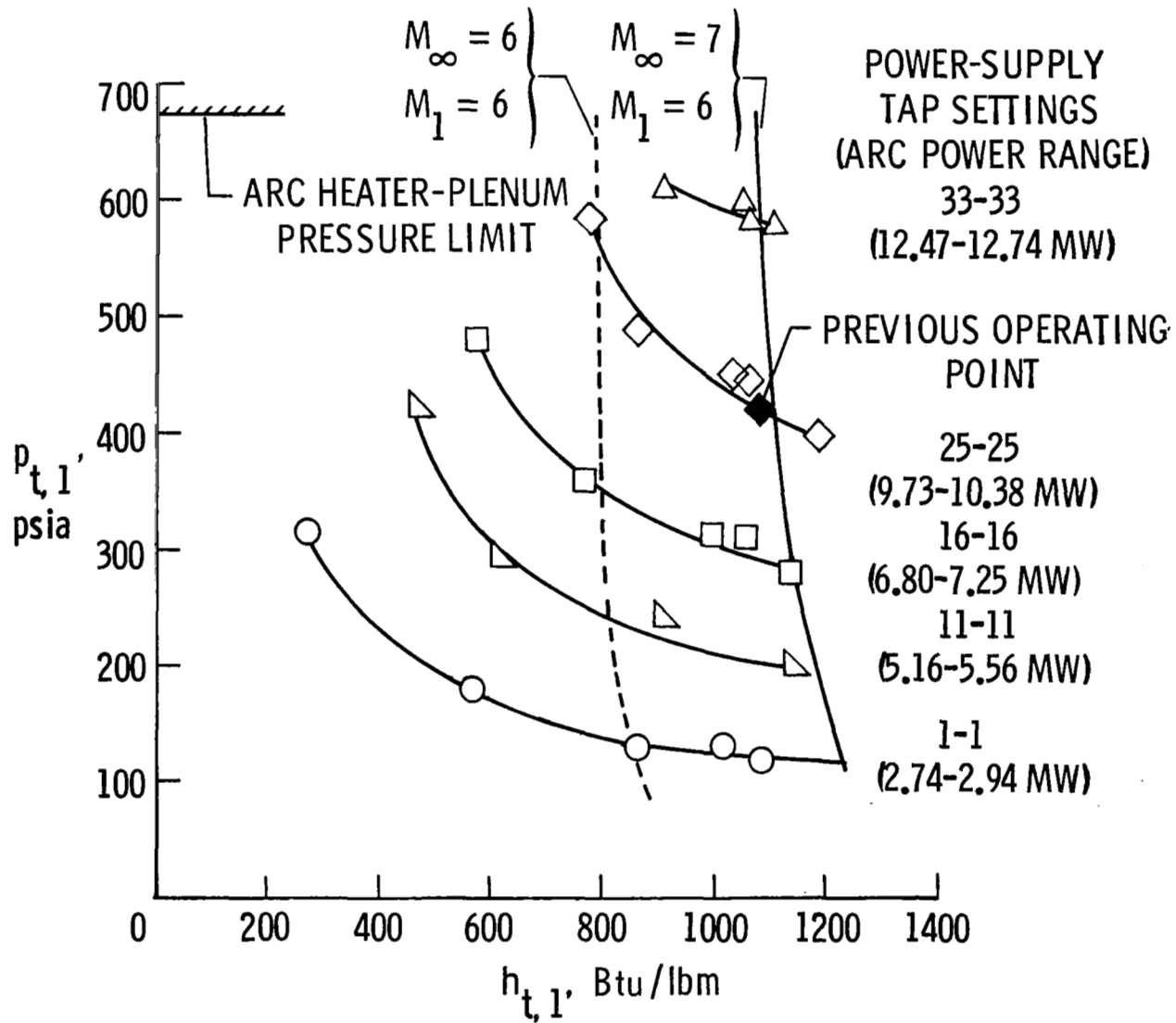
(a) Power-supply tap setting of 16.

Figure 38.- Effect of arc heater airflow rate on nitrogen oxide contamination level.



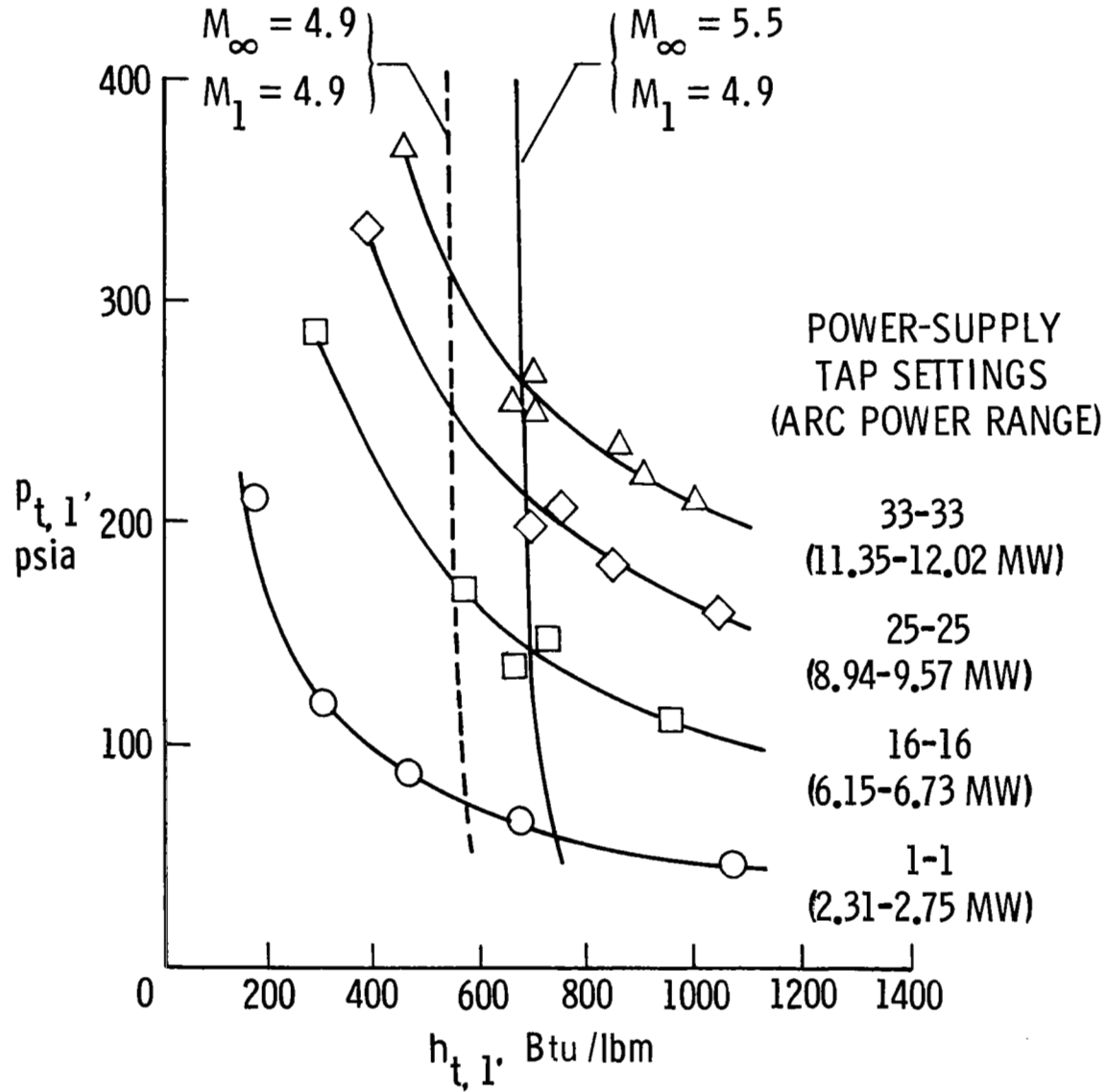
(b) Power-supply tap setting of 33.

Figure 38.- Concluded.

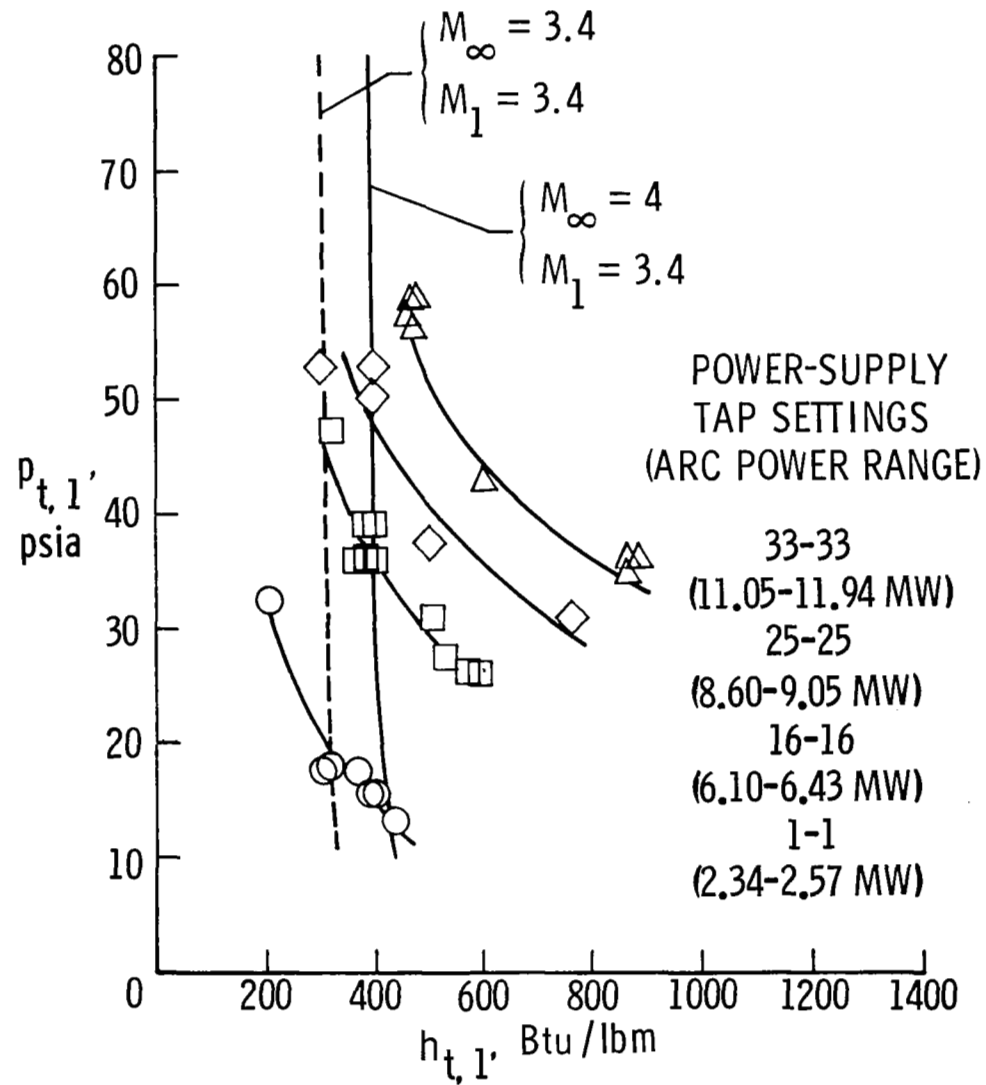


(a) 1.3-in-diameter metering nozzle.

Figure 39.- Facility operating range with ballast resistance of 1.304 ohms, new downstream electrode design, and equal tap settings on both power supplies.

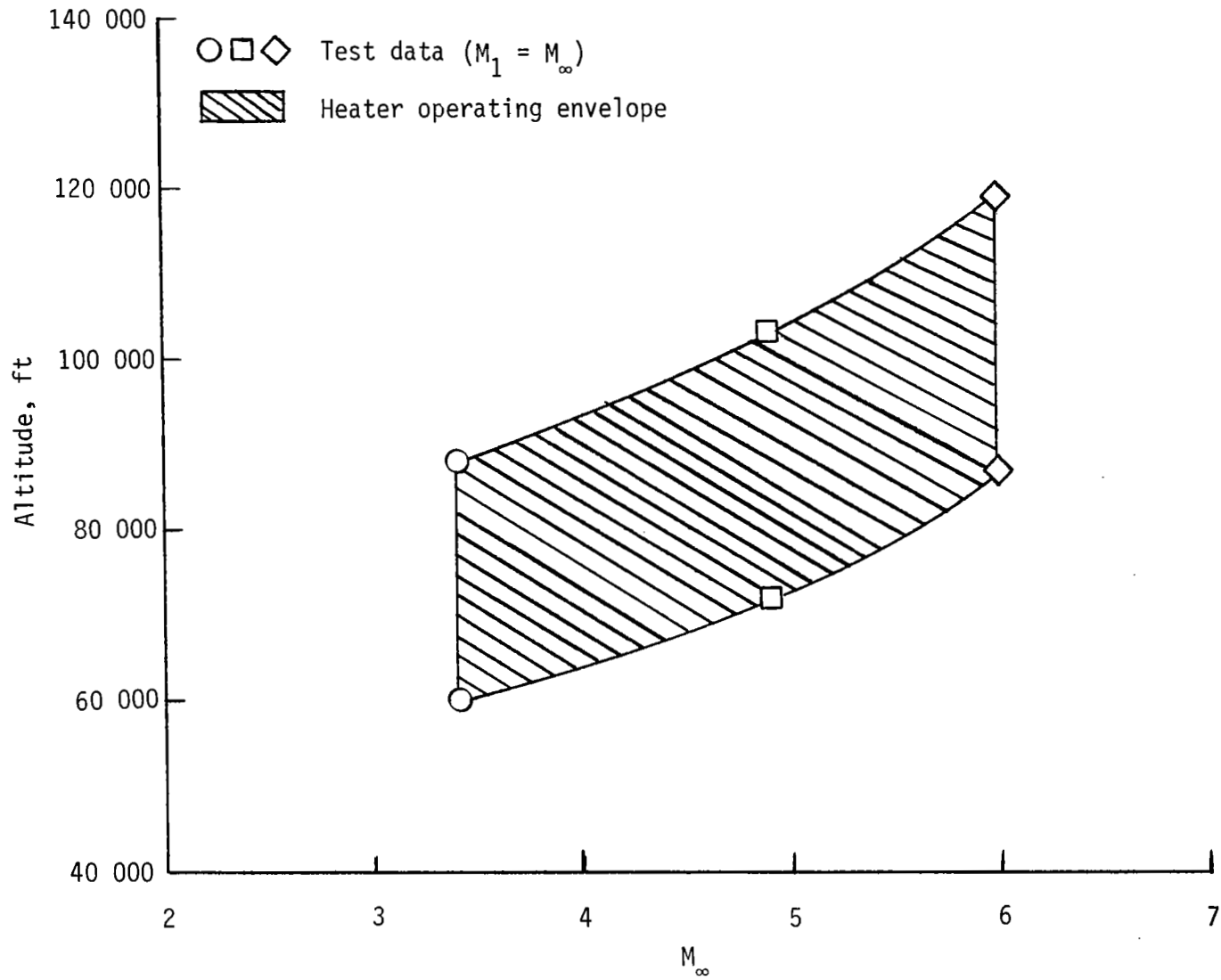


(b) 2.2-in-diameter metering nozzle.



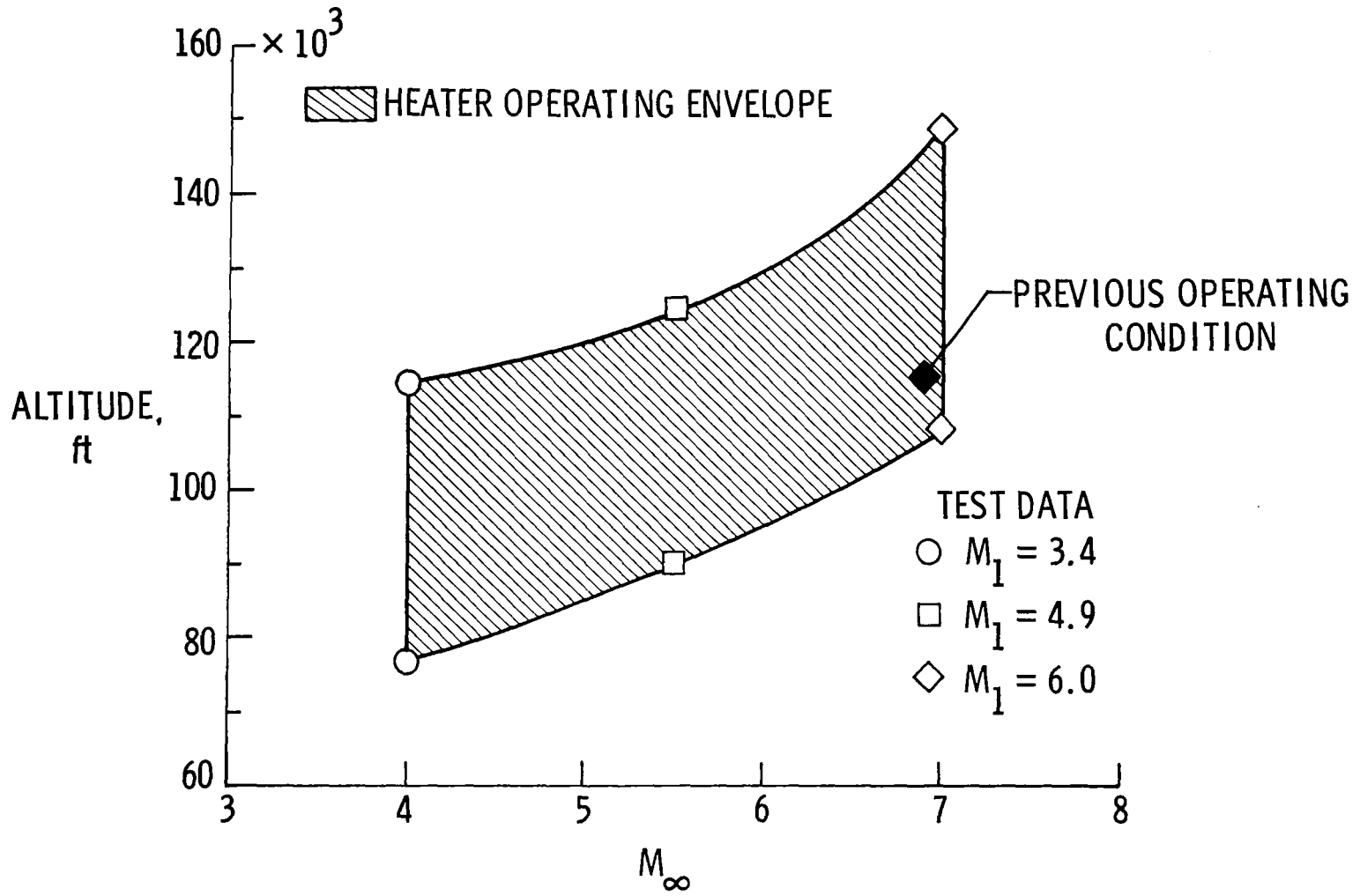
(c) 5.6-in-diameter metering nozzle.

Figure 39.- Concluded.



(a) Without precompression.

Figure 40.- New operating envelopes for the arc-heated scramjet test facility.



(b) With precompression.

Figure 40.- Concluded.

1. Report No. NASA TP-2186	2. Government Accession No.	3. Recipient's Catalog No.	
4. Title and Subtitle EXPANDED OPERATIONAL CAPABILITIES OF THE LANGLEY MACH 7 SCRAMJET TEST FACILITY		5. Report Date October 1983	
		6. Performing Organization Code 505-43-83-03	
7. Author(s) Scott R. Thomas and Robert W. Guy		8. Performing Organization Report No. L-15565	
		10. Work Unit No.	
9. Performing Organization Name and Address NASA Langley Research Center Hampton, VA 23665		11. Contract or Grant No.	
		13. Type of Report and Period Covered Technical Paper	
12. Sponsoring Agency Name and Address National Aeronautics and Space Administration Washington, DC 20546		14. Sponsoring Agency Code	
		15. Supplementary Notes	
16. Abstract An experimental research program conducted to expand the operational capabilities of the NASA Langley Mach 7 Scramjet Test Facility is described. Previous scramjet testing in this facility was limited to a single simulated flight condition of Mach 6.9 at an altitude of 115 300 ft. The arc heater research demonstrates the potential of the facility for scramjet testing at simulated flight conditions from Mach 4 (at altitudes from 77 000 to 114 000 ft) to Mach 7 (at altitudes from 108 000 to 149 000 ft). Arc heater electrical characteristics, operational problems, measurements of nitrogen oxide contaminants, and total-temperature profiles are discussed.			
17. Key Words (Suggested by Author(s)) Arc-heated facility Scramjet testing		18. Distribution Statement Unclassified - Unlimited Subject Category 09	
19. Security Classif. (of this report) Unclassified	20. Security Classif. (of this page) Unclassified	21. No. of Pages 72	22. Price A04

National Aeronautics and
Space Administration

Washington, D.C.
20546

Official Business
Penalty for Private Use, \$300

THIRD-CLASS BULK RATE

Postage and Fees Paid
National Aeronautics and
Space Administration
NASA-451



2 1 1U,A, 830929 S00903DS
DEPT OF THE AIR FORCE
AF WEAPONS LABORATORY
ATTN: TECHNICAL LIBRARY (SUL)
KIRTLAND AFB NM 87117

NASA

S

POSTMASTER: If Undeliverable (Section 158
Postal Manual) Do Not Return